博 士 学 位 論 文

TLZ Model for Assessing Long-Term Permafrost Changes in the Qinghai-Tibetan Plateau Region

（青海チベット高原地域における長期的な永久凍土の変化を評価するための TLZ モデル）

令和 5 年 6 月

茨城大学大学院理工学研究科

社会インフラシステム科学専攻

Zhao Zhijian

Abstract

As an important component of the global cryosphere, permafrost plays an important role in global climate stability and environmental sustainability of inland areas. Permafrost is also an important component of the global carbon pool, which can help reduce greenhouse gas emissions and thus serve to curb climate change. In recent years, scientific research has revealed that the continued degradation of permafrost not only affects the global climate, but may also trigger catastrophic consequences, the most alarming of which is the re-emergence of ancient viruses. Due to the continued degradation of permafrost, these ancient viruses that have disappeared may be released, posing a serious threat to human health. Therefore, we should enhance the protection of permafrost to prevent the re-emergence of ancient viruses.

Remote sensing technology is becoming increasingly indispensable in observing large areas of permafrost to assess the effects of global climate change and to protect important social frameworks. Using satellite and aerial photography, this technology can provide important information about permafrost and its impact on the environment and human activities. However, the usual remote sensing permafrost models have some problems that need to be improved in terms of analysis scale, applicability range and parameter accuracy.

Especially, the Top Temperature Of Permafrost (TTOP) permafrost model and Land Surface Temperature (LST)-zero-curtain permafrost model, which have been applied more in recent years, have some problems that must be improved in these aspects. For example, the TTOP model should improve the overall resolution of the data, improve the accuracy of the soil thermal conductivity, and reduce the error caused by the temperature observation range, etc. And the LST-zero-curtain model needs to remove the influence of vegetation and snow layer, and set the lower limit of temperature for curve change.

To address these issues and the relevance of both models, in this study we propose a new permafrost analysis model for more accurate permafrost assessment than the traditional TTOP and LST-zero-curtain models. The new model's active permafrost layer is temperature controlled by the LST and the TTOP. By using these two parameters, the model provides an accurate and reliable picture of temperature changes in the permafrost zone.

Because the water content of the soil must be taken into account when determining the TTOP level for curve changes. Here, the soil thermal conductivity at the net water content state is introduced to correct the soil thermal conductivity at the saturated water content state in the original TTOP equation. After that, the corrected TTOP value is used as the lower limit temperature of the new model, and the LST replaces the 2-10m air temperature value as the upper limit temperature of the new model, and then the lower and upper limit temperatures are used together to determine the temporal and spatial extent of the occurrence of the zero-curtain effect in the subsurface. Then the change of zero-curtain effect and the duration are used to analyze the existence of permafrost and the change law of stability. This new approach to permafrost analysis is referred to as the TTOP LST-zero-curtain (TLZ) permafrost model in this study.

In order to better apply, analyze, and validate the TLZ model, the most representative region in permafrost research, the central-eastern part of the Qinghai-Tibetan Plateau was selected as the study area for the TLZ model. There are not only a lot of long-period satellite observations from National Aeronautics and Space Administration (NASA) but also a variety of meteorological data from the China-Meteorological-Data_service-Centre (CMDC) in the study area, which provides a rich data guarantee for the smooth implementation of this study. After extensive data processing and analysis required for the TLZ model, the permafrost changes, classification and stability in the study area for the period 2012-2021 were evaluated and mapped according to the principles of the TLZ model. The results of the analysis showed that the permafrost in the study area showed an overall significant degradation trend in terms of stability and continuity during the period 2012-2021, but the permafrost that continued to degrade around 2018-2019 showed a certain degree of recovery, which we believe may be more related to the increase in vegetation and rainfall in these two years.

Later, to validate the results of the TLZ model, the Mean Anuual Ground Temperature (MAGT) model was constructed using twice-daily ground temperature data from 27 CMDC sites near the center of the study area, where daily average ground temperature data at 300, 60, 50, and 30 cm depths at each site were used to calculate daily average ground temperatures at each of the 27 sites for the period 2012-2021. Afterwards, the MAGT model results were compared with the TLZ model ground temperature estimates for validation.

Here, the comparison of ground temperature at 300 cm depth was done to verify the accuracy of TTOP values after adding the net moisture content soil thermal conductivity factor, while the comparison of ground temperature at 60, 50, and 30 cm was done to verify the accuracy of determining the zero-curtain effect in this study. The validation results showed an average SE of 0.25 °C, an average MAE of 0.27 °C, and an average RMSE of 0.19 °C at different depths. Finally, the superiority of the TLZ model was demonstrated by comparing the results with those of the TTOP and LST-zero-curtain models in the traditional study.

The TLZ model not only identifies areas where large- and medium-scale permafrost exists, but also allows for detailed small-scale stability analysis, periodic change patterns, permafrost type conversion, and degradation predictions. These features of the TLZ model offer significant advantages over traditional permafrost analysis methods. The TLZ model provides insight into permafrost conditions in a region and is expected to be a useful tool for assessing the impact of climate change on permafrost in other parts of the world. Such a detailed analytical model will help to better inform permafrost management decisions in these regions. It also provides a new direction for the development of multi-scale analytical models for permafrost with a high degree of accuracy. Further research work will be conducted on LST and 0cm ground temperature conversion, and removal of tall vegetation to better refine the TLZ model.

Contents

Chapter 1 Introduction

1.1 Background of the Study

According to common definitions, permafrost refers to ice-rich soils and rocks that are lower than 0 ℃ [1,2]. It is a typical cold-zone geological environment, widel y distributed in polar and high-altitude regions such as the Himalayas and the Arctic. Permafrost is a very fragile ecosystem with lower temperature, higher humidity, higher weathering and lower plant growth rate. Typical characteristics of permafrost include a hard surface layer, glacial action, and vertical sliding. In addition, permafrost is affected by human activities, such as climate change and pollution, which may have a negative impact on it. Permafrost is a significant part of the cryosphere, 1 of the 5 global spheres, and it covers a significant portion of the planet's land surface [3]. In today's global warming, the importance of permafrost has become more and more prominent. It has a variety of surface forms, such as glacial, rocky permafrost, permafrosty sandy soil, clayey clay, etc. These changes in surface characteristics also make the surface state of permafrost layer complex and variable. Every year, around 50×10^6 km^2 of the planet's soil experiences a freeze-thaw transition due to permafrost [4]. The freeze-thaw process of permafrost is a complex physical process that affects the surface temperature, water level, and the movement of materials, and is an important part of the Earth's climate change. The freeze-thaw process not only affects the surface geomorphology and its ecological environment, but also affects the human life and living environment. Therefore, it becomes very important to protect the permafrost layer and its ecological environment.

According to how long the permafrost remains frozen, it may be divided into three types: ephemeral permafrost, seasonal permafrost and permafrost. Ephemeral permafrost freezes in the fall of each year and melts in the spring for a relatively short period of time, generally no more than 15 days; Seasonal permafrost continues to freeze in the spring and fall of each year, generally for a longer period of time, about 15-200 days; Permafrost continues to freeze, generally for more than 700 days, and may last for several years [5].

The soil and rock layer over the permafrost layer that freezes and melts during the cold and warm seasons is known as the active layer [6,7]. Active layers greatl y influence the changes in the soil and rock layers that make them up. When they freeze, they push the ground up, creating specific landform patterns; when they melt, they make the ground more barren, making plant growth limited. When the active layer becomes deeper it causes water to accumulate in the surface layer of permafrost, making the surface wet and forming a distinctive feature of permafrost deterioration. In addition, deepening of the active layer leads to thinning of the surface soil, resulting in changes in the microbial activity and nitrogen and phosphorus nutrient concentrations of the permafrost vegetation and soil material. Therefore, the active layer becoming deeper is thought to be an indication of permafrost deterioration [6,7]. At the same time, th e principal location for gaseous, hydrothermal, and energy exchange between the outside world and the permafrost is the active layer [8,9].

Numerous variables, including air temperature, snow cover, plant cover, soil moisture, geotechnical characteristics, evapotranspiration, precipitation, geomorphology, and unfrozen water content, have an impact on the permafrost active layer's energy exchange [10–12]. Among them, air temperature is the main factor affecting energ y exchange, snow cover can reduce the melting of frozen soil, while plant cover can change soil temperature and humidity, and also affect soil albedo. Changes in soil moisture can also have an impact on energy exchange. Geotechnical properties, transpiration and precipitation can also change soil temperature and moisture, while topography and unfrozen water content can also influence the energy exchange process from a hydrological and geological point of view.

Warnings of permafrost deterioration have been made in recent years as a direct result of the greenhouse effect's global warming deepening the permafrost's active layer over a significant portion of the planet [13–16]. Since permafrost has characteristics closel y related to ecological environment and climate change, the impact of global warming on permafrost will not only affect the polar regions, but also affect the climate change in other regions, thus bringing far-reaching effects on the ecological environment of the earth. Therefore, in the context of global warming, protecting permafrost, slowing down the process of global warming, and thus protecting the ecological environment of the earth, has become an important issue that the global society must face.

The permafrost has deteriorated as a result of the extraordinary hydrothermal energy shifts in the permafrost's active layer [17,18], as well as to a number of environmenta l issues, such a notable decrease in the amount of plant cover [19], an increase in the soil's organic matter emissions of carbon-containing components, a decline in the soil's microbial stability and diversity [20–23], which has serious implications for the socia l environment and human health, a rise in precipitation makes the environment more humid and affects the normal life of people [24,25]. Milder winters [26], which affec ts the ecological balance. And the resurgence of ancient viruses in the permafrost layer [27] poses some unknown risks and poses a health threat to humans.

And that is why, it is crucial to execute long-period interactive monitoring, high temporal and spatial mapping, and evaluation of permafrost-related shifts in the thickness of the active permafrost layer according to an accurate understanding of the patterns of temperature and soil factor fluctuation. Such high-precision monitoring and assessment helps to detect early signs of permafrost changes, take early measures, and effectively avoid the adverse effects of permafrost changes on the environment. In addition, such monitoring and assessment can also help to better reveal the mechanisms of permafrost change, thus providing a basis for scientific research and environmental management.

1.2 Permafrost Research Model Development Process

The majority of permafrost study first half of the 1990s was done by groups working in the area [28], utilizing field observations and boreholes to gather information on the local distribution and kind of permafrost. Therefore, the government and related research institutions are working to form research teams to support more permafrost research in the larger region to provide a scientific basis for protecting the local permafrost environment and to help make better use of permafrost resources, financial and geographic restrictions, however, make it difficult to conduct long-term permafrost research across a large region.

The study of permafrost at this time is constrained to a primitive planimetric and two-dimensional mapping stage due to the sparse field data and small-scale. This mapping method can only give a basic description of the morphology, spatial distribution and development of permafrost, but it cannot deeply study the internal soil characteristics, active layer characteristics, geographic and natural environment, energy status, changes, transformation types, etc. Therefore, there is still much room for further exploration and in-depth expansion of permafrost research at this stage.

On the basis of physics principles and earlier research, scientists have presented a range of empirical, physical, semi-physical, and semi-empirical models for permafrost research to solve fieldwork's limitations. These models are designed to address the limitations of field work by allowing researchers to simulate the field permafrost environment indoors for in-depth studies. This also provides an easy way to think about the nature of permafrost and better utilize them in this period of permafrost research.

Among them, the empirical models mainly use the main natural geographic factors related to the conditions of permafrost occurrence to establish the relational expressions that can be deduced step by step, and then seek the laws of permafrost change on a large spatial scale. The natural geographic factors required in the empirical models are generally relatively easy to obtain, but because of the limitations limited by objective geographic factors and human cognition, the empirical models have large errors.

The physical model is based on the principle of energy conservation and makes full use of the law of water and heat energy conversion between the outside world and permafrost to simulate and analyze the distribution and changes of permafrost, which largely avoids the limitations of human perception in the empirical model, but most of the physical models require many model parameters, which generally require long period of continuous observation to obtain, which also causes a relatively large limitation in the temporality of the physical model for permafrost analysis. Although the subsequent semi-empirical and semi-physical models combine the advantages of the empirical and physical models and avoid the limitations of the empirical and physical models to a certain extent, there are still limitations in monitoring permafrost changes dynamically on a large scale and for a long period.

Remote sensing technology can greatly improve our ability to observe and study the Earth's surface, it can be used to monitor changes in the geographic environment, and it can also acquire information at a very fast rate. It can dynamically monitor information about the geographic environment over long distances, large areas, and long periods of time, and it can record a variety of permafrost-related environmental data, such as information about soil, vegetation, and water sources, for analysis and prediction. In addition, remote sensing technology can be used to study large-scale permafrost changes and help people better cope with various impacts caused by permafrost degradation.

The study strategy of mixing semi-physical and semi-empirical models with remote sensing technology has emerged as the most well-liked method for permafrost study due to the continuing growth and advancement of remote sensing technologies in the twenty-first century. This research strategy can improve permafrost research in many ways and help identify and address the spatial distribution and evolution of permafrost and its cyclical effects on environmental factors. In addition, this strategy can effectively improve the efficiency and accuracy of permafrost research, providing permafrost researchers with practical and valid information.

The combination with remote sensing technology fully solves the problems of geographical, spatial and temporal aspects of the previous semi-empirical and semi-physical models, and makes it possible to monitor the changes of permafrost on a global scale over a long period of time. As a result, scientists have proposed many models for permafrost analysis combined with remote sensing techniques.

More specifically, this approach is best represented by the permafrost models listed in Table 1.1 by time and by examples of current permafrost studies. These permafrost models each have their own benefits and drawbacks and may be used to analyze permafrost at various temporal and geographical dimensions.

Table 1.1: The most representative models and examples of permafrost studies.

Time of Presentation	**Models and Examples**
1891	The Stefan permafrost (Original) model [29]
1943	The Stefan permafrost (Modified) model [30]
1983	The Nelson permafrost (Original) model [31]
1996,1997,2002,2004	The Nelson permafrost (Modified and Examples) model [32–35
1974	The Kudryavtsev permafrost (Original) model [36]
1999	The Kudryavtsev permafrost (Examples) model [37]
2005	The mean annual ground temperature (MAGT) permafrost (Original) model [38]
2018	The mean annual ground temperature (MAGT) permafrost (Examples) model [39]
1996	The temperature at the top of the permafrost (TTOP)-MAAT permafrost (Original) model [40]
2002	The temperature at the top of the permafrost (TTOP)-MAAT permafrost (Modified) model [41]
2021,2007,2021,2021, 2022,2021,2019	The temperature at the top of the permafrost (TTOP)-MAAT permafrost (Examples) model [42–48
2020	The LST–zero-curtain permafrost (Original) model [49]
1990,2017,2022	The zero-curtain permafrost (Examples) model [50–52

1.3 Several Representative Permafrost Research Models

1.3.1 The Stefan Permafrost Model

Josef Stefan initially put out the Stefan model [29] in 1891 to analyze the thawing and freezing of Arctic lake ice and determine its thickness, and its basic principle is that when the heat inside the lake ice changes uniformly and rapidly, the phase change temperature between ice and water is equal to the temperature at the location of ice and water contact in the lake ice, i.e., the heat release from ice to water is equal to the heat absorption from water to ice in a certain time space the absorption of heat [29]. In other words, the variation law of ice thickness is inferred from the variation law of heat with time in a certain space, and the early Stefan model is widely used in the calculation of ice thickness in many cold regions because of its few parameters and simple calculation. It provides an effective calculation method that allows us to better understand the variation pattern of ice thickness. At the same time, it provides a basis for subsequent researchers that can be further improved so that they can better study the variation pattern of ice thickness.

To determine the broad spread of permafrost by using characteristics and qualities of the soil, Berggren analyzed soil ice rather than pure lake ice in 1943 [30]. He used the principles of the Stefan model to calculate the depth of the active layer in the frozen zone and came up with a more accurate result. Since permafrost and lake ice behave almost identically during freeze-thaw and their change patterns are close, it can be said that there is not much difference between them [30].

Therefore, the parameters of permafrost can be replaced by those of soil during the freeze-thaw process without much effect. Also because the distribution of soil ice is mainly influenced by the type and composition of the soil, climatic conditions and topography. For example, in polar regions, with lower temperatures and higher snowfall, soil ice covers a wider area, while in temperate regions, with lower temperatures and rainfall, the distribution of soil ice is smaller. In addition, the type and composition of the soil can also affect the distribution of soil ice. Soil ice can form and develop more readily in coarse and fine sandy soils, and more slowly in clay and gravel. Thus, Berggren's study provides an important practical basis for the distribution and depth variation of permafrost.

In the next time, scientists introduced some factors related to surface temperature into the Stefan permafrost model applied to permafrost, which include surface temperature change rate, surface emissivity, surface albedo, atmospheric pressure, etc. These factors can better reflect the actual situation of permafrost heat transport. to improve the applicability of the Stefan permafrost model in permafrost analysis and calculation. Because of its small computational size, the Stefan permafrost model is well suited to analyze and predict large-scale permafrost by year without pursuing accuracy. It can help us grasp the trend of permafrost changes in a holistic manner and effectively predict the environmental changes caused by permafrost changes on a large scale scale.

1.3.2 The Nelson Permafrost Model

The Nelson permafrost model [31] sometimes known as the Nelson freeze-thaw index model, was proposed by Nelson et al. in 1983 and is based on Stefan's permafrost model. The Nelson permafrost model is mainly based on the heat transfer properties of the soil, using the extreme monthly temperature method to calculate the surface temperature, and then the Stefan permafrost model applied to permafrost to estimate the thickness change of permafrost during the freeze-thaw period, and then infer the distribution of permafrost.

The Nelson permafrost model is identical in principle to the Stefan permafrost model in that it starts from the perspective of the effect of potential soil heat on the thickness of the active layer and uses the corrected air temperature to derive the surface temperature, so that it can more accurately reflect the temperature change of the actual environment. The Nelson permafrost model also takes into account the loss and gain of energy transfer, as well as the humidity and wind speed in the atmosphere, which are not taken into account by the Stefan permafrost model, when calculating the surface temperature. In addition, the Nelson permafrost model uses a more accurate numerical algorithm, which reflects the temperature variation of the actual environment more precisely.

But, on a broad regional scale, this model has difficulty determining the attenuated air temperature and the amount of unfrozen water in soils. For example, in winter in some regions, air temperature may decrease more rapidly than the amount of unfrozen water in the soil, while in other regions, the amount of unfrozen water in the soil may decrease more rapidly. In addition, the model is unable to determine under which climatic conditions this attenuation is most pronounced and in which areas it will be most affected. Therefore, the accuracy of this model may also vary at different regional scales, and further research is needed to determine its accuracy at different regional scales. Nelson et al. made some local improvements to the Nelson permafrost model in the following decades [32–35] to increase the applicability of the Nelson model at hig h latitudes, and these improvements helped to improve the computational accuracy of the Nelson permafrost model to better reflect the state changes during soil freezing and thawing.

However, these improvements do not take into account the effects of snow and vegetation, and therefore, the accuracy of the Nelson permafrost model in snow and vegetation-covered areas may be lacking. To solve this problem, some researchers now try to develop Nelson permafrost models that take snow and vegetation into account. Because the Nelson model is able to simulate the temperature change during the freeze-thaw period and because it requires fewer parameters, it is more applicable in the field of large-scale permafrost analysis where the freeze-thaw period needs to be considered.

As described in Sections 1.3.1 and 1.3.2, the Stefan permafrost model and Nelson permafrost model, which are large-scale models for predicting the distribution of permafrost, depend mainly on latitude and longitude, soil characteristics, elevation, and unfrozen water content. Both models can predict the distribution of permafrost by calculating the thickness variation of permafrost on a large scale. However, in practice, geographic and climatic variables at small and medium scales are also important factors affecting permafrost distribution. For example, climate change affects the distribution of permafrost in a given area, and geomorphic topography affects the vertical distribution of permafrost.

Therefore, large scale models alone may not be able to accurately capture these small and medium scale variables, thus making the large scale models limited in the accuracy of simulating permafrost distribution. Therefore, for permafrost distribution studies that require higher accuracy, these two models may not be very useful.

1.3.3 The Kudryavtsev Permafrost Model

In order to solve the shortcomings of Stefan's permafrost model in permafrost research, Kudryavtsev proposed the Kudryavtsev permafrost model in 1974 [36], which changed the assumptions of Stefan's permafrost model and took the temperature variation into account as an independent variable, thus reflecting the dynamic characteristics of permafrost more accurately. The emergence of the Kudryavtsev permafrost model has brought new ideas to the study of permafrost, making it more accurate and more in-depth. It is based on the effects of temperature and climate on permafrost, including effects on permafrost cover, temperature, moisture, humidity, vegetation, snowpack, wind speed and direction.

When the temperature decreases, the permafrost cover increases; the moisture content increases and the humidity increases; the wind speed decreases and the wind direction changes. As a result of these changes, the biodiversity and ecosystem function of permafrost will change, and the structure and properties of permafrost will also change. The Kudryavtsev permafrost model aims to comprehensively explore the various layers of the permafrost system through the study of the thermal state of the soil. It takes into account the influence of soil water content and temperature on permafrost, combines surface and subsurface meteorological factors, and studies the movement characteristics, water transport, energy exchange and hydrogeological processes of the layers in the permafrost system, thus providing an in-depth analysis of the formation mechanism of permafrost and its natural laws.

The algorithm takes into account not only the effect of potential soil heat on the active layer, but also the heat capacity and heat conduction effects of the soil itself. For example, the heat capacity can affect the rate of change of soil temperature and the heat conduction effect can change the distribution characteristics of soil temperature. In addition, heat conduction effects can also affect the direction of change of soil temperature and increase the gradient of soil temperature. Theoretically, the Kudryavtsev permafrost model is a comprehensive improvement of the Stefan permafrost model, which more accurately simulates the soil thermal effect. However, a large number of model parameters need to be entered to achieve a more accurate simulation.

These parameters need to take into account the structural and compositional properties of the soil, as well as the surface morphology of the soil, which are important factors in the soil thermal effect. In addition, the variation of the internal soil temperature field, moisture field and flux field need to be considered, and these parameters are also important factors influencing the soil thermal effect.

This model benefits from a more thorough consideration of the heat transfer mechanisms that occur between the atmosphere and the soil in the permafrost zone, which improves the prediction of climate change in the permafrost zone to some extent. Although this model has been utilized in the Kuparuk area of the northern Alaska, USA [37], it is less frequently used than other permafrost models for permafrost study, mostly because the model needs more parameters and some specific parameters are difficult to obtain periodically in some study areas with relatively harsh geographic environments, plus the high accuracy requirements of individual parameters can easily lead to errors in interlayer simulations.

1.3.4 The Mean Anuual Ground Temperature (MAGT) Permafrost Model

The MAGT permafrost model [38], the mean annual ground temperature model, was initially applied in 2002 in a borehole empirical study of the eastern Qinghai–Tibetan Plateau along the highway by Nan et al. After that, in 2005, Nan et al. presented the MAGT permafrost model in a forecast of the future permafrost distribution on the Qinghai Tibetan Plateau, which is generally understood to be the subsurface temperature at the level where the annual temperature variation of permafrost is 0.

This permafrost model was formulated by correlating temperature data from multiple boreholes in the east of the Qinghai–Tibetan Plateau with their elevational coordinates and latitudinal, and this correlation was used to set the boundary between permafrost and non-permafrost regions. This model can help us understand more accurately the distribution of permafrost on the Qinghai-Tibet Plateau and the impact of permafrost on the surrounding environment by using real measurement data.

Aalto et al. [39] and Qin et al. [15] both successfully explored the evaluation o f permafrost on the Tibetan Plateau using the MAGT permafrost model in 2018 and 2017, respectively. These studies give a quantitative evaluation of the geological changes of permafrost and lay the foundation for the studies related to the measured permafrost model.

In addition, these studies also provide an important reference and validation basis for mapping permafrost distribution in the Qinghai-Tibetan Plateau area. Therefore, the studies related to the MAGT permafrost model are of great significance for better understanding the permafrost geological conditions and developing the resources in the Qinghai-Tibetan Plateau area.

In summary, the MAGT permafrost model has two main advantages: firstly, it can accurately predict the cyclical variation pattern of subsurface temperature using long-term subsurface temperature data collected at various depths, and secondly, it can better evaluate the correlation between permafrost and elevation change considering the geographic elevation change in the Qinghai-Tibetan Plateau area. At the same time, because the Qinghai-Tibetan Plateau is a research area with large and relatively concentrated permafrost coverage, the research results using the MAGT permafrost model are more reliable and can be used to evaluate the research results of other models to achieve comparative verification between different permafrost models.

However, in the absence of real measurement data, this model cannot perform its function. Without these data, the reliability and accuracy of the model cannot be guaranteed. Therefore, before model modeling, it is necessary to have enough real measurement data to achieve the best analysis results only when the model can rely on valid data. This is the limitation of this permafrost model.

1.3.5 The Top Temperature Of Permafrost (TTOP) Permafrost Model

Smith and Riseborough's TTOP permafrost model, first suggested in 1996, is a semi-physical and semi-empirical permafrost analysis model that examines the energy conversion and balance link between climate and permafrost [40]. This model fully considers the influence of climate and energy changes on the development and evolution of permafrost, and can predict the distribution and performance characteristics of permafrost relatively accurately.

TTOP represents the temperature value at the contact between the subsurface permafrost layer and the active layer, which is generally referred to as the temperature at the top of permafrost. TTOP is an important thermal characteristic that can help us better understand changes in subsurface permafrost levels and respond accordingly in a timely manner. In addition, this indicator can also help us better analyze the effects of climate change and the possible causes of surface temperature changes.

The TTOP permafrost model, which analyzes the relationship among air temperature and temperature of the permafrost layer at the top in multi-year permafrost from the viewpoints of negative temperature displacement after removing the effects of snow cover and vegetation cover. It was found that the variation of permafrost is mainly influenced by the temperature difference between air temperature and subsurface temperature and the thermal conductivity of the soil in different seasons.

Therefore, by defining the heat transfer of permafrost, we can infer the distribution and changes of permafrost. In addition, the model can be used to study the effects of permafrost and other factors on the environment, as well as to predict the degradation of permafrost due to climate change.

According to the principle of TTOP model, if the sum of air temperatures in the thawing period is greater than the sum of air temperatures in the freezing period within a certain time period, then the value of TTOP is greater than zero, which means there is no permafrost or seasonal permafrost. Conversely, if the sum of the air temperatures during the thawing period is less than the sum of the air temperatures during the freezing period, then the value of TTOP is less than zero, which means that permafrost exists [40]. In other words, permafrost exists when the rate of change in temperature is not sufficient to compensate for the drop in temperature during the freezing period.

Riseborough updated the TTOP permafrost model in 2002 to account for the frozen season [41], and in the following two decades, as shown in Table 1.2 TTOP permafrost model has been widely used in different regions.

Table 1.2: The TTOP permafrost model has been applied in different parts of the world in recent years.

Time	**Areas of Application**
2021	Canada [42]
2007	Norway [43]
2021	Daxinganling in northeastern China [44]
2021, 2022, 2021	Qinghai–Tibetan Plateau in China [45–47
2019	The Arctic Circle as a whole [48]

Compared with the Nelson and Stefan permafrost model, the TTOP permafrost model fully considers the freeze-thaw conditions and soil properties of permafrost. the TTOP permafrost model can be used for small to medium-sized permafrost studies, and it takes into account the effects of snow cover, vegetation, and temperature more than the Nelson and Stefan permafrost model, where snow cover and vegetation can affect the temperature of permafrost and keep soil temperature at a minimum level, thus hindering the melting of permafrost. Temperature, on the other hand, is the main factor affecting permafrost ablation, and if the temperature increases, permafrost will ablate. In addition, the TTOP permafrost model can also consider the effect of soil moisture on permafrost ablation to better simulate the permafrost ablation. Therefore, the TTOP permafrost model is more comprehensive than the Nelson and Stefan permafrost model and can more accurately simulate the permafrost ablation.

Compared to the Kudryavtsev model, it uses a simpler structure and a simpler model algorithm, making parameter acquisition easier and reducing the number of possible errors. In addition, it is also efficient to run, which can save a lot of time and effort. Moreover, compared with the MAGT permafrost model, the TTOP permafrost model has better adaptability and can simulate the surface permafrost distribution and change trend more effectively in the absence of observation data, while the MAGT permafrost model relies more on the support of observation data.

Therefore, the TTOP permafrost model is very suitable for some research areas with poor objective geographical conditions, and can effectively simulate the distribution and change characteristics of permafrost from the perspective of energy transformation.

But, in earlier studies [42–48], rather than better direct observation or dail y measurement data, measurements and satellite data of the snow factor, vegetation factor, air temperature factor, soil properties factor, Land Surface Temperature (LST) factor and other factors used in the TTOP permafrost model were primarily consisted of low-resolution large-scale observations, and there is still space for enhancement in input data.

In addition, although the soil composition does not change, the soil moisture content is not constant because of yearly freeze-thaw conditions inside the active layer, changes in evaporation and precipitation, this is because the soil thermal conductivity utilized is predicated on the assumption that the soil moisture content is saturated. Therefore, to better study permafrost, higher resolution observations are needed and combined with changes in soil water content to obtain more accurate results.

Furthermore, the TTOP permafrost model primarily incorporates the yearly mean air temperature in the 2-10 m range to estimate the occurrence of permafrost, while the wide spatial range of temperature and the increase of extreme temperature weather are prone to observation errors. Therefore, the TTOP permafrost model must be enhanced in several ways as described above.

1.3.6 The LST-zero-curtain Permafrost Model

Gillespie et al. suggested in 2020 to utilize MODIS LST data to detect and record the thermodynamic isothermal phase, also known as the zero-curtain phase, during freeze-thaw of the active permafrost layer and use it as a critical phase for permafrost identification [49]. This strategy is known as the LST-zero-curtain permafrost model in this research.

In permafrost research, the zero-curtain effect is the name given to the phenomenon that causes the active layer of permafrost to remain close to 0°C for a certain period of time due to the stored heat of the lower layers during the thawing or freezing process [50]. This is a widespread natural phenomenon, which is influenced by the depth of permafrost, heat storage and climatic conditions. In general, the greater the thickness of the active layer of permafrost, the longer the duration of the zero-curtain effect, and when the temperature decreases, the temperature of the active layer also decreases, and the duration of the zero curtain effect is prolonged.

In addition, the surface heat output in the permafrost region also affects the occurrence of the zero-curtain effect, and the temperature of the active layer will be affected in the case of snow and waterfall, which will change the time of the zero-curtain effect. During the thawing (spring) or freezing (fall) periods of the active permafrost layer, the zero-curtain effect prevents the energy from directly altering the temperature of the active soil, however, it does cause the ground ice to melt or the groundwater to freeze in the active layer [51]. The zero-curtain effect is an important manifestation of the active soil temperature change during the thawing or freezing of the active permafrost layer.

As a result, the stability or existence of permafrost can be determined by observing the duration of the zero-curtain phenomenon during the annual freezing or thawing phase, of which the former is usually often significantly longer than the latter, which helps to detect the presence of permafrost. In addition, the zero-curtain phenomenon can also help us to determine the stability of permafrost, and if the duration of the zero-curtain phenomenon is relatively short, it indicates that the permafrost may be less stable. When used to describe permafrost, the zero-curtain effect can often be used without considering the effects of geographic features such as ice, hydraulic and soil conductivity. This is due to the fact that permafrost has small water consumption and relatively small changes in temperature during the duration of the zero-curtain effect, so their effects can be ignored. In addition, the active layer temperature during this period is less affected by factors such as atmospheric heat exchange, so the zero curtain effect can describe the thermal properties of permafrost well.

The LST-zero-curtain permafrost model can distinguish the freeze-thaw state of permafrost well compared with the Stefan permafrost model, while it can avoid the errors caused by too many model parameters and complicated geographical stratification compared with the Kudryavtsev permafrost model. For instance, Gillespie et al. demonstrated that MODIS LST data supported the concept of the zero-curtain effect by altering the temperature at different depths in the permafrost of the Atacama Andes, Chile, ranging from 2-40 cm [49]. The LST-zero-curtain permafrost model has developed a revolutionary technique for identifying and delineating permafrost using the long-standing MODIS LST product, which not only effectively and accurately identifies permafrost, but also enables the use of MODIS LST products with higher spatial resolution to effectively improve the accuracy of permafrost modeling. This is a major advancement in the field of permafrost modeling and makes permafrost modeling more accurate and reliable.

But most active permafrost levels are often approximately 3 m deep [53]. Without entirely eliminating the impact of snow and plants, the LST-zero-curtain model in Gillespie et al's study calculated the zero-curtain effect at only around 40 cm under earth's surface [49], this should be more precise as the zero-curtain effect can occur farther below the surface and is frequently obscured by snow or plants. In addition, the calculation of the zero-curtain based on LST alone may lead to errors because the lower limit temperature is not taken into consideration. This is because the LST may decrease significantly at low temperature conditions, resulting in a lower calculated zero-curtain than the actual case.

Therefore, the lower limit temperature must be considered to estimate the zero-curtain more accurately. In addition, other factors such as precipitation, humidity, and evapotranspiration need to be considered to ensure that the calculated zero-curtain matches the actual situation. Therefore, there is opportunity for development and certain drawbacks for the LST-zero-curtain permafrost model.

1.4 Purpose of the Study

Through the introduction of the principles related to the representative models of permafrost and the comparison of the advantages and disadvantages of various models, it is clear that by describing soil energy changes through temperature differences, the LST-zero-curtain permafrost model and the TTOP permafrost model have both been used to evaluate permafrost distribution.

Compared with other permafrost models, these two permafrost models have obvious advantages. First, they have obvious advantages in the accuracy of model calculation, which can reflect the change pattern of permafrost more accurately; second, they can handle larger scale of permafrost analysis, which can better support the design of large-scale projects; third, they also have obvious advantages in the accessibility of relevant parameters, which can better support the accurate analysis of permafrost models; finally, in recent years, they also have obvious advantages in the application of can better support the design implementation of permafrost engineering.

However, they have some problems that must be solved. Among them, for the TTOP permafrost model, the accuracy of the model can be improved by increasing the overall resolution of the satellite data and the measured data. In addition, the original soil thermal conductivity in the TTOP permafrost model can be corrected by calculating the soil thermal conductivity at net water content to reflect the actual situation more accurately.

In addition, to reduce the observation error, the temperature variation can be reflected more accurately by reducing the temperature observation range. In conclusion, by optimizing these aspects of the TTOP permafrost model, the actual situation can be more accurately reflected, and thus the accuracy of the model can be improved. For the LST-zero-curtain permafrost model, the effects of vegetation and snow can be removed to improve the accuracy of the LST-zero-curtain permafrost model. In addition, to further analyze the zero-curtain effect at deeper locations, a lower temperature limit for the curve change can be set to obtain more accurate results.

Thus, a TTOP LST-zero-curtain (TLZ) permafrost model is revealed in this study. The model combines the correlations of the TTOP permafrost model and the LST-zero-curtain permafrost model and makes improvements to address the improvement needs of both models. Specifically, the model uses a modified TTOP as the lower limit temperature, while the upper limit temperature is modified from the ground air temperature utilized in the standard TTOP permafrost model to LST. This permafrost model is expected to be more accurate than the conventional TTOP permafrost model and plays an important role in studies that simulate permafrost depth structure and predict permafrost properties and changes.

In addition, the model is also expected to predict the zero-curtain effect more accurately than the conventional LST-zero-curtain permafrost model. The novel permafrost model proposed in this paper is expected to provide new ideas and methods for the study and prediction of permafrost.

And the TLZ permafrost model was tested in the central-eastern part of the Qinghai-Tibetan Plateau, which is a representative permafrost study area with a large amount of measurement data. These data were analyzed with an effective method to determine the performance of the TLZ permafrost model under different environmental conditions, and the accuracy and applicability of the model were analyzed, and finally the results were discussed.

1.5 Composition of the Paper

This thesis is comprised of several distinct components. The primary components include a comprehensive introduction, a thorough review of relevant literature, an in-depth analysis of the research topic, and a comprehensive conclusion. Each component provides a comprehensive overview of the topic, allowing for a comprehensive understanding of the research. Additionally, all components are written in a professional and concise tone, ensuring that the thesis is both persuasive and informative. The relevant description of each chapter is as follows:

In Chapter 1, the research background of this study, the development process of permafrost models, representative models are highlighted, and the advantages and disadvantages of various models are described in subsections, as well as the research objectives based on the problems of permafrost models at the present stage. Finally, the contents of Chapter 1 are summarized.

In Chapter 2, the proposed new TLZ model related to permafrost analysis, which is based on the experimental purpose presented in Chapter 1, addresses the problems of the TTOP model and the LST-zero-curtain model at the present stage. The details revolve around the basic principles of the TLZ model, the modification of the TTOP model, the specific steps of the TLZ model for permafrost analysis, and the research area of the TLZ model in this study, and finally, a summary of the contents of Chapter 2.

In Chapter 3, based on the study area of the TLZ model introduced in Chapter 2, the data sources used in the study and the geographic information of the meteorological stations in the study area are highlighted, as well as the specific information of the various parameter used in the TLZ model, and the method of determining the parameters from the perspective of upper and lower temperatures is presented. Finally, a summary of the contents of Chapter 2.

In Chapter 4, the process of processing each parameter and the obtained parameter results based on the various data and parameter processing methods introduced in Chapter 3 are shown, and the obtained parameter results are analyzed and interpreted, which also includes some subsections of the results of the multiple data processing required for the net water content soil thermal conductivity (NWC) proposed in this study, followed by a detailed presentation of the results and validation analysis methods for the soil thermal conductivity after the addition of the NWC coefficient, and finally a summary of the contents of Chapter 4.

In Chapter 5, based on the various parameter factors required for the TLZ model obtained in Chapter 4, and based on the formulas and principles of the TLZ model, various results of the TLZ model are illustrated graphically, mainly including the map of permafrost classification in four-level, map of the LST statistics, the average subsurface temperature at various depths, and map of permafrost classification in seven-level. After that, the MAGT model is compared with the TLZ model for verification, and finally, the contents of Chapter 5 are summarized.

In Chapter 6, the various results of the TLZ model obtained in Chapter 5 are first discussed, and then the conclusions of this study are described in the context of the previous five chapters and discussions.

Finally, thanks are given to all those who contributed to the research and development of this thesis, including mentors, friends, and family, by way of reviewing my research process. References or web links are given to the sources of information used in the research and development of this dissertation, including books, articles, and websites. This compilation is provided to ensure the accuracy and integrity of the research for this dissertation.

1.6 Summary

In Chapter 1, the concept, hierarchical classification, composition, influencing factors, and degradation effects of permafrost are first described, pointing out the parts of permafrost research that still need improvement. The importance of permafrost research for future environmental and social development is also recognized, which provides an important basis for the research background of this study. Permafrost is a special geological feature that can not only alter vegetation, but also affect local climate, hydrological movement, and surface thermodynamic conditions. Its effects cover the hydrological, ecological, physical and chemical properties of the ground surface.

Then, the development of permafrost research starting from the early 1990s is described in detail in the historical events. Initially, the development of permafrost research focused on planimetric operations and field observations on small areas, and with the development of permafrost models, permafrost research entered a new phase in which permafrost was studied as a model system. Researchers have carried out a holistic understanding of the permafrost environment and analyzed the impact of permafrost on global climate change. In recent years, with the development of remote sensing technology permafrost modeling combined with remote sensing technology has become a mainstream research trend.

Subsequently, some of the most representative models in permafrost research in recent years are introduced, including Stefan permafrost model, Kudryavtsev permafrost model, TTOP permafrost model, LST-zero-curtain permafrost model, and so on. For different permafrost models, the advantages and disadvantages between them are compared in detail according to their principles.

After that, the solution of this study, a new TLZ permafrost analysis model, is proposed in this study based on the problem points that can be improved on the traditional TTOP model and the LST-zero-curtain model and the correlation that exists between the two models to illustrate the research objectives of this study.

Finally, the overall structure of this paper and the research content of each chapter are explained in detail.

Chapter 2 The Principle of TLZ Model and Study Area

2.1 The TLZ Model's Principle and Formula

The principle of TLZ model is to use the modified TTOP value as the lower limit temperature of the active layer of permafrost and the LST value instead of air temperature as the upper limit temperature of the active layer of permafrost according to the solution proposed in Section 1.4. The lower and upper limit temperatures of the active layer are used to determine and plot the zero-curtain effect of permafrost in a certain physical space range, and then the stability of permafrost, distribution, degradation, year-to-year change pattern, transformation type, etc. are analyzed in a hierarchical manner from the perspective of zero-curtain effect.

Following is the equation that represents the *TLZ* model:

$$TTOP = \frac{DDt \cdot L_t - DDf \cdot L_f}{L_f \cdot Z} \tag{2-1}$$

where

- *DDt* and *DDf*: the thawing and freezing indices, respectively,
- L_t and L_f: the thermal conductivities of soil in the thawing and freezing periods, respectively,
- *Z*: the number of days per year (365 or 366),

The unit of the thermal conductivity is in W/(m·°C), and that of temperature is in degree C. Figure 2.1 [54] shows the conceptual diagram of the TLZ model.

The TLZ model is expected to have the following advantages:

- Though the TTOP model determines the distribution of permafrost by analyzing the lower limit temperature of the active layer and the air temperature at 2 to 10 m above the surface, the TLZ model is expected to better reflect the state of the active layer using LST instead of the air temperature.
- The TLZ model reduces the errors caused by the use of low-resolution satellite data and measured data in previous TTOP model studies by using high-resolution satellite data and measured data.
- Compared with the LST-zero-curtain model, the TLZ model determines the lower limit temperature of the active layer of permafrost with a curvilinear variation, so that the zero-curtain can be well evaluated even without complex and expensive drilling operations.
- The TLZ model reduces the effects of vegetation cover and snow cover through an inversion-based approach.
- The TLZ model can analyze the permafrost variation pattern in large, small, medium and multiple scales, which is beneficial for more accurate permafrost distribution and mapping.

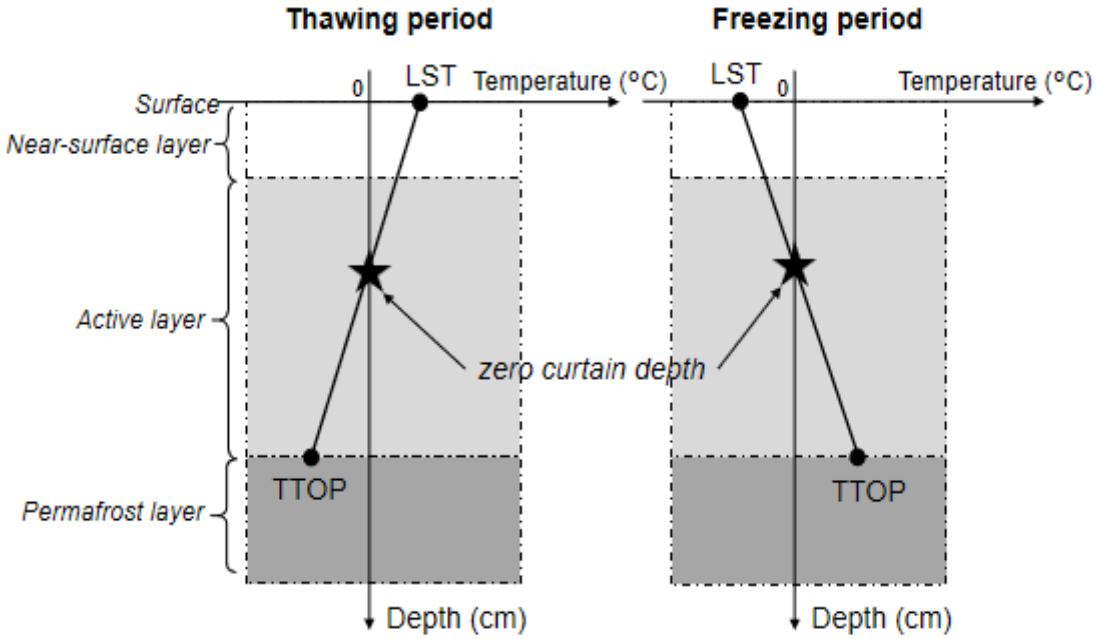

Figure 2.1: The TLZ model's conceptual diagram. Reproduced from Zhao and Tonooka (2022) [54].

2.2 Modification to the TTOP Permafrost Model

In addition to improving the resolution of the data used, an attempt was made to improve the TTOP model by calculating the thermal conductivity of the soil at the net water content state.

With regard to the soil thermal conductivity, there are two main models that can be applied to the Tibetan Plateau region. One is the K model proposed by Kersten in 1949 [55], which distinguishes properties between frozen and melted soils and is applicable to per-mafrost regions in the Northern Hemisphere where the main soil types are clay and chalk, but its applicability is less satisfactory in permafrost intervals that require subdivision of soil types. The other is Johansen's J model, which was introduced in 1975 and derived soil thermal conductivity by combining the impacts of thermal conductivity of the soil at saturation, coefficient of saturation correlation and thermal conductivity of dry soil [56].

Researchers from various permafrost research fields, including permafrost on the Qinghai-Tibet Plateau, are increasingly focusing on soil thermal conductivity studies to investigate the response of soil thermal conductivity to climate change. Because of the strong characterization of the J model in soil thermal conductivity studies, more and more researchers have started to use the soil thermal conductivity data provided by the J model. This is because the J model can better reflect the effects of different soil properties on soil thermal conductivity and can describe the changes in soil thermal conductivity more effectively. Therefore, in the field of permafrost research, the J-model has become the first choice for studying soil thermal conductivity.

Since the inception of the J model, no less than 40 improved J model models have been derived through continuous improvement. However, most of the improved models only consider the thermal conductivity of soil in the saturated or dry state, and ignore the thermal conductivity of soil in the net water content state, which makes the improved J models still have a certain degree of error in the analysis and application of permafrost. Therefore, based on the soil thermal conductivity in the net water content state, the improved J model can better improve the accuracy of permafrost analysis and is an important direction in the field of permafrost research in the future.

Net soil water content is the amount of water left in the soil minus organic matter, inorganic salts and other harmful substances [57]. It has a great influence on soil thermal conductivity and is one of the important factors affecting the thermal conductivity of soil. The higher the soil net water content, the higher the soil thermal conductivity, the lower the soil thermal index, and the better the soil thermal conductivity. In addition, the soil net water content can also affect the elastic modulus of the soil and thus the impact resistance of the soil.

In general, precipitation in permafrost zones has three main destinations: first, it can flow into water bodies such as lakes, rivers, and wetlands through surface runoff; second, it can form vegetation structures such as root systems, leaf surfaces, etc., which participate in plant transpiration; and finally, it can be absorbed directly by vegetation and snow layers [57]. Also, atmospheric deposition may occur in the permafrost zone, a phenomenon that can have an impact on climate elements such as temperature, precipitation and precipitation patterns. That is, the true soil thermal conductivity in the permafrost region depends on the net water content in the active layer.

As a result, we use precipitation, evapotranspiration and subsurface seepage data to develop a modified TTOP model based on the three main factors affecting net water content. The model takes into account not only the variation of water content in the active layer, but also the influence of heat due to seasonal variations.

On the basis of the J model, the NWC_f and NWC_t (NWC) factors are introduced in this model to dynamically evaluate the net water content factors for each of the thawing and freezing phases, soil thermal conductivity is predicted to vary from 2012 to 2021, and our model is anticipated to capture this fluctuation more precisely.

The *NWC* factors are calculated as follows:

$$NWC_t = \frac{W_t}{P_t - (E_t + C_t + G_t)} = \frac{W_t}{SW_t} \tag{2-2}$$

$$NWC_f = \frac{W_f}{P_f - (E_f + C_f + G_f)} = \frac{W_f}{SW_f} \tag{2-3}$$

where

- *NWC* represents the net water content factor,
- *f* and *t* represent freezing and thawing phases, respectively,
- *P* represents for precipitation,
- *E* represents for potential soil evapotranspiration,
- *C* represents for snow or vegetation cover effect,
- *G* represents for groundwater seepage factor,
- *SW* represents for saturated soil water content,
- *W* represents for net soil water content.

And the updated TTOP is written as follows:

$$TTOP = \frac{T_t \cdot F_t \cdot l_t \cdot NWC_t - T_f \cdot F_f \cdot l_f \cdot NWC_f}{l_f \cdot NWC_f \cdot Z} \tag{2-4}$$

where

- *Z* represents the annual day count (365 or 366),
- *T* represents factor for cumulative temperature,
- *F* represents factor for snow or vegetation cover,
- *l* represents the soil thermal conductivity [W/m/°C],
- The *NWC* factors can be used to adjust the soil thermal conductivity, and $L_t = l_t \times NWC_t$ and $L_f = l_f \times NWC_f$ (called "adjusted soil thermal conductivity").

When daily temperature data for the whole year of interest are available for the place of interest, the value of T_t is supplied by the sum of all daily average temperatures over 0 °C, and the value of T_f is given by the total of all absolute daily average temperatures under 0 °C. As demonstrated in Table 2.1 [54,56], the values of l_t and l_f in the researc h region can be known to as J model's calculated value. Except for organic matter, we used the lowest ("*1.15*") and highest ("*2.92*") values from the table for l_t and l_f in this research 's analysis.

Table 2.1: According to Johansen (1975) [56], the Qinghai-Tibetan Plateau's typical soil types' thermal conductivities during freezing and thawing seasons. (Except for organic matter, the values utilized in this analysis's highest and lowest ranges are denoted by italicized numbers.) Modified from Zhao and Tonooka (2022) [54].

Soil Type	**Dry Density (kg·m^{-3})**	l_t **(W·m^{-1}·K^{-1})**	l_f **(W·m^{-1}·K^{-1})**
Sloping soils	1400	*1.15*–1.54	1.61–2.69
Lacustrine soil	1475	1.21–1.62	1.82–2.74
Wind-deposited soil	1500	1.39–1.60	1.63–2.47
Ice and water deposition	1550	1.26–1.66	1.65–2.50
Alluvial soils	1600	1.30–1.72	1.59–2.53
Moraine	1750	1.41–1.98	1.68–*2.92*
Organic matter	300	0.52	1.7

2.3 Analysis of Permafrost Using the TLZ Model

In this research, the existence and stability of permafrost are analyzed on a small scale based on the zero-curtain effect, so it is crucial to accurately determine the occurrence time, duration period, and location distribution of the zero-curtain effect.

Table 2.2 describes in detail the specific aspects of using the TLZ permafrost model to determine the properties related to the zero-curtain effect, and how the determined zero-curtain effect properties are used to evaluate and analyze the permafrost accordingly.

Table 2.2: Specific steps to determine the zero-curtain effect and permafrost analysis based on the TLZ permafrost model.

Step Number	**Operation Method**
1	Every pixel in the research area's yearly TTOP was computed (The altered formula (2-4) published in Section 2.2 was used to calculate the TTOP values stated in this Chapter.). Only permafrost pixels with yearly TTOP values below 0 were analyzed after assuming that pixels with annual TTOP values above 0 were not permafrost.
2	The research area's yearly temperature data were used to determine the freezing season, which was supposed to run from 10 to 4, and the thawing season, which ran from 5 to 9. After that, the seasonal TTOP ($TTOP_f$, $TTOP_t$) was determined for every permafrost pixel. It was expected that during the course of a year, pixels that fulfilled the condition "$TTOP_f > 0 > TTOP_t$" would freeze in the winter and melt in the summer, e.g., that the zero-curtain effect would take place. As a result, only the pixels that match this requirement were retrieved, and the rest were disregarded. It should be noted that among the excluded pixels, those that fulfill $TTOP_f$ below 0 can be considered to be stable permafrost because they did not melt throughout the summer.
3	Since the ice freezes during the freezing season, the LST as a whole

	has a negative value. In contrast, the ice melts throughout the thawing process, and LST is generally positive. Thus, it may be considered that the overall connection is "$TTOP_f > 0$ and $LST < 0$" for the freezing period and "$TTOP_t < 0$ and $LST > 0$" for the thawing period, despite the fact that it is influenced by mistakes, coverage, and daily fluctuations in LST. As a result, only the pixels that met these requirements were retrieved, and the rest were not.
4	We assume that the subsurface temperature for the pixels retrieved in the preceding phase fluctuates linearly between seasonal TTOP and the LST between the lower surface and the surface of the active layer, and determined the depth where the subsurface temperature was within ± 0.1 °C (There must be a solution because the seasonal LST and TTOP are showing the opposing indications), where based on the research done by Wang et al., a consistent depth of 3 m was assumed to exist under the active layer in the research region [53]. The obtained depth might be regarded as the zero-curtain range. This strategy is known as the TLZ permafrost model in this research. A conceptual representation of the TLZ model is presented in Figure 2.1. (The next Chapter provides more information on the aforementioned technique.)

2.4 Area of Study

In order to better verify the validity of the TLZ model and the possibility of comparing the results of the TLZ model with the MAGT model, the most representative region in the field of permafrost, the Qinghai-Tibetan Plateau, was chosen as the study area for this experiment.

The Qinghai–Tibetan Plateau is not only the source of the Yangtze and Yellow Rivers, but also the origin of many lakes such as Qinghai Lake and Namucuo Lake, and a large number of snow and glaciers on the plateau have nurtured these rivers and lakes. The size of this plateau ranges from 1.05×10^6 to 1.5×10^6 km^2 [58]. It is the largest plateau-type permafrost distribution region in Asia as well as the highest and largest permafrost distribution area in the globe. It is known as the third level and roof of the planet [59].

The physical topography of this plateau region is very special, with its high terrain, which makes its topography very characteristic. In addition, the climate here is also very special, most of the time in a cold and dry climate, the temperature difference between the four seasons, the night temperature is low, the day temperature is high, precipitation is also relatively low, sunshine is abundant, so it is known as "sunrise and sunset two places clear". The plateau low-temperature zone is famous for its plateau topography, and the climate is cold, especially in winter, when the temperature is low and frost lasts for a long time. The plateau cold zone has lower temperatures, more snowfall in winter, cooler summers, and more rain in spring and autumn. Plateau temperate areas have higher temperatures, hotter summers, warmer winters, and sometimes light rains in spring and autumn. Subtropical and tropical areas have higher temperatures, hotter summers, warmer winters, and higher air humidity.

Grassland, meadow, shrubland, and woodland make up the vegetation distribution from northwest to southeast, shrublands and woodlands is formed. Most of the areas are well endowed with geothermal heat and sunshine, and the daily temperature difference is large, which makes this vegetation distribution belt more colorful. Moreover, with the direction from northwest to south, the precipitation is gradually increasing, which is more favorable environmental conditions for this vegetation distribution belt.

Consequently, the plateau is frequently referred to as a region of climate change start [60]. In recent years, permafrost research in the Qinghai–Tibetan Plateau region is becoming the focus of the scientific community, and the permafrost's resilience and durability in this plateau have enormous practical implications for Asia's climatic and ecological harmony as well as for the rest of the planet.

The Qinghai-Tibetan Plateau is home to several mountain ranges, the most famous of which is Mount Everest, the highest peak in the world. In the east-west direction, there are countless mountain ranges, large ones towering like lofty peaks, and small ones as slender and slim as thin willows, winding all the way along the mountain ranges to see the scenery in the valleys. And in the north-south direction, there are various mountain ranges of different heights, some with high peaks and some with short peaks, and one can see that the mountains of different heights are arranged together to form a complete system of mountain ranges. In addition, there are numerous marshes, grasslands, plateau surfaces, river systems and other natural features that form a unique area of natural scenery.

It also has a wide geographical depth in the north-south and east-west directions, and covers six provinces in China and many countries in Southeast Asia. The general topography has a tendency toward high northwest and low southeast, with the mean elevation of the northwest section above 5000 m [61], and the excessive altitude causes significant plateau effects such as thin air and little dust and water vapor this does not convenient for long-period continuous geographic observation research.

And the east-central part of the plateau, on the other hand, is the site concentration of the "China-Meteorological-Data_service-Centre (CMDC) " sites, with relatively low altitude, high air and water vapor density, high people's actions, low forest cover, and high precipitation; such geographical features make the climate conditions here relatively suitable for human habitation and research activities.

In addition, data from CMDC sites can be used to analyze changes in the natural environment, including permafrost, and can provide important data information for the study and validation of permafrost models.

As a result, it was decided to study the "H25V05 tile" covering the MODIS image of the east-central part. The maps were interpolated based on geographical information such as latitude, longitude and weather stations in the study area, as shown in Figure 2.2 [54], the CMDC sites are highlighted with asterisks in red, and the research region is denoted by a blue polygon.

The region contains 54 CMDC sites and is located between "26°00′ and 39°47′N latitude and 73°19′ to 104°47′E longitude " ("around 2800 km to the east-west and around 300-1500 km to the north-south") [62]. In addition, in order to reduce the errors that arise when the observation area is too large for subsequent analyses such as temperature, the study area was divided into six sub-regions as shown in the image from A to F.

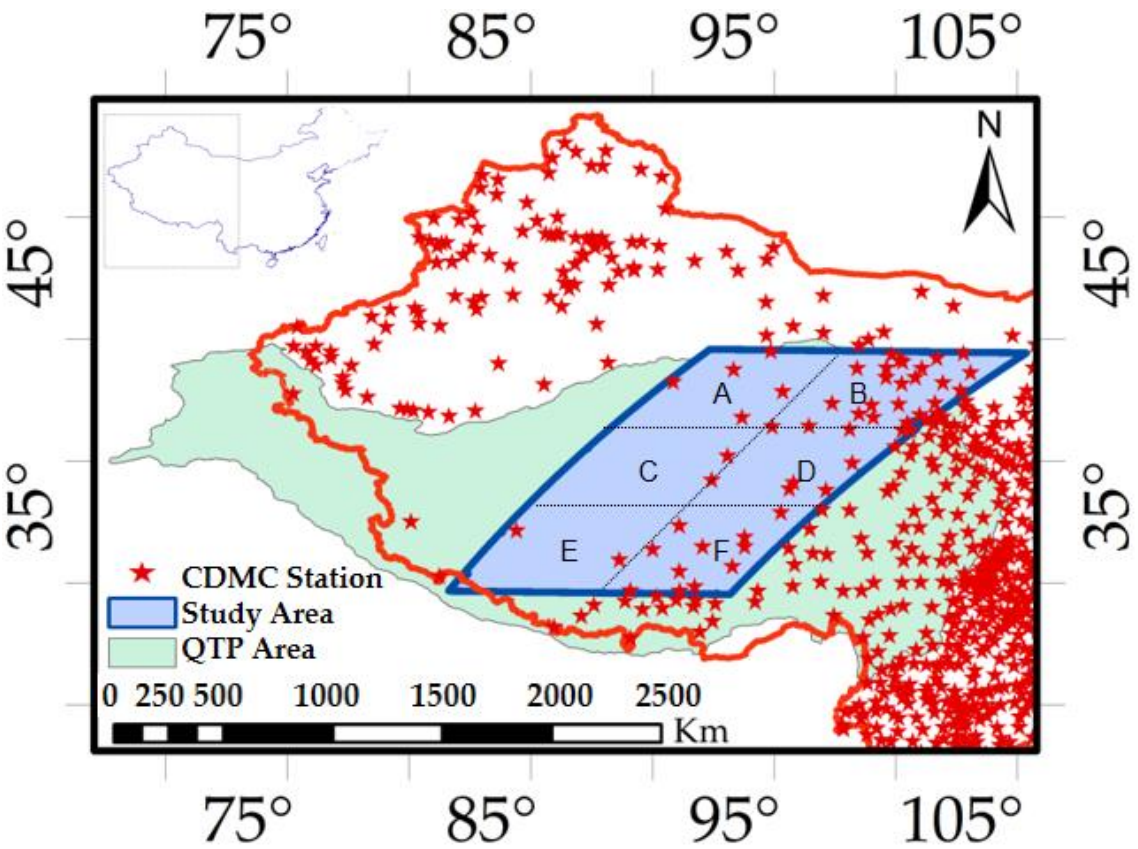

Figure 2.2: The locations of CMDC sites are shown by red asterisks. The research region (blue polygon) and its 6 subregions (A to F) are shown on a map of China's Qinghai-Tibetan Plateau. Reproduced from Zhao and Tonooka (2022) [54].

2.5 Summary

In Chapter 2, the basic concepts, principles, equations and parameters of the TLZ permafrost model are first explained, including the "lower limit temperature value" TTOP, which is a key parameter in the model.

The principle of the correction of the "lower temperature limit value" TTOP in the TLZ model, the equation and the main soil thermal conductivity parameters are explained in detail to ensure the accuracy of the permafrost model. Next, the different parameters used in the model and their specific effects are discussed in depth to determine the feasibility and reliability of the model.

Then, a table is presented in depth on how to determine the properties related to the zero-curtain effect using the TLZ permafrost model. In addition, how to use the TLZ permafrost model to analyze and evaluate permafrost is also presented.

Finally, in order to further apply and validate the TLZ permafrost model, the east-central region of the Qinghai-Tibetan Plateau was selected as the research area for this experiment, and detailed information related to the water system, geography, nature, and CMDC sites distribution in the research area was provided for better data collection and analysis. In the next chapter, the specific information of the study data and data processing methods, etc. in this study will be detailed according to the parameter requirements of the TLZ model and the distribution of meteorological observation stations in the study area.

Chapter 3 Utilized Data and Parameter Determination

3.1 Information about Geographic Data Sources and Meteorological Stations

Various data collected by CMDC sites in the research region and a range of MODIS images served as the major sources of data for our analysis.

The *China Meteorological Administration's* website (*http://data.cma.cn/en*; *visited on 7 July 2022*) provided the subsurface and meteorological data that were utilized in the CMDC. And the *National Aeronautics and Space Administration* (NASA) website, (*https://ladsweb.modaps.eosdis.nasa.gov/*; *visited on 7 July 2022*), is where all of the MODIS images utilized were obtained from.

Table 3.1 provides specific information on the MODIS data that were primarily used in this study and the associated uses of this study. Table 3.2 presents the geographic information of the 54 CMDC meteorological stations.

Table 3.1: MODIS data used in this study.

Parameter in this study	Product name	Platform	Spatial Resolution	Temporal Resolution	Product type
F_t	MO/YD13Q1	Terra, Aqua	250m	16 Days	Vegetation index
	MCD12Q1	Combined	500m	Yearly	Land cover type
F_f	MO/YD09GA	Terra, Aqua	500/1000m	Daily	Surface reflectance (bands 1–7)
LST	MO/YD11A1	Terra, Aqua	1000m	Daily	Land surface temperature
	MO/YD11A2			8 Days	

Table 3.2: The geographic information of the 54 CMDC meteorological stations.

ID	Site name	Latitude (N)	Longitude (E)	Elevation (m)
01	CH04	29°38′44″	91°8′7″	4450
02	CH05	29°39′57″	89°5′44″	4452
03	CH06	29°49′44″	91°43′36″	4335
04	NQ01	30°27′40″	91°5′40″	4339
05	NQ02	30°38′41″	93°16′36″	4423
06	NQ05	30°55′49″	88°37′36″	4366
07	NQ06	31°21′31″	90°0′48″	4378
08	NQ07	31°27′38″	92°4′24″	4320
09	KM01	31°27′38″	93°47′11″	4280
10	KM03	31°50′53″	93°47′11″	4278
11	KM05	32°19′2″	91°5′40″	4205
12	ALI01	32°8′59″	84°25′0″	4174
13	XDT01	32°52′4″	95°16′31″	4151
14	XDT02	33°48′22″	95°37′19″	4137
15	XDT03	33°45′55″	97°7′52″	4080
16	XDT05	34°11′37″	92°26′25″	4052
17	XDT07	34°5′29″	95°48′20″	4018
18	XDT09	34°54′26″	98°12′44″	4005
19	TGL02	35°11′34″	93°4′22″	3956
20	TGL03	36°23′46″	94°55′43″	3945
21	TGL04	36°46′33″	93°40′52″	3928
22	TGL05	36°24′59″	96°26′16″	3826
23	TGL06	36°16′25″	98°5′23″	3815
24	TGL07	36°54′22″	98°28′38″	3811
25	TGL09	36°45′48″	99°5′21″	3756
26	TSH03	36°15′9″	100°16′6″	3721
27	TSH05	36°15′39″	100°37′10″	3689
28	TSH07	36°34′12″	100°29′8″	3701
29	TSH08	36°40′43″	101°14′45″	3568
30	TSH09	36°53′15″	100°58′43″	3547
31	TSH11	36°56′45″	101°40′49″	3588

32	ZNH01	37°50′10″	95°20′43″	3754
33	ZNH03	37°20′3″	97°23′47″	3735
34	ZNH05	37°16′23″	99°0′27″	3602
35	ZNH07	37°22′49″	101°36′48″	3545
36	ZNH08	37°19′19″	100°8′5″	3526
37	ZNH09	37°54′24″	102°39′58″	3502
38	QT01	37°49′25″	95°21′25″	3689
39	QT03	38°14′57″	90°51′0″	3756
40	QT05	38°44′44″	93°20′3″	3652
41	QT07	38°46′56″	98°24′58″	3501
42	QT08	38°37′0″	103°5′1″	3402
43	LDH02	38°12′26″	101°55′51″	3407
44	LDH04	38°47′33″	101°5′3″	3426
45	LDH05	38°25′44″	100°48′53″	3452
46	LDH06	38°10′51″	100°15′0″	3455
47	LDH07	38°25′29″	99°35′9″	3523
48	LDH09	38°49′36″	99°37′1″	3556
49	AYK01	39°30′53″	94°52′1″	3703
50	AYK03	39°24′7″	102°46′59″	3586
51	AYK04	39°12′26″	101°40′58″	3568
52	AYK05	39°4′44″	100°17′3″	3605
53	AYK07	39°8′51″	100°9′52″	3621
54	AYK09	39°21′41″	99°50′7″	3637

The data processing methods mentioned below are centered on two aspects.

The first aspect is to determine the temperature of the lower active layer, TTOP, which includes methods to determine the positive and negative cumulative temperature coefficients T_t and T_f for the thawing and freezing periods, methods to determine the vegetation and snow cover interchange coefficients F_t and F_f, and methods to determine the net water content coefficient NWC to correct for soil thermal conductivity, as proposed in this study. In the second aspect, the temperature of the upper active layer, i.e., the land surface temperature (LST), needs to be determined. This requires us to collect information about the LST data and to determine the correct determination method to ensure the reliability and accuracy of the measurement results.

3.2 T_t and T_f (the Cumulative Temperature Factors)

Because the TTOP model is combined with air temperature to determine the distribution of permafrost, it is very important to have an accurate grasp of air temperature. In combination with equation (2-5), the accumulation coefficients T_f and T_t for the freeze-thaw period must first be determined from the air temperature. Kukkonen et al. (2020) employed a technique employing the temperatures of extreme monthly to calculate the cumulative temperature parameters in the freezing and thawing phases of the TTOP model [63]. Due to the study of the yearly freeze-thaw temperature utilizing data from just two months, a obviously error remains even if this approach incorporates some degree of temperature fluctuation.

In essence, a discrepancy between the yearly fluctuation in the yearly average temperature and extreme temperatures exists, and this disparity is more pronounced in the lengthy research period. Additionally, the temperature readings sent to 54 CMDC sites were derived from the air temperature each day observations made by the meteorological satellite of China's Fengyun, thus there will inevitably be brief gaps in the data and occasional abnormalities.

The air temperature data for this study were processed in the manner of Table 3.3 to obtain greater accuracy.

Table 3.3: Specific processing steps to improve the accuracy of temperature data in the study area and to determine the cumulative temperature factors T_t and T_f.

Step Number	Operation Method
1	In order to gather air temperature data between 2 and 10 meters below the ground surface for the years 2012 to 2021, the 54 CMDC sites were first separated into six groups that correspond to subareas A, B, C, D, E, and F in Figure 2.2.
2	After removing outliers, averages for the previous three days for every group were used to fill in any gaps in the temperature data.
3	Then, using these data, the average annual air temperature value for the research region was calculated for every year between 2012 and 2021.
4	Utilizing thin plate spline approach [64], spatial interpolation was carried out in this estimate by creating temperature buffers at 54 sites.
5	After removing the incorrect values from the air temperature data, we calculated the T_f and T_t parameters by performing negative and positive cumulative temperature computations.

The Thin Plate Spline method expressed by:

$$TPS = t(a,b) + \sum_{i=1}^{o} \theta_i \, r(\mu_i) \tag{3-1}$$

$$t(a,b) = L_1 + L_2 a + L_3 b \tag{3-2}$$

$$\mathrm{r}(\mu) = \frac{1}{2\pi}\left\{\frac{\mu^2}{4}\left[\ln\left(\frac{\mu}{2\nu}\right) + J - 1\right] + \nu^2\left[O_k\left(\frac{\mu}{\nu}\right) + J + In\left(\frac{\mu}{2\pi}\right)\right]\right\} \tag{3-3}$$

where

- i: the number of temperature value points,
- θ_i: the correlation coefficient obtained by solving the linear equation,
- μ_i: the distance between point (a,b) and point i,
- L: the coefficient obtained by solving the equation in t (a,b),
- μ: the distance from the point to the sample,
- v^2: the threshold weight,
- O_k: the modified Bessel coefficient,
- J is a constant (0.577 in this study).

3.3 F_t (the Reciprocal of Vegetation Cover Fraction)

After introducing the method of determining the influence factor of freeze-thaw accumulation temperature, the next step is to explain how to exclude the influence of snow and vegetation during the freeze-thaw period, and in this subsection the method of excluding the influence of vegetation is focused.

The reciprocal of the fraction of vegetation cover (FVC), which is necessary for FVC to be precise enough, was used in this work to calculate the F_t factor. To address the problems of FVC derivation in previous TTOP studies, the use of data and derivation methods were enhanced to achieve a more accurate FVC.

Zhang et al. [44] examined the permafrost zone in northeastern China using the TTOP permafrost model. The daily or monthly variations in plant cover, however, were not completely taken into account since the MCD12Q1 (MODIS_500/1000 m_yearly_land cover image) of the "International-Geosphere-Biosphere-Programme" (IGBP) was used to estimate the impacts of thawing and freezing on vegetation. Additionally, the land cover categories according on the IGBP must be reclassified to fit every research region.

As a result, in this research, we calculated the fraction of vegetation cover (FVC) used to determine the fraction of vegetation (F_t) from the "enhanced-vegetation-index" (EVI) and the "Normalized-Difference-Vegetation-Index" (NDVI) for every month in the MYD13Q1 and MOD13Q1 (MODIS_250 m/16 day_vegetation indices images) using the formula below [65]:

$$\mathrm{FVC} = \frac{(VI - VI_s)}{(VI_v - VI_s)} \tag{3-4}$$

$$\mathrm{FVC}_1 = \frac{(NDVI - NDVI_s)}{(NDVI_v - NDVI_s)} \tag{3-5}$$

$$\mathrm{FVC}_2 = \frac{(EVI - EVI_s)}{(EVI_v - EVI_s)} \tag{3-6}$$

where

- *v* and *s* stand for pure vegetation and pure soil pixels, respectively,
- *VI* stands for the vegetation index (EVI or NDVI).

when the range of the confidence was defined at 0.5% to 99.5%.

- Pixels that had more than 99.5% of grass type accumulation were considered as pure vegetation,
- Pixels that had less than 0.5% of grass type accumulation were considered as pure soil.

Finally, the element dichotomous approach [65] was used to combine the FVC values for EVI and NDVI, and the resultant FVC value was employed.

3.4 F_f (the Reciprocal of Snow Cover Fraction)

After describing how to exclude the effect of vegetation during the freeze-thaw period, in this subsection, the focus is on the method to exclude the effect of snow cover. In this work, the reciprocal of the snow cover (FSC), which is necessary for the FSC to be accurate enough, is used to calculate the F_f factor. Comparing the methods of determining FSC in previous studies, the method with less error was selected to determine FSC in this study.

Regional and temporal regional variations in snow cover were not taken into account in the aforementioned research by Zhang et al. [44] since the snow depth was specified as being below 30 cm and the yearly snow parameter was defined uniformly by a fixed value [44]. The advantage of this method is that it is less computationally intensive and simpler to handle, but the disadvantage is that it ignores the effect of the dynamics of snow cover on permafrost and is prone to errors in multi-year time-series monitoring, especially when analyzed through the TTOP permafrost model.

In order to better grasp the dynamic impact of snow cover on permafrost research, scientists have since carried out many relevant studies, such as: Jiang et al. (2022) employed the MYD09GA and MOD09GA (MODIS-surface-reflectance_daily_L2G global_1 km and 500 m images) to analysis of the snow cover layer around the water tower area, with a resultant Root-Mean-Square-Error (RMSE) around 0.14 [66]. Comparison with actual snow measurement data demonstrates a high degree of accuracy and therefore we calculated the fraction of snow cover (FSC) used to derive F_f after their research employing the same materials.

And the "Multiple Endmember Spectral Mixture Analysis-Automatic-Selected Endmembers" (MESMA-ASE) approach suggested by Jiang et al. [66] was used in this computation, which, repeatedly, analysis for each and every spectral library endmember combination, gets a suitable unmixing result by adjusting the quantity and kind of snow endmember spectra in every pixel. This method not only greatly reduces the missing data caused by the omission of spectral information, but also can capture the cyclic change pattern of snow cover more effectively. Through this method, the data of snow cover variation can be more accurately captured, thus providing reliable information support for snow monitoring and permafrost analysis. At the same time, it also provides good support for other researches and applications, such as hydrological studies, glacier movement observation, vegetation distribution, etc.

3.5 NWC_t and NWC_f (the Net Water Content Factors)

After describing how to exclude the effect of snow accumulation during the freeze-thaw period, in this subsection we present the method for determining the net water content factor related to the thermal conductivity of the soil proposed in this study.

The values of precipitation (P), potential soil evapotranspiration (E), net soil water content (W), groundwater seepage factor (G) and snow or vegetation cover impact factor (C) during thawing and freezing phases can be used to compute the NWC factors.

And the various data information and related operations used to calculate the NWC factor are shown in Table 3.4.

Table 3.4: Data and operations required to determine the NWC factor.

Data Name	Data Information or Operation
precipitation (P)	Daily in situ measurements taken by CMDC during that time period provided the precipitation (P) information and spatially interpolated by the Thin Plate Spline method [64].
potential soil evapotranspiration (E)	The CMDC reprocessed the MODIS/Terra net evapotranspiration (E) 8-day L4 global 500 m SIN grid product and used monthly data to calculate the evapotranspiration (MOD16A2).
net soil water content (W)	In situ measurements taken by CMDC every half-hour at four different depths between 2012 and 2021 yielded the net soil water content (W): 5 cm, 50 cm, 150 cm, and 200 cm.
groundwater seepage factor (G)	Since in situ measurements were not carried out in the research region, by averaging several sets of observations made by Tarnawski et al. (2015) for soil thermal conductivity [67], the groundwater seepage factor (G) was calculated and given a constant value.
snow or vegetation cover impact factor (C)	In this study, we define the normalized annual averages of the vegetation cover change and the snow cover change as the positive influence factors of vegetation cover and snow cover, respectively, based on the original meaning of the FVC and FSC. First, the average values of FVC and FSC for each year were calculated. Then they were subtracted from their corresponding base amounts, where the base amount of FVC was 0 and that of FSC was 120, and the subtracted values were normalized by one percent.

3.6 LST (the Land Surface Temperature)

After introducing the various factors required for the lower limit temperature (TTOP) of the TLZ permafrost model, in this section we focus on the relevant information and processing methods for the upper limit temperature (LST) of the TLZ permafrost model.

The MYD11A1 and MOD11A1 (MODIS-LST/E_daily_L3-global-1 km_SIN-grid images), which cover the years 2012 to 2021, provided the LST data required for the zero-curtain study. And the MYD11A2 and MOD11A2 (MODIS-LST/E_8-day_1 km images) were used to fill in the gaps left by some MODIS observation difficulties, such as those that occurred in 2016 from Days 50 to 58.

The MYD11A1 and MOD11A1 datasets were merged after being supplemented, and the daily average LST maps that were acquired for the time period were utilized. And the average, maximum, minimum, and standard deviation of LST were computed and produced in graphs on an annual basis in order to compare the general change in LST from 2012 to 2021.

Based on the above description, the information and processing of all parameters required for the TLZ permafrost model are presented in detail. In the next chapter, the results of the processing of each parameter described in this section will be graphically displayed and analyzed.

3.7 Summary

In Chapter 3, the various parameters required for the TLZ permafrost model are discussed in depth in terms of lower limit temperature (TTOP) and upper limit temperature (LST), the definitions and characteristics of these parameters are described, and data information on the parameters is also presented, and methods for determining the parameters are given to ensure the accuracy of the model.

The details are as follows:

First, information related to measured air temperature data from 2-10 m is presented. Based on the relevant air temperature data, the cumulative temperature factors were calculated as the reference values for the thawing (T_t) and freezing (T_f) periods, respectively, by combining the characteristics of the air temperature changes during the freezing and thawing periods through methods such as zoning and TPS interpolation. By comparing the air temperature data and cumulative temperature factors, the thawing and freezing periods of each season are determined, thus providing a reference basis for the freeze-thaw cycle division of the TLZ model.

Then, the methods for determining the inverse of vegetation cover and the inverse of snow cover (F_t and F_f) using satellite observation data are presented, combining the treatment of vegetation and snow cover effects in previous studies with appropriate data or methodological improvements in the context of the actual situation. And the F_t and F_f factors are used to exclude the interference caused by vegetation and snow cover during the analysis of TLZ permafrost model.

After that, the net water content (NWC) factor associated with the soil thermal conductivity correction proposed in this study were presented, and provide detailed information or treatments for determining the multiple parameter variables associated in the NWC factor. Among them are precipitation (P), potential soil evapotranspiration (E), net soil water content (W), groundwater seepage factor (G) and snow or vegetation cover impact factor (C).

Above, after introducing the various parameter information required for the lower limit temperature (TTOP) and its processing method. Finally, data information and processing methods related to the upper limit temperature (LST) are explained.

Chapter 4 Processing of the Parameters and the Acquired Factors

4.1 Obtained T_t and T_f (the Cumulative Temperature Factors)

The temperatures are processed according to the method proposed in Section 3.2, and the results obtained are shown and illustrated one by one.

The daily fluctuations of air temperature for each of the six groups (from A to F) from 2012 to 2021 are displayed in Figure 4.1 [54]. While the Group A has the least yearly variance in temperature, the Group F exhibits the biggest. Elevation has a major role in how different groups differ from one another. The Group F, which is situated southeast, is close to 3600 m above sea level, whereas the Group A, which is situated northwest of the research region, is above 4000 m above sea level.

Figure 4.2 shows a graph of the average air temperature for each year obtained by the Thin Plate Spline method [64]. The results indicates that the air temperature in the study area has a small oscillation slowly increasing trend from 2012 to 2021, where the maximum increase in the annual extreme low temperature in the period is 3.4 degree C, that in the annual extreme high temperature in the period is 2.3 degree C, and the overall average temperature increases by about 0.21 degree C in the period.

Figure 4.3 [54] displays the predicted cumulative temperature factors for the freezing and thawing phases for every year from 2012 to 2021, after abnormalities in the air temperature data have been eliminated. It is clear that from 2012 to 2021, the T_t values (freezing duration) have a decreasing tendency while the T_f values (thawing duration) have a rising trend.

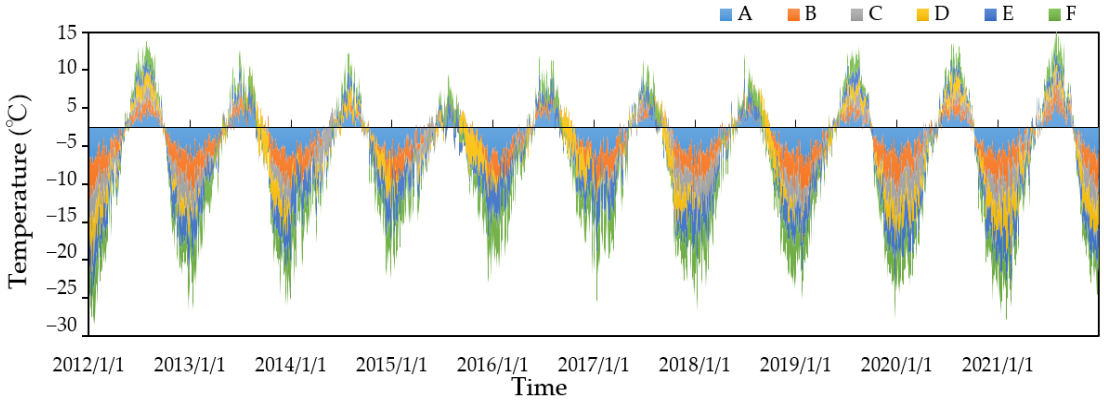

Figure 4.1: Fluctuations in the 6 groups A through F of the daily average air temperature from 2012 to 2021. Reproduced from Zhao and Tonooka (2022) [54].

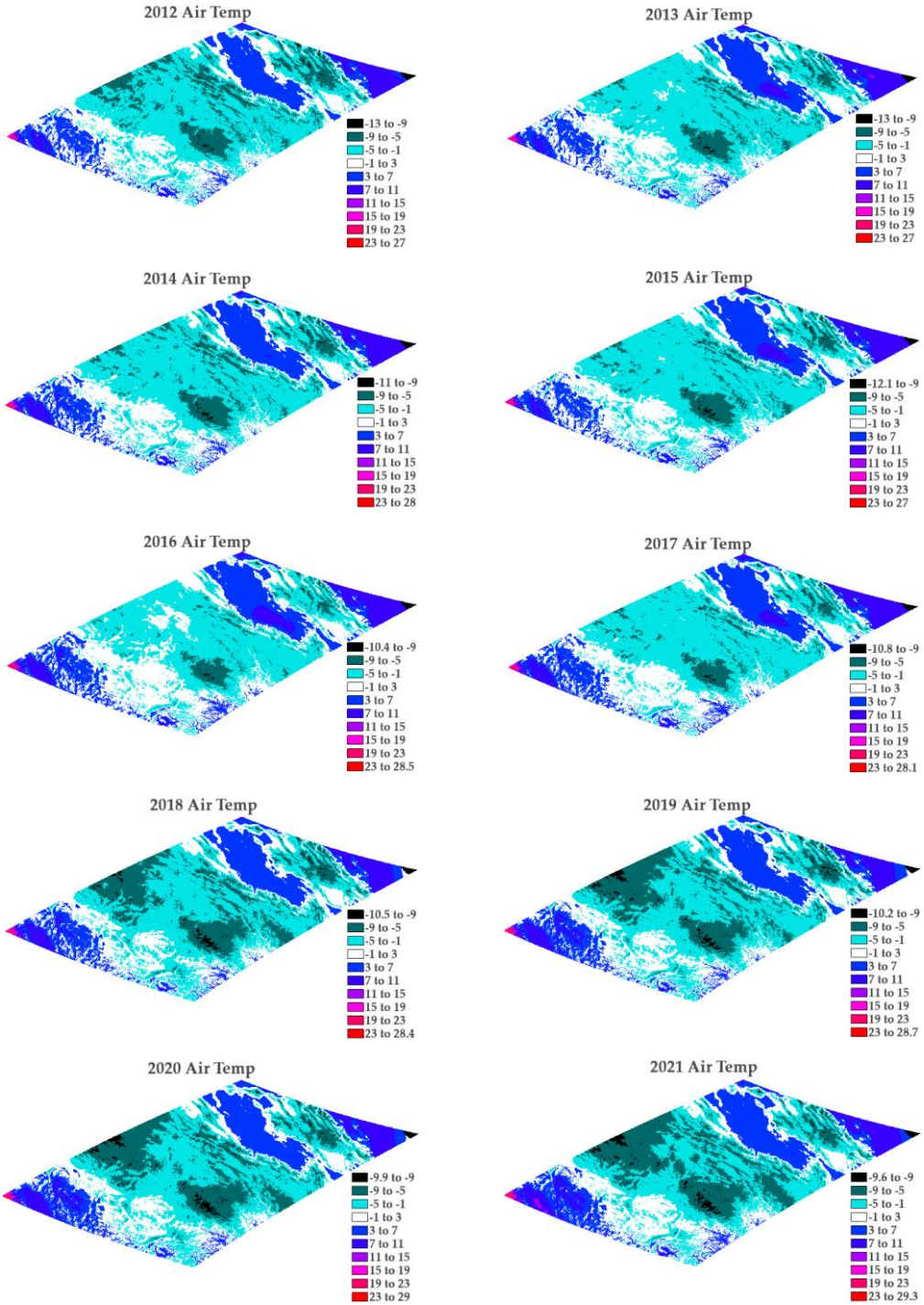

Figure 4.2: The average air-temperature map for each year from 2012 to 2021 (unit: degree C).

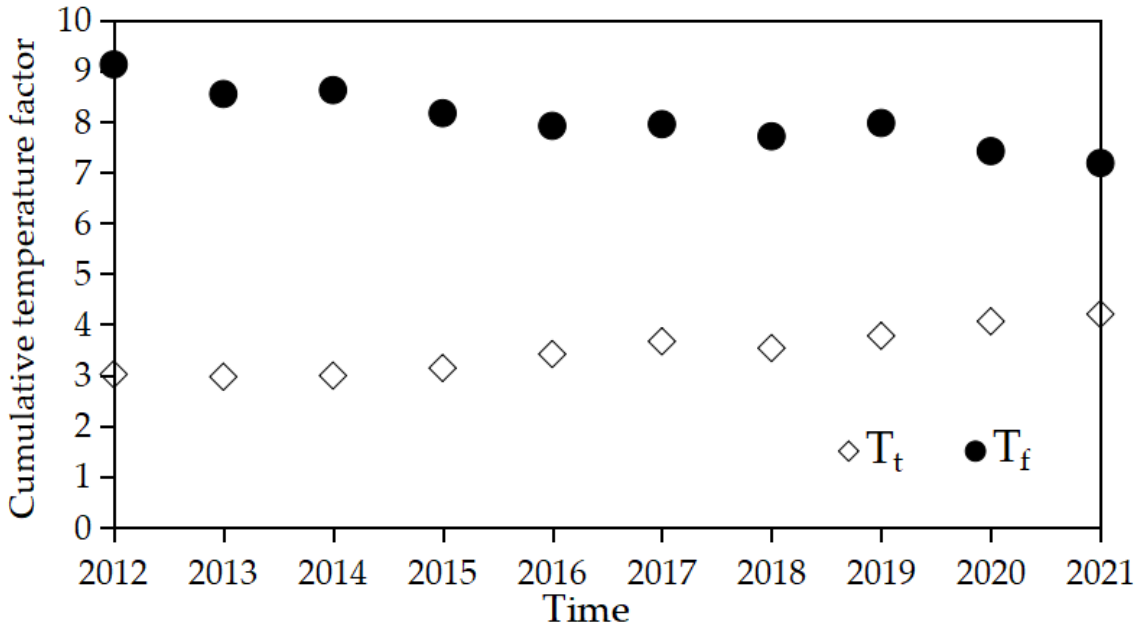

Figure 4.3: T_t and T_f (the cumulative temperature factors) from 2012 to 2021. Modified from Zhao and Tonooka (2022) [54].

4.2 Obtained F_t and F_f (the Reciprocals of Vegetation and Snow Cover Factors)

First we have to obtain the F_t factor by FVC according to the treatment presented in Section 3.3, so we have to determine the values of the VIs needed in Equations (3-4), i.e., NDVI and EVI. Figure 4.4 and Figure 4.5 show the changes in the statistical values of NDVI and EVI from 2012 to 2021, respectively.

After determining the values of NDVI and EVI, we calculated the results of FVC year by year. Figure 4.6 demonstrates the FVC map calculated for each year from 2012 to 2021, showing that the west part is less vegetated, and the east part is more vegetated but the whole area is not highly covered by vegetation.

Because the MODIS MCD12Q1 Land Cover products for 2021 were not yet available, we compared the results of the IGBP land classification in MCD12Q1 for 2012-2020 with those of FVC obtained in this study by using the MCTK module in the extension of the ENVI software for pre-processing and reclassification and other related processing. The total count of pixels classified as each IGBP class is given by Figure 4.7.

Figures 4.6 and 4.7 indicate that the west area is dominated by sparse vegetation (class no. 16-17) in red and the east area is dominated by alpine meadow (class no. 10-11) in dark green with little forest cover, while there are also a few scattered stable snow cover areas. The vegetation cover maps based on MCD12Q1 500m show a high agreement with the FVC maps based on MOD13Q1 (Terra) 250m_16day and MYD13Q1 (Aqua) 250m_16day, but the MOD13Q1 and MYD13Q1 based maps in this study were much better than the MCD12Q1 based maps in terms of spatial and temporal resolution, thus providing more accurate results.

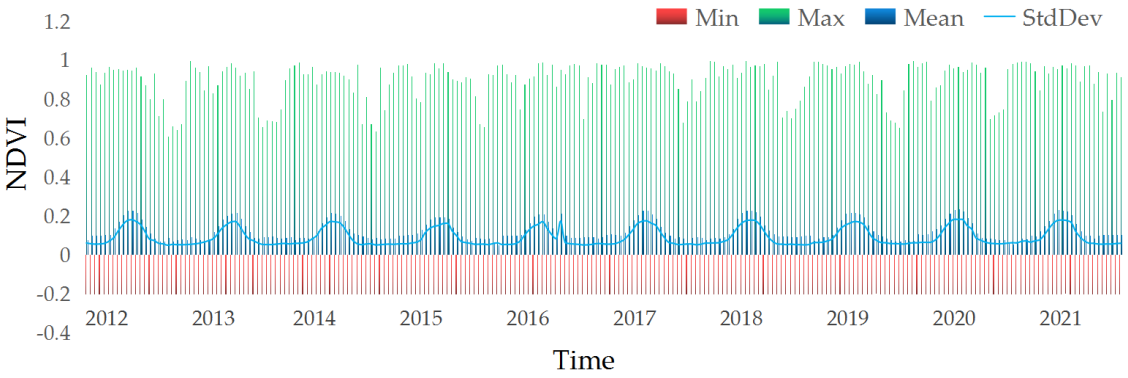

Figure 4.4: The change in the statistics of NDVI from 2012 to 2021.

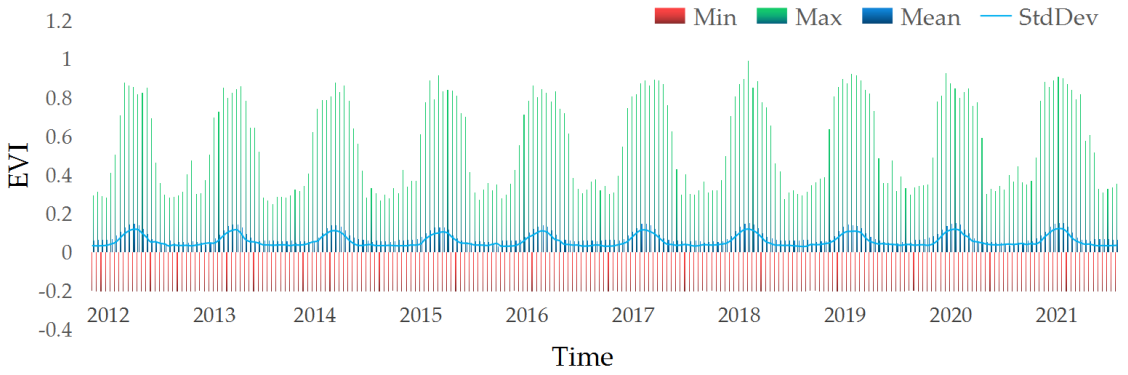

Figure 4.5: The change in the statistics of EVI from 2012 to 2021.

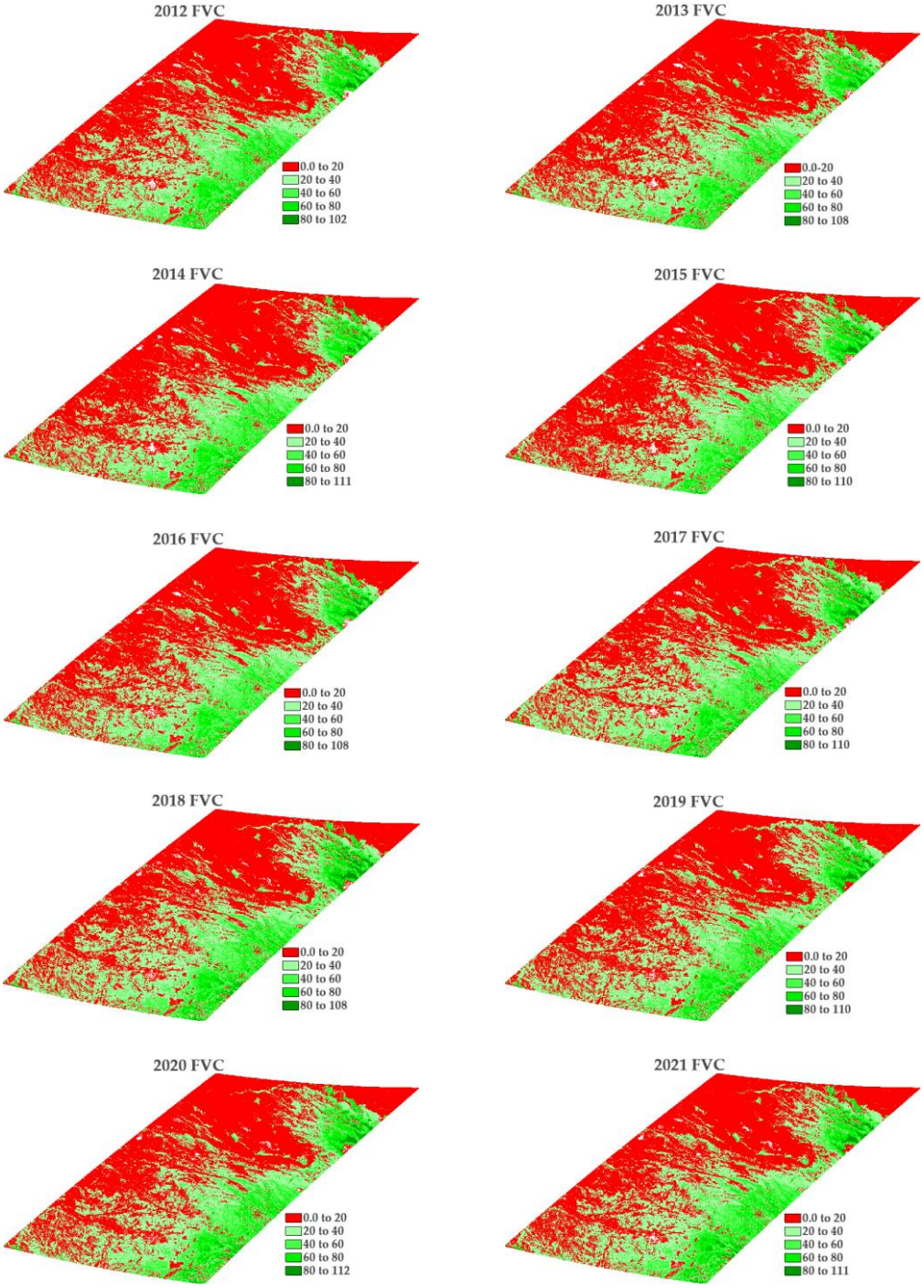

Figure 4.6: The FVC map derived for each year from 2012 to 2021.

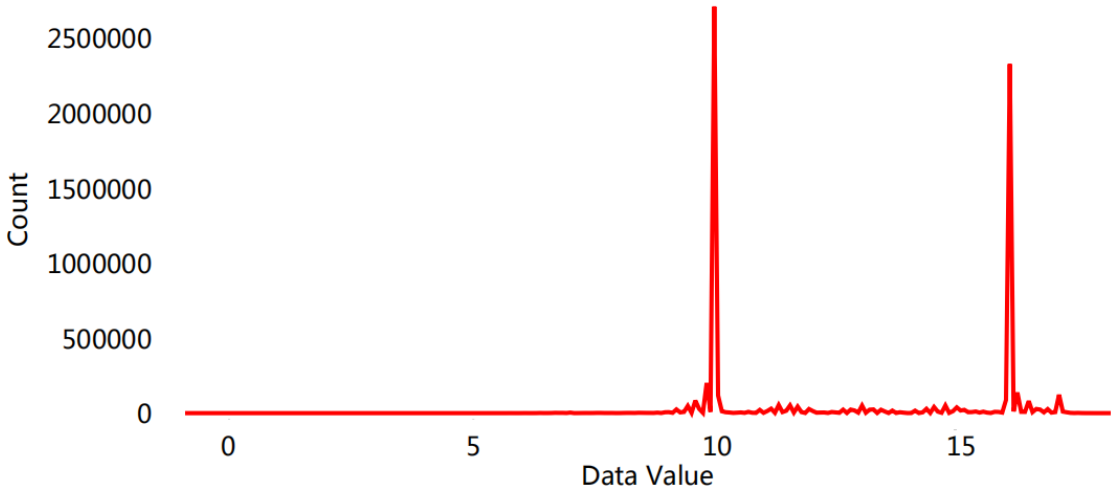

Figure 4.7: The total count of pixels classified as each IGBP class.

After determining the FVC, we then determine the FSC according to the method of processing in Section 3.4. Figures 4.8 and 4.9 demonstrate the FSC maps for January to December in 2012 and 2021, respectively, and Figure 4.10 shows the daily average trend of FSC in the period from 2012 to 2021. These results indicate the followings for the study area:

- The area enters the freezing period from October every year. The average FSC value is in the 120-130 range in October, and then gradually increases. The average FSC value is around 130 in November, reaching the peak of snow cover (130-140) in December-February, and exceeds the 140 range in several months.
- From March, the weather starts to warm up slightly and the average FSC value drops back to the 125-135 range, and from April to May, the FSC average drops to the 120-130 range.
- From May to September, the snow melt coverage is relatively stable during the thawing period and the FSC average stays around 120.

In the thawing period (May to September) from 2012 to 2021, the snow cover fluctuates slightly locally with no significant changes overall, but the mean snow cover in the freezing period (October to April) shows a decreasing trend yearly, thus indicating that the mean-temperature increase of 0.21 degree C in the period from 2012 to 2021 would decreas snow cover in this area to some extent. These results for FSC indicate a thin snow cover and relatively low snow cover stability in the study area, which is consistent with the annual snow cover trend of IGBP in Figure 4.7.

Using the obtained FVC and FSC, we eliminated the effect of vegetation cover and snow cover during the thaw and freeze periods by reverse normalization. Figure 4.11 [54] shows the annual average values of F_t and F_f from 2012 to 2021.

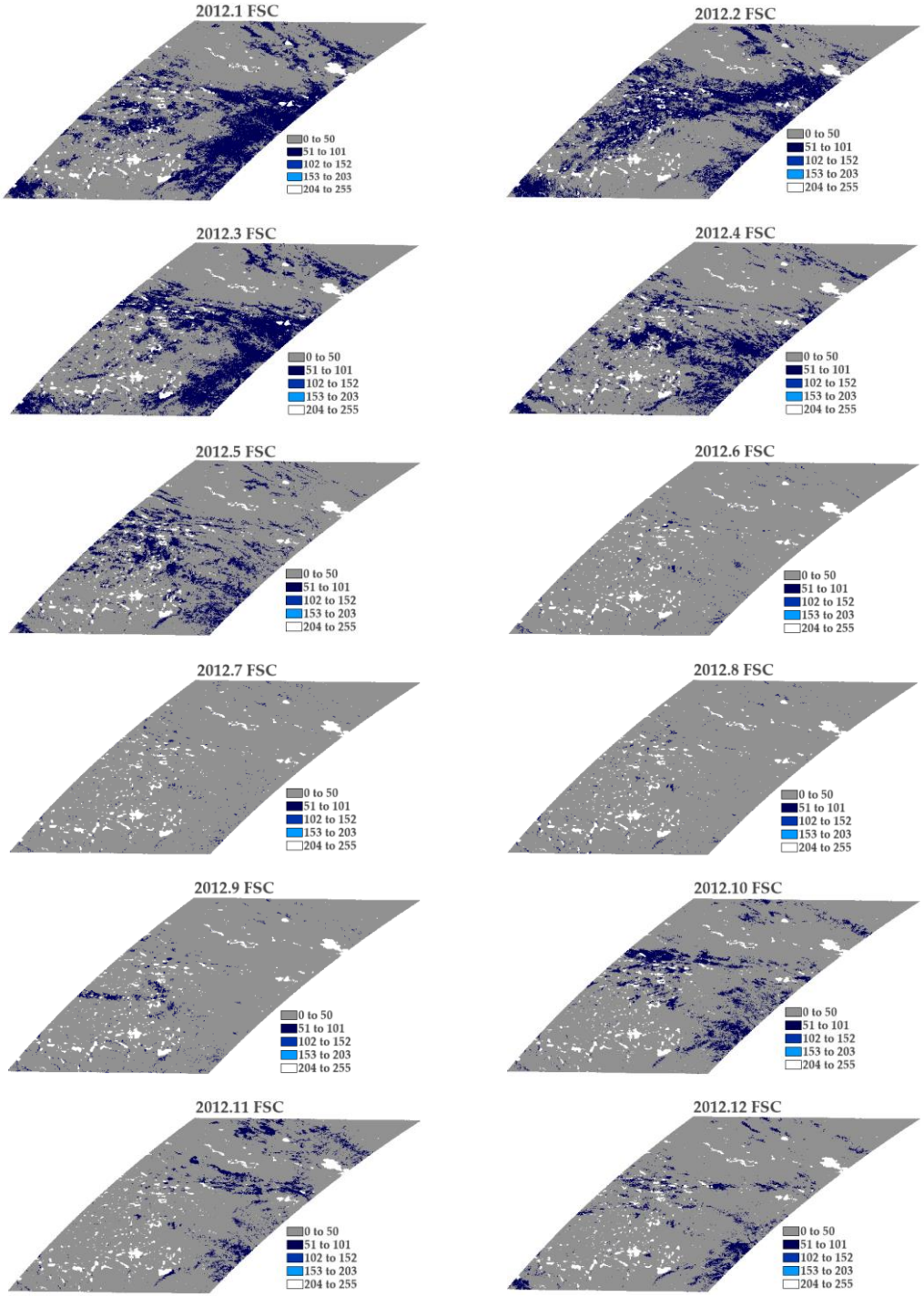

Figure 4.8: The FSC map obtained for each month in 2012.

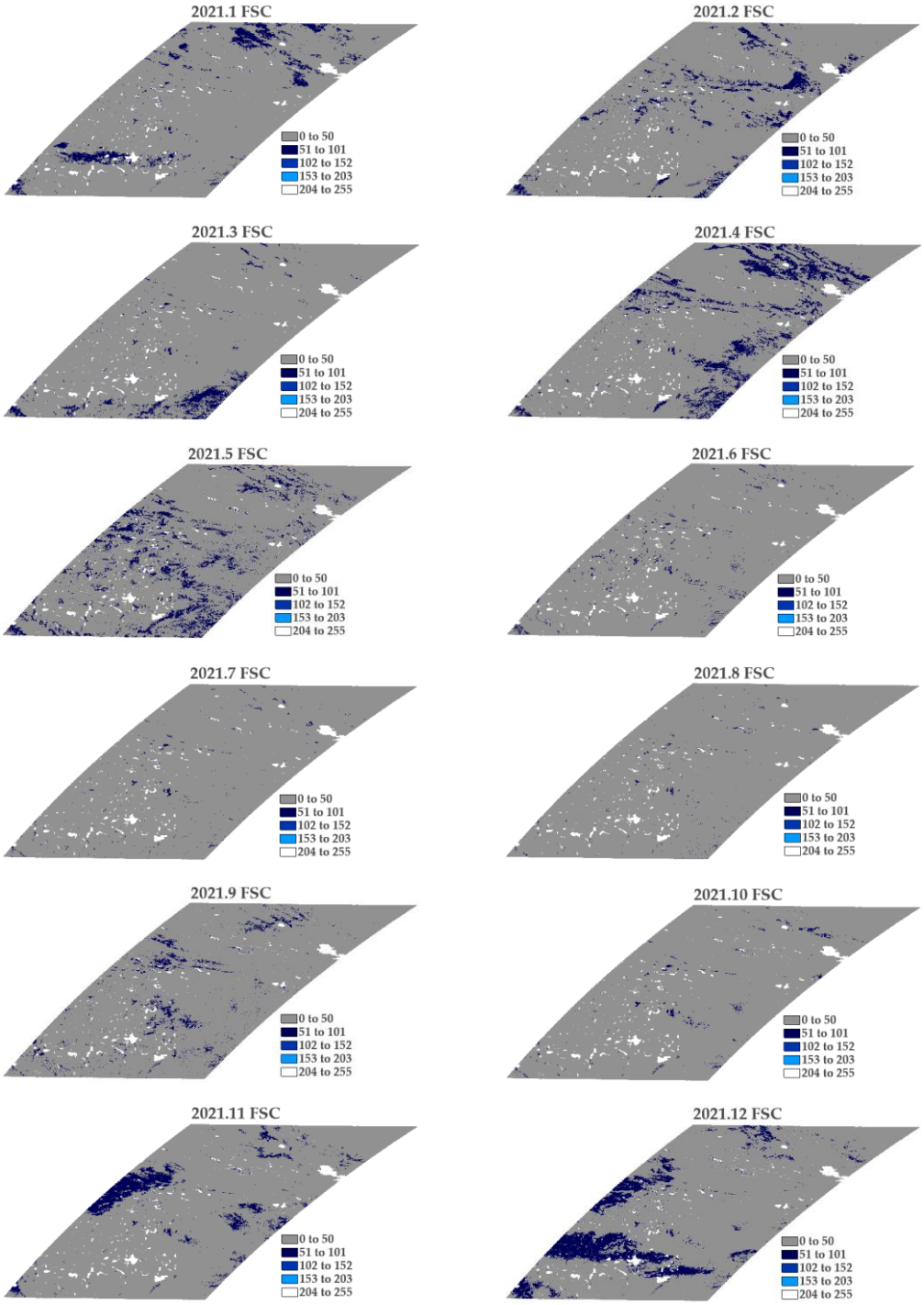

Figure 4.9: The FSC map obtained for each month in 2021.

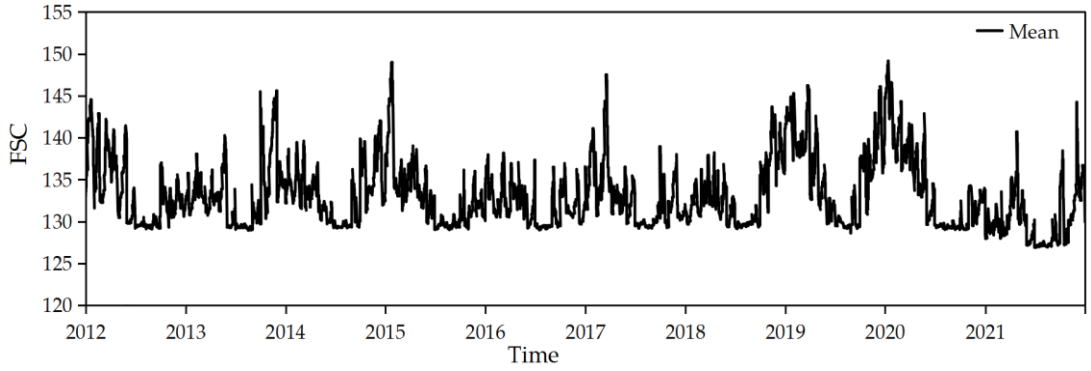

Figure 4.10: Daily average trend of FSC in the period from 2012 to 2021.

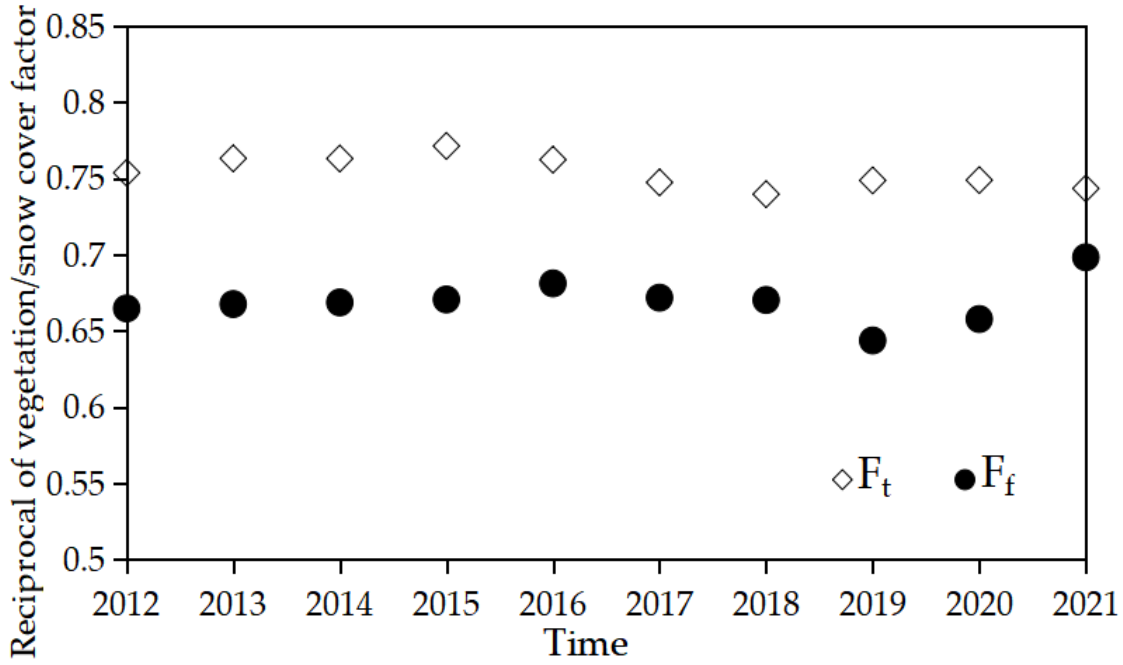

Figure 4.11: F_t and F_f (the reciprocals for vegetation and snow cover) for the years 2012 through 2021. Modified from Zhao and Tonooka (2022) [54].

4.3 Obtained NWC_t and NWC_f (the Net Water Content Factors)

4.3.1 The Value of Precipitation (P)

To determine the NWC factors for the freeze-thaw period, we need to determine the precipitation (P), potential soil evapotranspiration (E), net soil water content (W), groundwater seepage factor (G) and vegetation or snow cover impact factor (C) for the freeze-thaw period based on Equations (2-3) and (2-4) and the data content in Section 3.5.

The precipitation results obtained by the Thin Plate Spline method are shown in Figure 4.12. Some negative intervals within -16 to 0 are shown in the figure, which were produced by small amounts of clouds. The mean value of precipitation in the freeze-thaw period was then calculated for each year and shown in Figure 4.13.

Figures 4.12 and 4.13 show that the mean precipitations in the thawing period from 2012 to 2021 are around 300-400 mm, and the mean precipitations in the freezing period are around 200 mm. As shown in Figure 4.12, the precipitation increases from the northwest area with less rainfall covered by bare soil or sparse vegetation to the southeast area with more rainfall covered by alpine meadows, indicating to be consistent with the land classi-fication map of IGBP.

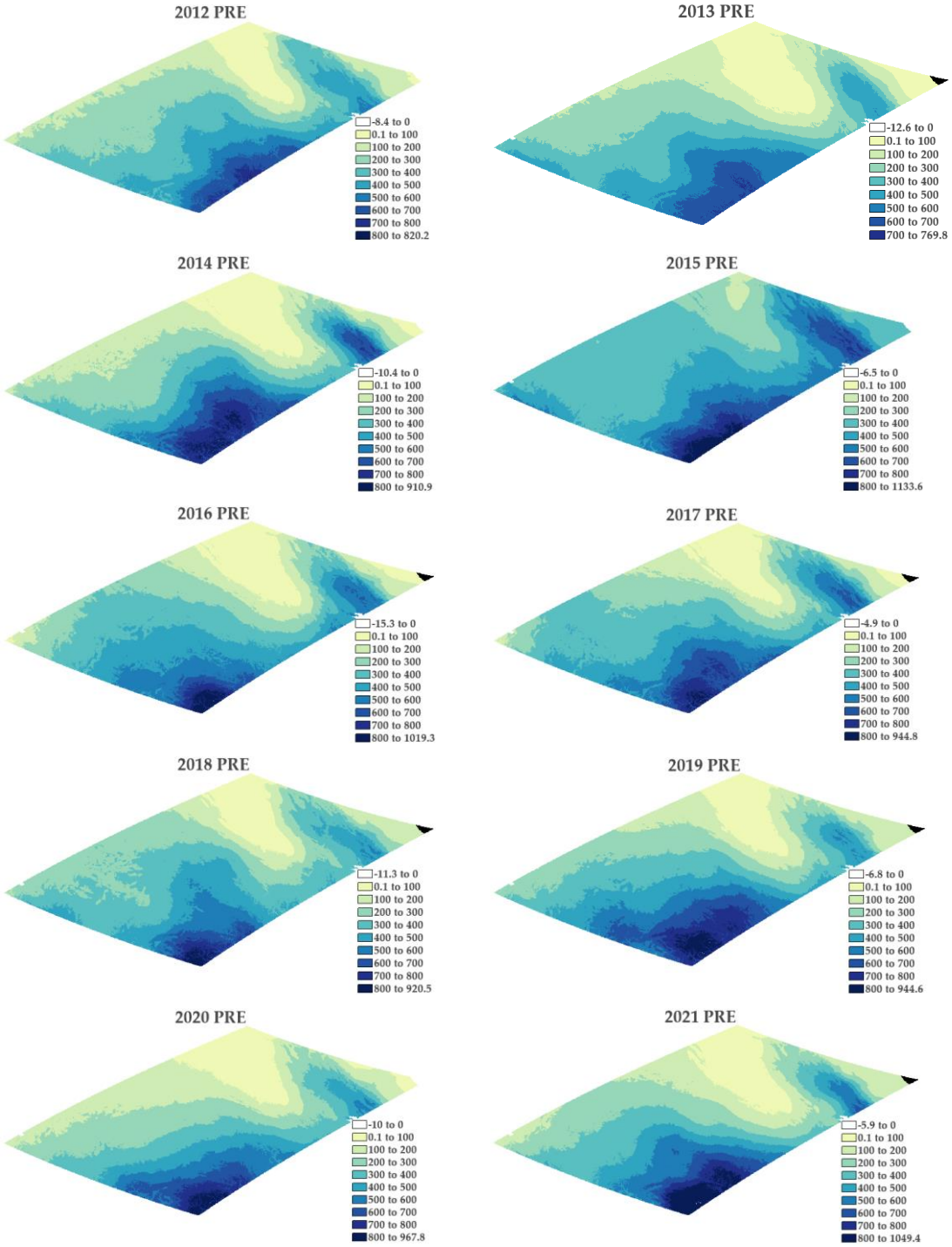

Figure 4.12: The average precipitation map for each year from 2012 to 2021 (unit: mm).

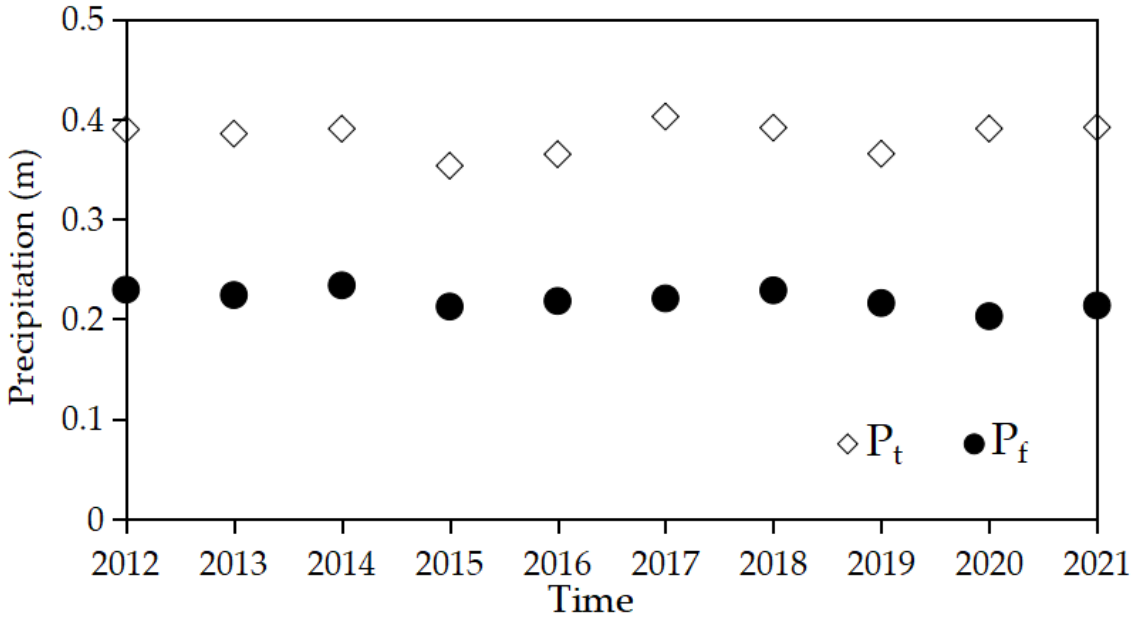

Figure 4.13: The average precipitation (m) in the thawing and freezing periods for each year from 2012 to 2021.

4.3.2 The Value of Potential Soil Evapotranspiration (E)

The monthly evapotranspiration data were statistically analyzed, showing the results in Figure 4.14. In annually, the evapotranspiration is relatively stable, while the max-imum value is larger in 2015 and has a slightly increasing trend from 2019 to 2021. The mean value of evapotranspiration in the freeze-thaw period was then calculated for each year and shown in Figure 4.15.

The results indicate that the mean values in the thawing period are around 70 and those in the freezing period are around 20. The changing trends of evapotranspiration and soil water content in the thawing and the freezing periods are relatively consistent, both of which are several times higher in the thawing period than in the freezing period.

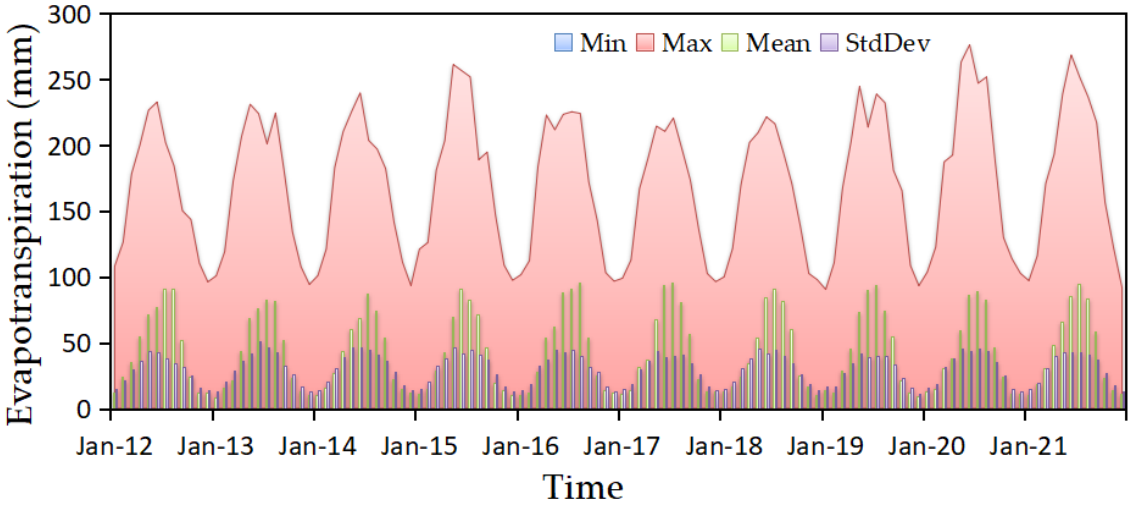

Figure 4.14: The statistics (min, max, mean, and standard deviation) of potential soil evapotranspiration in the period from 2012 to 2021, as a function of time.

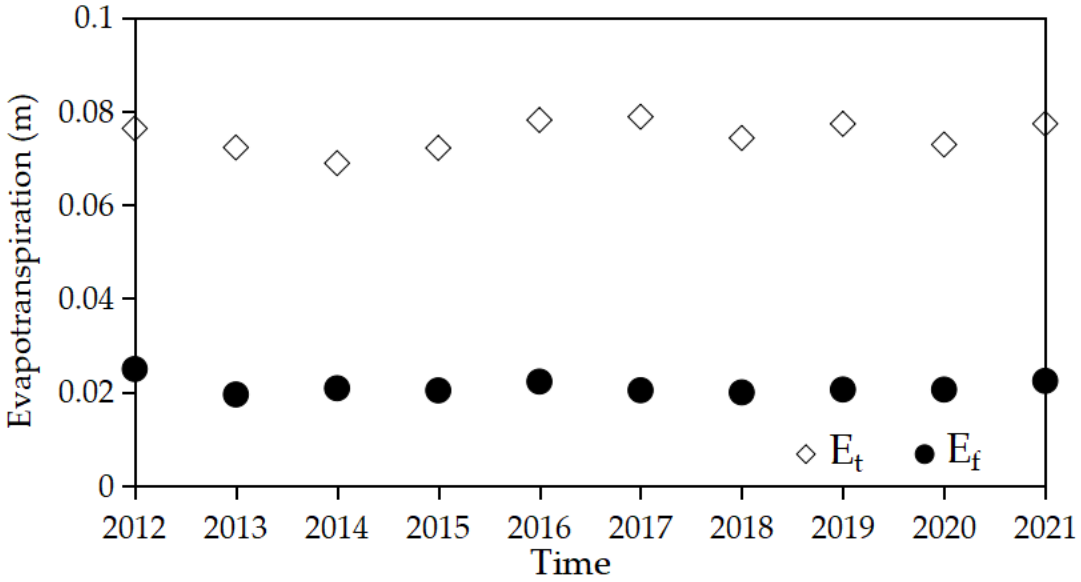

Figure 4.15: The average potential soil evapotranspiration (m) in the thawing and freezing periods for each year from 2012 to 2021.

4.3.3 The Value of Net Soil Water Content (W)

Figure 4.16 displays the mean soil water contents at four depths in the period as a function of time. Next, the mean soil water contents of the thawing and freezing periods were calculated for each year as shown in Figure 4.17.

The results indicate that the soil water content of the freezing period is in the range of 0.05% to 0.15%, and that of the thawing period is in the range of 0.15% to 0.25% in the period from 2012 to 2021.

Because of a large amount of ice in the active layer in the freezing period, the soil water content is much smaller than that in the thawing pe-riod. The soil water content in the freezing period is characterized by large fluctuations due to the variance of precipitation in individual years.

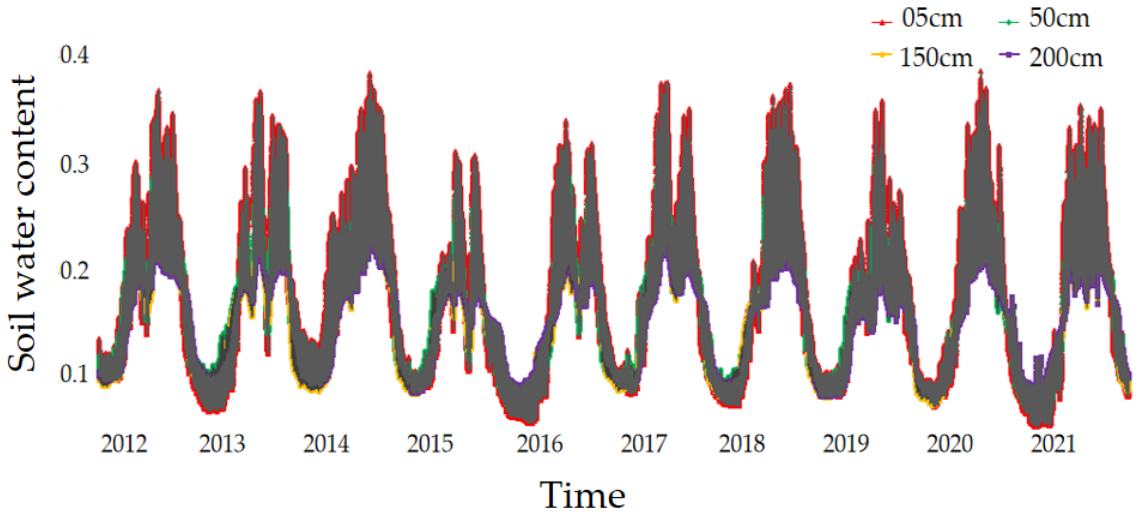

Figure 4.16: The average soil water contents at depths of 5, 50, 150 and 200 cm in the period from 2012 to 2021, as a function of time.

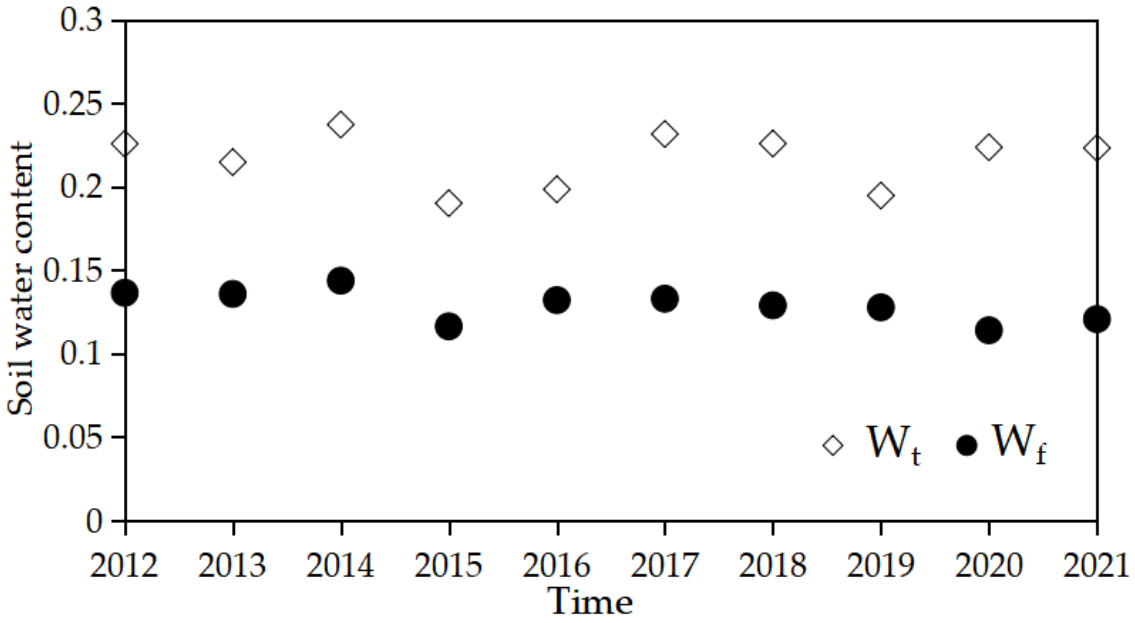

Figure 4.17: The average soil water contents (%) in the thawing and freezing periods for each year from 2012 to 2021.

4.3.4 The Value of Groundwater Seepage Factor (G)

The seepage factors are not available for the study area in the period from 2012 to 2021, because Tarnawski, et al. (2015) also used the improved J model [56].

Thus in this study, we averaged the seepage factors measured by Tarnawski, et al. for the soil thermal conductivity in each of the freezing and thawing periods [67]. As a result, the seepage fac-to in the freezing period was taken as 0.05 m and that in the thawing period was taken as 0.06 m.

4.3.5 The Value of Vegetation or Snow Cover Impact Factor (C)

The results of the Vegetation or Snow Cover Impact Factor are shown in Figure 4.18, with C_t values between 0.22 and 0.27 and C_f between 0.12 and 0.14 for the period 2012 to 2021.

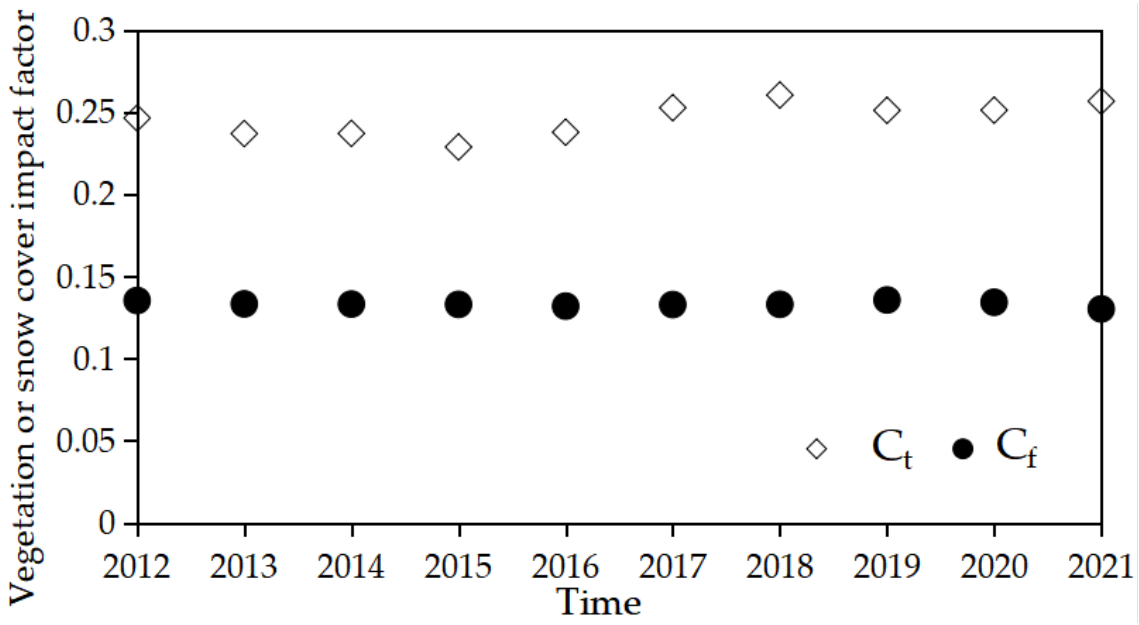

Figure 4.18: The vegetation or snow cover impact factors for each year from 2012 to 2021.

The result of NWC factors for every year are shown in Figure 4.19 [54] as points on every interpolation curve.

Throughout the time, the NWC_t factor is greater than the NWC_f factor, but only in 2013, which is probably owing to less precipitation, is the NWC_f factor greater.

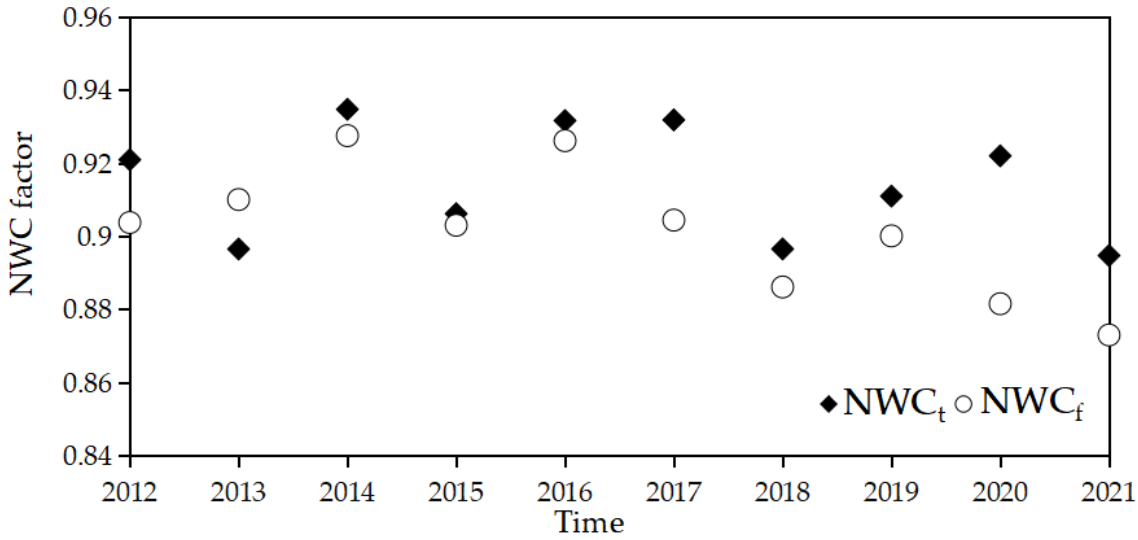

Figure 4.19: Changes over time in the NWC factors (NWC_f and NWC_t) for the years 2012 through 2021. Modified from Zhao and Tonooka (2022) [54].

4.4 Data and Procedure for the Soil Thermal Conductivity Validation

After determining the NWC factor required to correct the soil thermal conductivity, we will describe the validation method of the corrected soil thermal conductivity in detail in this section in order to ensure the accuracy of the corrected soil thermal conductivity. We did pertinent pre-processing, such as recalculation and resampling, using the observed soil thermal conductivity data from prior research based on various research methodologies to enhance the J model as the sample dataset. There are 128 total datasets, 64 of which are during the freezing phase and 64 during the thawing phase. Those types of soil are equivalent to each of the groups in Table 2.1, with the exception of organic content.

The sources of the sample dataset are shown in Table 4.1, which lists these data sources by temporality.

Table 4.1: Source of sample dataset for validation of the soil thermal conductivity.

Time (Year)	**Source**
1981	McInnes [68]
1986	Hopmans and Dane [69]
1994	Campbell et al. [70]
2005	Côté and Konrad [71]
2007	Kasubuchi et al. [72]
2007	Lu et al. [73]
2008	Chen et al. [74]
2012	Tarnawski et al. [75]
2015	Tarnawski et al. [67]
2017	McCombie et al. [76]

Preprocessing was carried out taking into account the variations in soil characteristics between frozen and thawed soil. We organize the main properties of frozen and thawed soils samples and the range of values of their related properties for respectively, as shown in Tables 4.2 and 4.3.

Table 4.2: The main properties of frozen soil samples and their corresponding values.

Main Properties	**Corresponding Values**
soil porosity	between 0.02–0.06 m
soil temperature	between −37 to −1 °C
soil bulk density	between 900–2300 kg·m^{-3}
unfrozen water content	per unit volume of soil between 0–1

Table 4.3: The main properties of thawed soil samples and their corresponding values.

Main Properties	**Corresponding Values**
soil porosity coefficient	between 0.03–0.07 m
soil moisture content	per unit volume of soil between 0–1
soil dry density	between 400–2400 kg·m^{-3}
soil particle density	between 2500–3000 kg·m^{-3}

Here we need to provide additional information on the value of unfrozen water content in the frozen soil properties and how to handle it.

The details are shown below:

- The known water content of every sample was converted;
- Unfrozen water content saturation and the ice in its corresponding volume was determined using empirical formulae and temperature;
- This corrected the unfrozen water contents in the various frozen soil sample dataset;
- The unfrozen water saturation and the ice saturation for this are 1 and 0, respectively, for the unfrozen water content per unit volume.

Following that, using the sample dataset as a guide, we established the average, standard, minimum and maximum, deviation of the soil thermal conductivity for frozen and thawed soils. We then utilized these numbers as validation dataset for the soil thermal conductivity. In a similar manner, we computed the statistics of the soil thermal conductivity L_f and L_t using the NWC factors for the years 2012 through 2021 and compared them to the results of the validation dataset.

4.5 L_f and L_t (Corrections to the Soil Thermal Conductivities)

In Figure 4.20 [54], the soil thermal conductivity box plots are compared between the validation values (64 samples datasets for every phase) and the values estimated using the NWC factors for the freezing and thawing phases, where every box denotes a value from − 3σ to + 3σ. In the freezing and thawing periods, 96.3% and 95.7%, respectively, of the calculated values fulfilled the three sigma requirements of the validation values, demonstrating a good correlation between the calculated values and validation.

The calculated values' maximum value is less than that of the validation values' maximum values because the calculated values' maximum value is nearly the soil thermal conductivity under the net moisture content state after adding the NWC factor, while the validation values' maximum value is essentially the soil thermal conductivity under the saturated moisture content state. Because soil thermal conductivity is an important physical parameter of soil heat transfer, it is influenced by soil moisture and structural state.

Moisture in the soil has good thermal conductivity and when the soil water content increases, it increases the heat transfer properties of the soil, thus increasing the thermal conductivity of the soil.

On the contrary, in the state of net water content, the thermal conductivity of the soil decreases due to the lack of water in the soil. Therefore, it is consistent with the physical properties of soil thermal conductivity to arrive at such validation results.

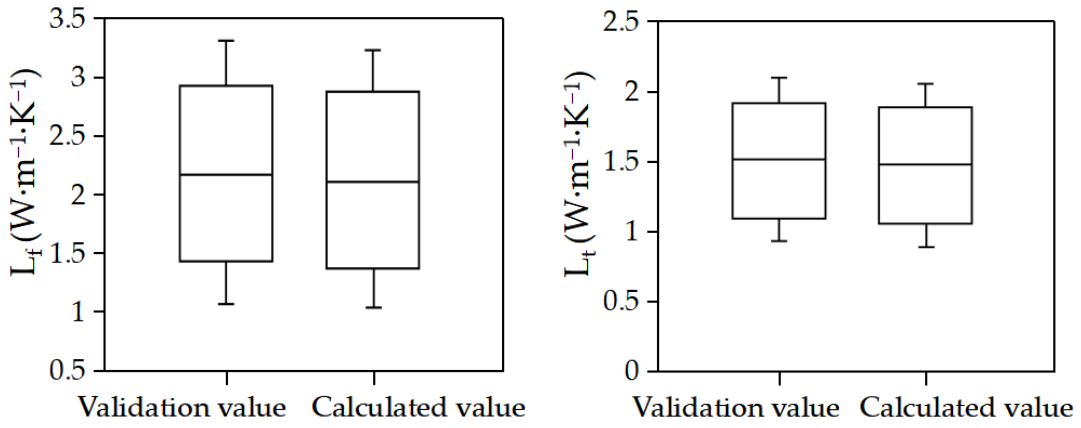

Figure 4.20: The values computed using the NWC factors for (a) the freezing phase and (b) the thawing phase, and the validation dataset (64 samples datasets for every phase) are compared in the box plots of the soil thermal conductivity. The box shows from − 3σ to + 3σ. Modified from Zhao and Tonooka (2022) [54].

4.6 Summary

In Chapter 4, we processed various parameters related to the lower and upper limit temperatures of the TLZ permafrost model according to the data and methods presented in Chapter 3, and the results of the various factors are presented and analyzed in a graphic manner in the following order.

First, we grouped the temperature analysis, which showed that the temperature variation in the six sub-areas in the study area was largely influenced by the elevation change. The mean values of temperature after removing anomalies were interpolated by TPS to calculate the cumulative temperature factors T_t and T_f. Between 2012 and 2021, the values of T_t showed a decreasing trend, while the values of T_f showed an increasing trend.

Then, we removed the influence of vegetation and snow in the study area by calculating the FVC and FSC reciprocals (F_t and F_f), where in the calculation of FVC, we analyzed in detail the trends of NDVI and EVI between 2012 and 2021, and the FVC mapping results derived by combining NDVI and EVI showed that there was less vegetation in the western region and more vegetation in the eastern region. However, the vegetation cover of the whole region is not high. This result is consistent with the IGBP land cover classification results. Meanwhile, in the FSC calculation, we analyzed the monthly snow cover mapping results for 2012 and 2021 as an example, and the results showed that the snow cover in the study area is very thin and the snow cover stability is relatively low, and the results are consistent with the annual snow cover trends of IGBP.

Then, we show and interpret the results of the net water content factors, i.e., NWC_t and NWC_f, presented in this study for the freeze-thaw period. In which we present the results of the five variables required to calculate the NWC factor (the precipitation (P), potential soil evapotranspiration (E), net soil water content (W), groundwater seepage factor (G) and vegetation or snow cover impact factor (C)). The results showed relatively consistent trends in evapotranspiration and soil water content during thaw and freeze periods, both being several times higher during thaw than freeze. Precipitation increases from the northwest (less precipitation in bare soil or sparse vegetation cover) to the southeast (more precipitation in alpine meadow cover), which is consistent with the land classification map of IGBP. The NWC factor were greater than the NWC_t factor overall between 2012 and 2021, but only in 2013, probably due to less precipitation, was the NWC_f factor greater. This also indicates that the NWC factor is strongly influenced by precipitation and evapotranspiration.

Finally, we show and explain the validation method of soil thermal conductivity and the results of soil thermal conductivity after adding the NWC factor. In the validation method, the soil thermal conductivity results of 128 groups of thawed and frozen soils from previous studies were used as validation data for comparison with the calculated data in this study, and the results show that the soil thermal conductivity after adding the NWC factor, i.e., the calculated data in this study, is closer to the physical properties of soil thermal conductivity.

After identifying the factors required for the TLZ permafrost model in this chapter, in the next chapter we use these factors to evaluate and analyze the permafrost changes in the study area between 2012 and 2021 according to the principles and formulas of the TLZ permafrost model, and present the final results.

Chapter 5 The Results and Validation

5.1 Utilization and Assessment of the TLZ Permafrost Model

We applied the results of each factor obtained in Chapter 4 to the TLZ permafrost model, and the specific steps for the application and evaluation of the TLZ model are shown in Table 5.1.

Table 5.1: TLZ permafrost model utilization and evaluation process.

Process	Utilization and Evaluation
1	Initially, the TTOP value for every pixel is first determined using (Equation (2-5)), and then every pixel is categorized using the following criterion. TTOP > 1.5 indicates short-term (ST) permafrost or non-permafrost. Permafrost is seasonal when TTOP is 0.5 to 1.5 and transitional when TTOP is 0 to 0.5. Permafrost occurs when TTOP < 0.
2	By measuring how long the zero-curtain effect lasted, we next evaluated every permafrost zone's stability. Permafrost zones with zero-curtain effects lasting (a) more than 4 weeks, (b) 3-4 weeks, (c) 2-3 weeks, and (d) 1-2 weeks or less were classified as (a) extremely stable, (b) very stable, (c) generally stable, and (d) unstable, respectively. And we assessed the research region in accordance with seven permafrost classes based on the TLZ model by adding three classes of (e) short-term/non-permanent, (f) seasonal, and (g) transitional permafrost zones.
3	Additionally, for the evaluation of the TLZ model, the MAGT model based on the subsurface temperature data taken twice daily at 27 CMDC stations close to the center of the research region was used. The daily mean subsurface temperatures among 27 sites at every depth for the years 2012–2021 were first calculated using subsurface temperature data at depths of 300, 60, 50, and 30 cm at every station. The MAGT values were derived by averaging every depth for every year, then comparing the MAGT results to the TLZ model's estimated subsurface temperature estimations for every year.

5.2 Maps of Permafrost Classification in Four-Levels

In this Section we discriminate the permafrost in the study area on a large and medium scale according to Process 1 in Table 5.1, with the following results and descriptions.

Using the adjusted TTOP data, Figure 5.1 [54] displays permafrost distributions for every year from 2012 through 2021. These distributions are broken down into four categories: short-term (ST) /non-permafrost, seasonal permafrost, transitional permafrost, and permafrost. The area represented by the dark purple color is the distribution area of permafrost. The distribution area of permafrost showed a relatively obvious overall degradation trend during the decade.

The total number of pixels for every class and every year are displayed in Figure 5.2 [54]. Permafrost regions may be shown to vary, shrink, and transform into transitional permafrost over time. Especially after 2016, the degradation of permafrost areas started to increase.

Additionally, it is clear that throughout this time both short-term/non-permafrost and seasonal permafrost zones remain stable, but the former tends to change into the latter. This also indicates that there is a tendency for some degree of recovery of permafrost in individual small intervals, influenced by environmental factors such as temperature.

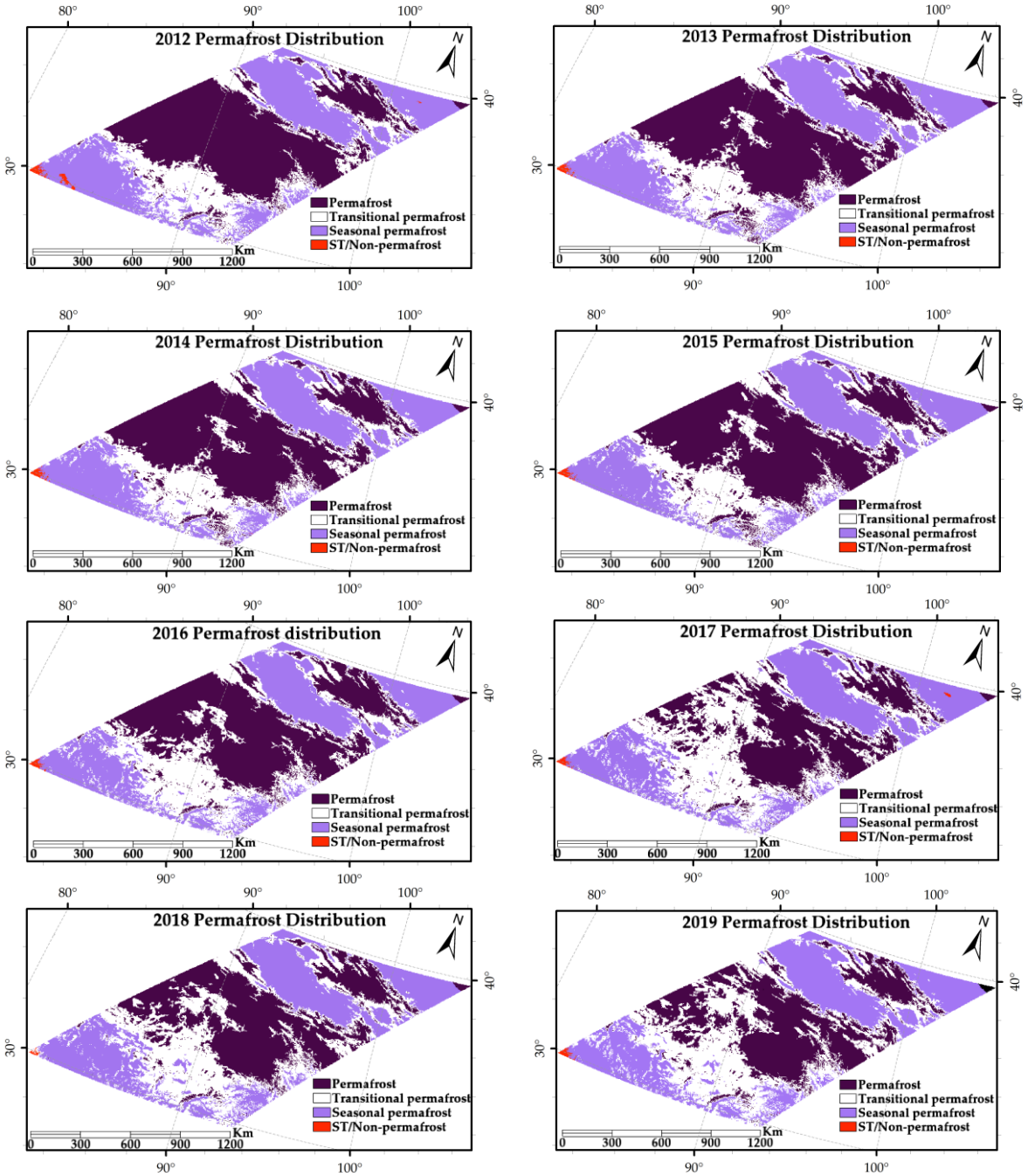
2012 Permafrost Distribution
2013 Permafrost Distribution
2014 Permafrost Distribution
2015 Permafrost Distribution
2016 Permafrost distribution
2017 Permafrost Distribution
2018 Permafrost Distribution
2019 Permafrost Distribution
Permafrost
Transitional permafrost
Seasonal permafrost
ST/Non-permafrost
Km
0 300 600 900 1200
80°
90°
100°
30°
40°
N

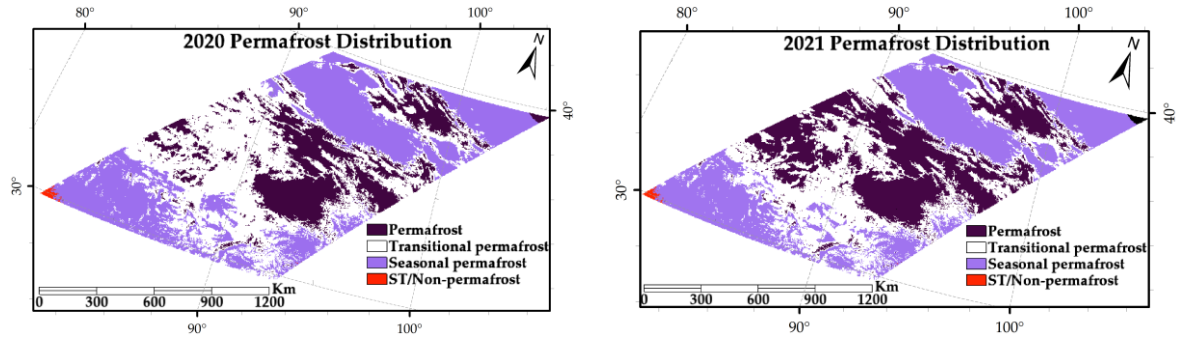

Figure 5.1: For every year from 2012 through 2021, permafrost distributions were divided into four categories: short-term (ST) / non-permafrost, seasonal permafrost, transitional permafrost, and permafrost. Modified from Zhao and Tonooka (2022) [54].

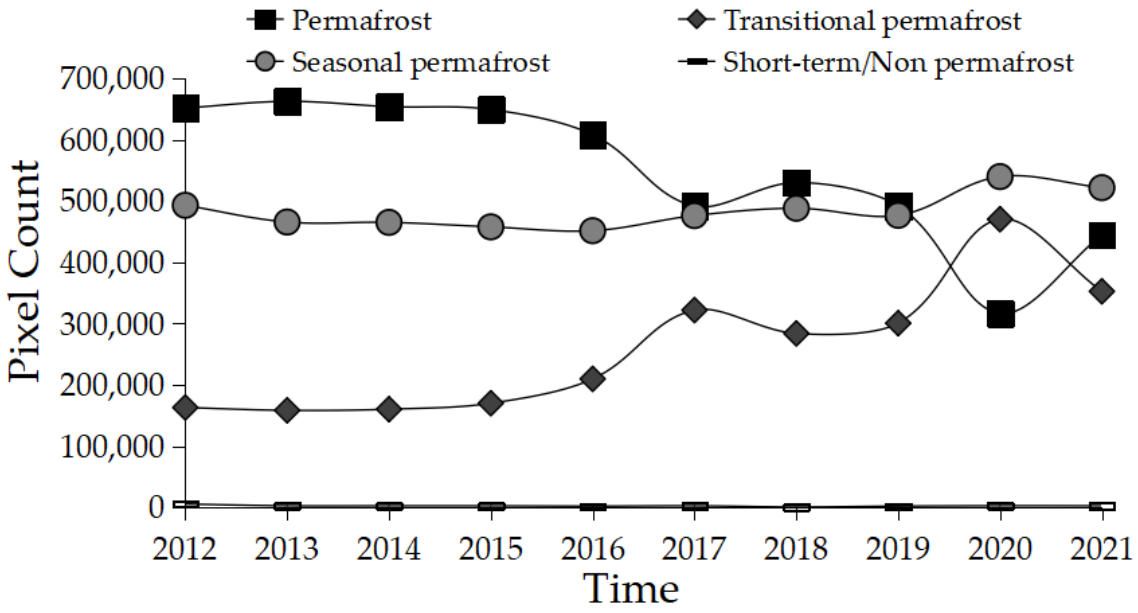

Figure 5.2: For every year from 2012 through 2021, the total number of pixels for every class—short-term (ST) / non-permafrost, seasonal permafrost, transitional permafrost, and permafrost—was calculated. Modified from Zhao and Tonooka (2022) [54].

5.3 Map of the LST Statistics

Based on the treatments presented in Section 3.6, we show and illustrate the results of the upper limit temperature (LST) treatment for the TLZ permafrost model for the period 2012 to 2021.

The mean, maximum and minimum of the LST maps derived from MODIS LST images are shown in Figure 5.3 [54] for every year.

The extent of the rise in LST can be clearly seen by the difference between the lowest and highest readings. For example, a clear trend in LST over time, with a significant change from low to high readings, indicates a large rise in LST. This change in conditions may be related to several factors:

- Related to changes in snow cover, a decrease in snow cover may lead to an increase in land surface temperature, which affects air temperature;
- Because vegetation absorbs solar radiation and reduces land surface temperatures, a decrease in vegetation can lead to an increase in land surface temperatures;
- A decrease in precipitation may also affect temperature. Precipitation removes heat and reduces the amount of heat in the air. When precipitation decreases, the amount of heat in the air and at the surface increases, which leads to an increase in air temperatures and land surface temperatures;
- An increase in evaporation also increases the movement of heat from the surface, which affects land surface temperatures;
- Global warming causes an increase in temperature due to a surge of greenhouse gases in the atmosphere caused by global warming, which allows more solar radiation to be absorbed by the Earth's surface, thus increasing the air temperature and land surface temperature;
- In addition, there are other factors that may affect land surface temperatures, such as human activities and atmospheric conditions.

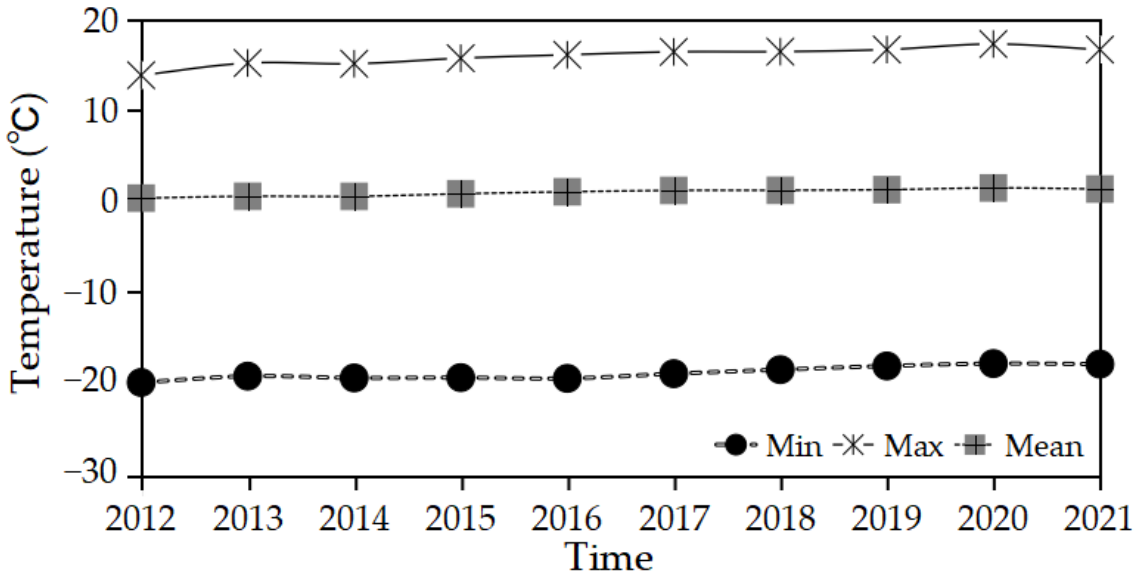

Figure 5.3: The mean, maximum and minimum of the LST maps were derived from MODIS LST images for every year from 2012 to 2021. Modified from Zhao and Tonooka (2022) [54].

5.4 The Average Subsurface Temperature at Various Depths

In this Section, we determine the time, location, and duration period of the zero-curtain effect based on the results of the upper limit temperature (LST) and lower limit temperature (TTOP) of the TLZ permafrost model for the years 2012 to 2021. We also present and illustrate the results of the zero-curtain effect for 2012-2021.

Figure 5.4 [54] reveals the subsurface temperature calculated by the TLZ permafrost model and its relationship with the cycle from 2012 to 2021. It can be seen from the figure that the average subsurface temperatures at different depths are significantly correlated with the cycle, where the average subsurface temperatures at depths of 60 cm, 50 cm, 40 cm, 30 cm, 20 cm, and 10 cm vary with the cycle, respectively. In addition, the average subsurface temperature showed a gradual increase with the increase of the depth of the active layer of permafrost in the same cycle. This indicates that the subsurface temperature of the active layer of permafrost is influenced by the depth, and the deeper the depth, the higher the temperature.

The zero-curtain effect was evident at depths of 60 cm, 50 cm, and 30 cm below the surface in 2012, according to Figure 5.5, however at 40 cm depth it was not evident owing to an absence of data. In addition, although the zero-curtain effect is obvious at the shallow surface, the effect of subsurface temperature on surface temperature deeper in the active layer cannot be completely ignored. In order to further study the effect of zero-curtain effect on climate change in terms of permafrost, analysis of subsurface temperature at greater depths and collection of more measured data on subsurface temperature are needed in the future.

Figure 5.5 [54] shows that during the thawing season from the beginning of April to the middle of June, the subsurface temperature at various depths briefly crosses the zero line for less a week, that is, the zero-curtain effect occurs briefly during the thawing season, and it is difficult to capture the changes brought about by such a brief zero-curtain effect to the permafrost because the duration period is so short, as a result, it is difficult to utilize the zero-curtain effect to assess the stability of permafrost during the thawing season and existence.

But, the freezing period, which starts in mid-October and lasts until mid-November, is a period during which the zero-curtain effect lasts for a relatively long time, around one month. Such a length of time can be utilized as a reliable measure of permafrost stability and presence.

As a result, the long period of persistence of the zero-curtain effect throughout the freezing period will play an important role and can help us better understand the condition of permafrost. In this study, we evaluate the stability of the permafrost distribution area utilizing the length of the duration period of the zero-curtain effect during the freezing period according to the method presented in Table 5.1 Process 2.

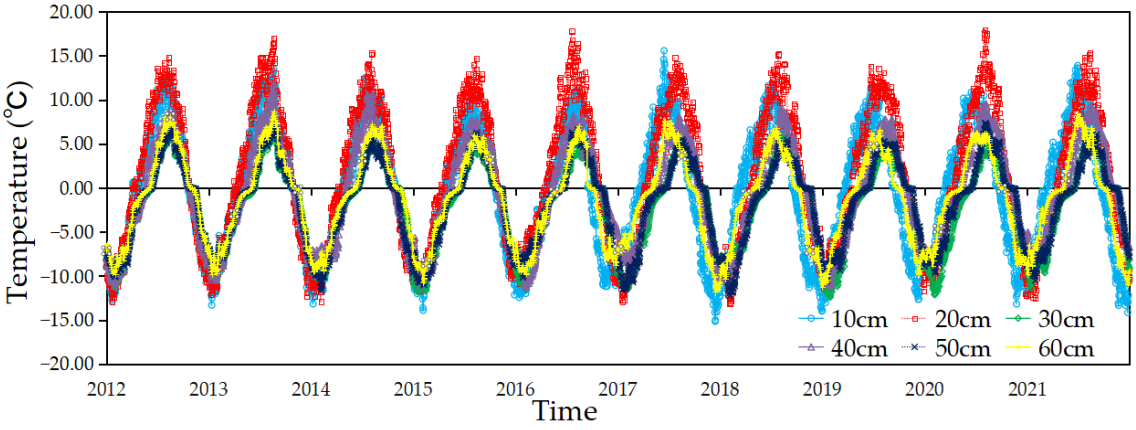

Figure 5.4: The TLZ model was used to determine the temporal variations in the average subsurface temperatures at depths of 60, 50, 40, 30, 20, and 10 cm for the years 2012 to 2021. Modified from Zhao and Tonooka (2022) [54].

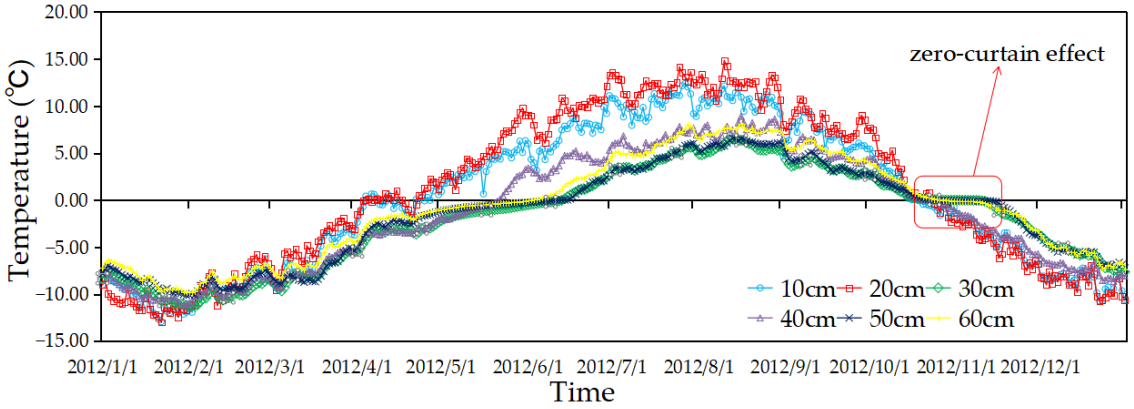

Figure 5.5: The TLZ model was used to determine the temporal variations in average subsurface temperatures in 2012 at depths of 60, 50, 40, 30, 20, and 10 cm. Modified from Zhao and Tonooka (2022) [54].

5.5 Maps of Permafrost Classification in Seven-Levels

After determining the duration of the zero-curtain effect for each year of the freezing period between 2012 and 2021, we present and illustrate the mapping results by combining the principles and evaluation methods of the TLZ permafrost model.

When the results of Figure 5.1 are combined with those from the TLZ permafrost model, permafrost distributions are shown in Figure 5.6 [54] and are divided into seven categories: unstable permafrost, general stable permafrost, very stable permafrost, extremely stable permafrost, short-term (ST) / non-permafrost, seasonal and transitional permafrost.

The total number of pixels for every type of permafrost is shown in Figure 5.7 [54] as a function of periodic variation. And from the variation of each curve in Figure 5.7 we can draw some conclusions as shown in Table 5.2 below.

Table 5.2: Conclusions drawn from the analysis of permafrost changes in the study area between 2012 and 2021 using the TLZ permafrost model.

Conclusions	Specific Content
1	The research period did not indicate any substantial changes in the short-term (ST) / non-permafrost and seasonal permafrost classes, but the latter exhibits a moderate rise from 2019 to 2020.
2	Changes from unstable permafrost and generally stable permafrost classes resulted in a definite growth in the transitional permafrost class throughout this time.
3	During the research period, the number of very stable permafrost and extremely stable permafrost classes marginally reduced. Changes from very stable permafrost to general stable permafrost classes and form extremely stable permafrost to very stable permafrost classes, respectively, were the major causes of these declines.

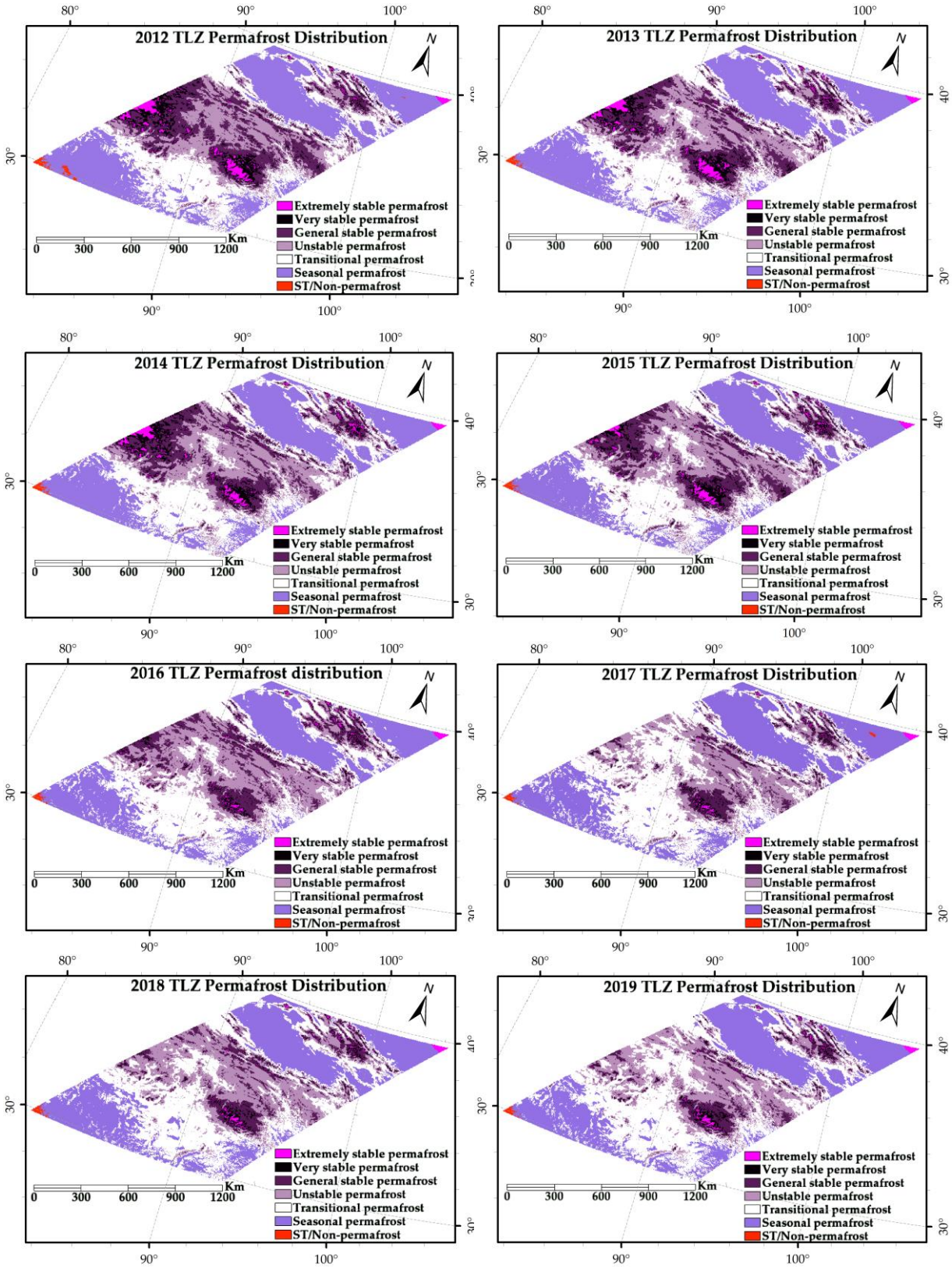
2012 TLZ Permafrost Distribution
2013 TLZ Permafrost Distribution
2014 TLZ Permafrost Distribution
2015 TLZ Permafrost Distribution
2016 TLZ Permafrost distribution
2017 TLZ Permafrost Distribution
2018 TLZ Permafrost Distribution
2019 TLZ Permafrost Distribution
Extremely stable permafrost
Very stable permafrost
General stable permafrost
Unstable permafrost
Transitional permafrost
Seasonal permafrost
ST/Non-permafrost
Km
0 300 600 900 1200
80°
90°
100°
30°
40°
N

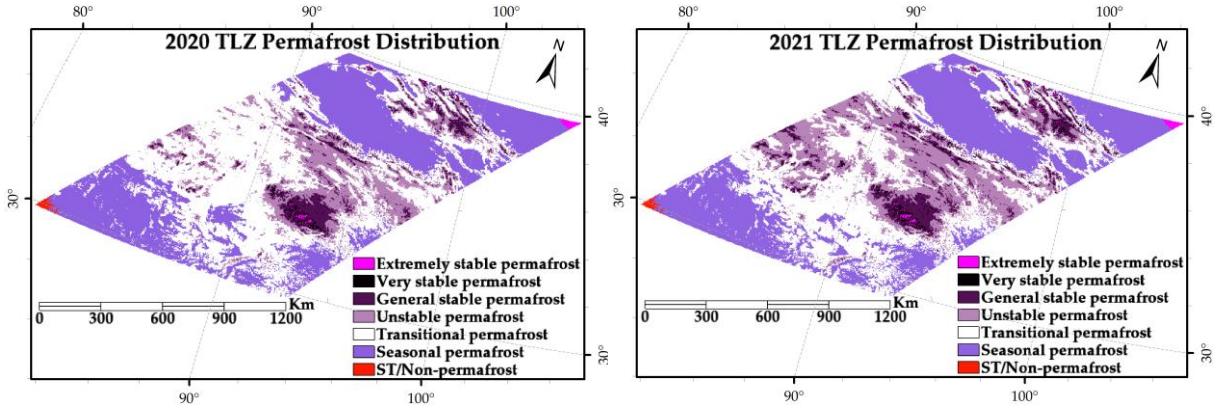

Figure 5.6: For every year from 2012 through 2021, permafrost distributions were divided into seven categories: short-term (ST) / non-permafrost, seasonal permafrost, transitional permafrost, unstable permafrost, general stablepermafrost, very stable permafrost and extremely stable permafrost. Modified from Zhao and Tonooka (2022) [54].

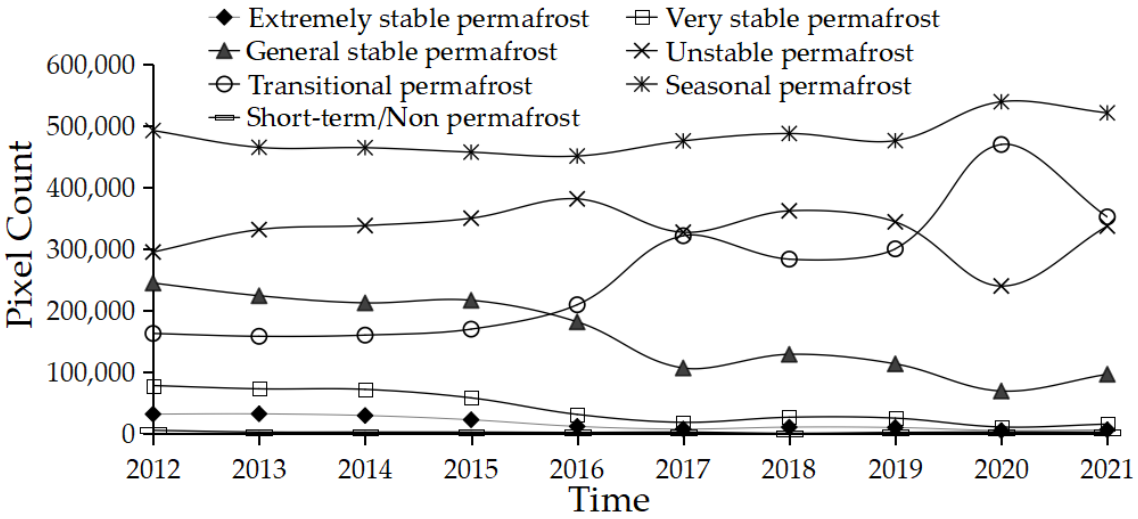

Figure 5.7: For every year from 2012 through 2021, the total number of pixels for every class—short-term (ST) / non-permafrost, seasonal permafrost, transitional permafrost, unstable permafrost, general stable permafrost, very stable permafrost and extremely stable permafrost—was calculated. Modified from Zhao and Tonooka (2022) [54].

5.6 The TLZ Permafrost Model is Validated by Comparison with the MAGT Permafrost Model

After obtaining the results of the application and evaluation of the TLZ permafrost model, in this Section we perform a validation analysis of the results according to the method presented in Table 5.1 Process 3.

From 2012 to 2021, the subsurface temperatures at the 27 CMDC sites show significant changes at different depths. At 300 cm depth, the average daily subsurface temperature shows a slow increase during this decade; while at 60 cm depth, the average daily subsurface temperature shows an oscillating increase; at 50 cm depth, the average daily subsurface temperature reaches its lowest point in 2014 and then starts to increase slowly; at 30 cm depth, the average daily subsurface temperature shows several oscillations during the decade, with the highest point occurring in 2020 year. It can be seen from Figure 5.8 [54] that the subsurface temperature at different depths has a clear trend of variation in this decade.

The annual averages of subsurface temperatures obtained by the TLZ permafrost model for the period for every depth are contrasted with the MAGT results calculated from this data in Figure 5.9 [54]. The comparison shows that the results obtained by the TLZ permafrost model are in high agreement with the MAGT results. At deeper depths, the differences are smaller; while at individual depths at shallow depths, some deviations occur, indicating that the TLZ permafrost model is more accurate in calculating the temperature at deeper depths. This should be related to the high accuracy of the corrected lower temperature limit (TTOP) in this research.

Based on the MAGT-based results, Table 5.3 [54] shows the simulation accuracy of the TLZ permafrost model for subsurface temperature at four depths. The RMSE (root mean square error) represents the deviation between the simulated and measured values, the Standard Error represents the accuracy of the simulated values, and the Mean Absolute Error measures the degree of deviation between the simulated and measured values.

Their respective average values are all substantially lower than 1 and the values are 0.19, 0.25 and 0.27, demonstrating the great accuracy of the TLZ model results in this investigation, which also indicates that the TLZ permafrost model can well simulate the trend of subsurface temperature changes and thus assess the changes of permafrost.

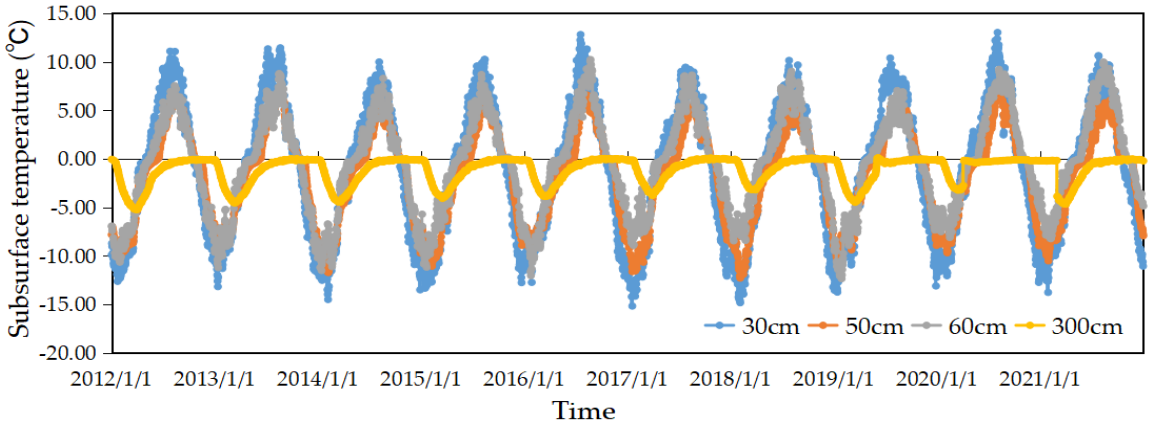

Figure 5.8: For the years 2012 to 2021, the average daily subsurface temperatures at 300, 60, 50, and 30 cm depths were calculated from 27 CMDC sites. Modified from Zhao and Tonooka (2022) [54].

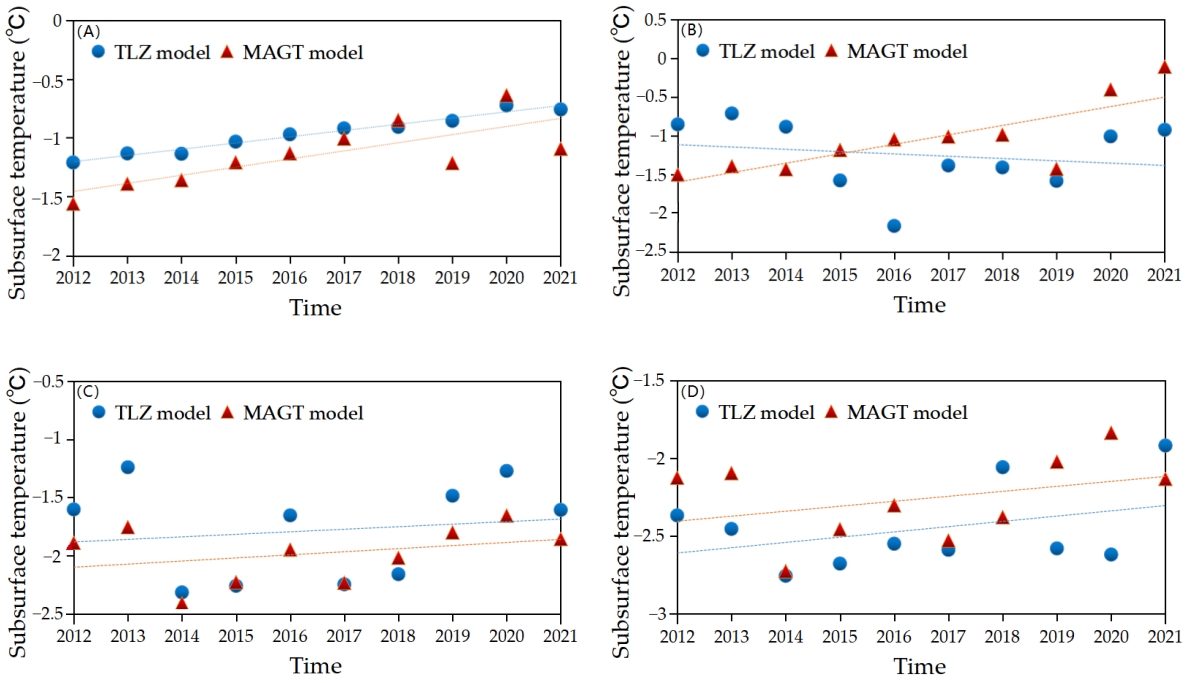

Figure 5.9: Comparison between the subsurface temperatures predicted by the TLZ permafrost model and the result of MAGT permafrost model for the years 2012 through 2021 at depths of (A) 300 cm, (B) 60 cm, (C) 50 cm, and (D) 30 cm. Modified from Zhao and Tonooka (2022) [54].

Table 5.3: RMSE, Standard Error and Mean Absolute Error, is the measurement of subsurface temperatures using the TLZ model at depths of 300, 60, 50, and 30 cm with reference to MAGT-based result. Modified from Zhao and Tonooka (2022) [54].

Depth (cm)	**RMSE (°C)**	**Standard Error (°C)**	**Mean Absolute Error (°C)**
300	0.165	0.094	0.189
60	0.198	0.478	0.355
50	0.200	0.158	0.291
30	0.192	0.279	0.238

5.7 Summary

In Chapter 5, we show and illustrate in detail the various results of the TLZ permafrost model based on the computational principles of the TLZ permafrost model using the various parameter factors obtained in Chapter 4. These results can be used not only as an important reference for the study and calculation of permafrost, but also as a validation of the permafrost model.

Firstly, we introduce the specific process of application and evaluation of the model, where process 1 is the application and evaluation of the T (TTOP) part, process 2 is the application and evaluation of the L (LST) and Z (zero-curtain) parts, and process 3 is the comparative validation of the model.

In the part of T, we classify permafrost and non-permafrost at large and medium scales in four levels, and analyze and illustrate the degradation trend and transition type of permafrost, etc. The results show that the permafrost zone changes, shrinks, and transforms into transitional permafrost over time. Especially after 2016, the degradation trend of permafrost areas started to increase.

In the part of L, we analyze in detail the mean, maximum, and minimum values of LST from 2012 to 2021 and other related changes, and we analyze and explain the various environmental and climatic factors that may cause the increase of LST during the decade.

In the part of Z, we determined the depth and time of occurrence of the zero-curtain effect, as well as the duration period of the zero-curtain effect, and determined that only the zero-curtain effect during the freezing period can be used to evaluate the stability of the permafrost distribution.

After that, we analyzed and evaluated the stability and transformation trends of permafrost regions, etc., on a small scale according to the duration period of the zero-curtain effect during the freezing period, combined with the classification results in part T. The results showed that the number of very stable permafrost and extremely stable permafrost classes decreased slightly during the study period. The shift from very stable permafrost to generally stable permafrost classes and from extremely stable permafrost to very stable permafrost classes, respectively, are the main reasons for these decreases.

Finally, to ensure the accuracy of the TLZ model analysis results, we constructed MAGT permafrost models at different depths based on the measured subsurface temperature data and compared them with the results of the TLZ permafrost model. The analysis showed that the error results of RMSE, SE, MAE, etc. were much less than 1°C. This proved that the TLZ permafrost model proposed in this study has high accuracy and can make accurate evaluation and analysis of permafrost changes at different scales, such as large, medium and small.

In the next chapter we discuss the experimental results and the problems encountered in the research, and summarize the final conclusions.

Chapter 6 The Discussion and Conclusion

6.1 The Discussion

Because, the model can help us better understand the characteristics and distribution pattern of permafrost, while the data can provide an objective and reliable reference for permafrost investigation. Therefore, to ensure the accuracy and feasibility of permafrost investigation, effective and accurate models and data must be grasped. First, we developed a revised TTOP permafrost model that incorporates a Net Water Content (NWC) factor to correct the soil thermal conductivity. This revised model can describe the soil properties of permafrost more accurately and provide more accurate lower limit temperature values (TTOP). In addition, a new TLZ permafrost analysis model is developed by fusing the revised lower limit temperature value (TTOP) and upper limit temperature value (LST) to accurately describe the specific conditions of permafrost according to the zero-curtain effect. We can use this model to conduct an in-depth investigation into the formation mechanism of permafrost, so as to better understand the environmental effects and change patterns of permafrost.

In order to better assess the permafrost in the Qinghai-Tibetan Plateau area, we have conducted a lot of research work. We used high-precision data, including remote sensing data, meteorological data, and topographic data, to analyze and describe the permafrost environment on the plateau in detail, as a way to achieve a more accurate and reliable assessment. In addition, we collected various meteorological parameters, such as temperature, precipitation, evapotranspiration, etc., to provide an important basis for the assessment of permafrost conditions. In addition, we collected a large number of field observations, including air temperature, subsurface temperature and subsurface water content, to verify the validity of the model. Through these studies, we try to complete a more accurate and reliable permafrost assessment in the Tibetan Plateau region as much as possible.

For identifying permafrost and non-permafrost at large and medium scales, this study used the modified TTOP model to classify and analyze permafrost in the study region. The results show that the largest shift in permafrost category occurs between transitional permafrost and permafrost; in addition, seasonal permafrost shows an increase between 2012 and 2021. This shows that the distribution of permafrost is influenced by the local climatic conditions and the trend of change is more obvious. Therefore, further in-depth studies on the distribution characteristics of permafrost and its changing trends in the study area will help to better understand the changes in the local climatic environment and provide a scientific basis for the effective use of permafrost resources.

Although the impact of global warming results on permafrost can be immeasurable, the observation in the past five years shows that permafrost has recovered to a small extent in some areas. For example, in 2021 and 2018, there is some recovery in the dark purple permafrost distribution area in the lower right as shown in Figure 5.1. During 2021 and 2018, although the warming trend persists in the study area, the average temperature is continuously increasing. However, the number of extreme weather events decreased during these two years, which may have contributed to the recovery of permafrost in the local region. Also the deterioration of permafrost may have been delayed during these two years due to the relatively stable average snowfall and rainfall and a certain degree of vegetation development. And due to the active layer's transfer of heat to the environment during the freezing phase, which raises the temperature at the active layer and permafrost layer's interface, the average value of TTOP during the freezing phase was greater than that during the thawing phase.

Even so, in the study area as a whole, the area of permafrost has been decreasing in the last decade, and this degradation is particularly evident in the central and western parts of the study area. At the same time, global warming is still increasing, which leads to a more fragile permafrost. This situation not only threatens the survival of plant and animal species on the Qinghai-Tibetan Plateau, but also may in turn affect the global climate change process. This requires us to analyze and study aspects such as the stability of permafrost at a smaller scale.

The stability types of permafrost are influenced by environmental factors, such as temperature, snow water depth, and soil energy changes, so it is necessary to gain insight into the transition processes between different stability types of permafrost. In addition, the stability transition process of permafrost can also help us better understand the effects of global climate change, thus providing us with useful information. By comparing the transitions between various stability types of permafrost, we can better understand these changes and help us to better formulate effective countermeasures. In order to further analyze the stability of permafrost and its changes in the research region in detail at a small scale, we subsequently added stability classifications of permafrost areas while merging the TTOP model classification results in the TLZ permafrost model-based permafrost mapping, i.e., the study area was classified into seven permafrost categories for every year from 2012 to 2021.

The results show a significant increase in the transitional permafrost category and some decrease in the very stable and extremely permafrost categories during this time period. No significant changes were seen in the short-term (ST) /non-permafrost and seasonal permafrost categories. In particular, changes from extremely stable permafrost to very stable permafrost categories and from very stable permafrost to general stable permafrost categories, respectively, were primarily responsible for the decreases in extremely stable permafrost and very stable permafrost categories, while changes from general stable permafrost and unstable permafrost categories were primarily responsible for the increase in transitional permafrost category. These changes indicate that the stability of permafrost areas in the study area is generally deteriorating, most likely as a result of the greenhouse effect that is currently starting.

Therefore, we must take effective measures to stop the effects of the greenhouse effect in order to mitigate this deterioration in stability before it causes greater permafrost degradation. In 2020, certain changes in specific patterns in the atmosphere have occurred due to the occurrence of multiple extreme weather conditions. This phenomenon has a clear impact on climate warming, and the findings show that climate patterns in 2020 differ from those of previous years. Among them, temperature changes were particularly significant, with extreme temperatures in some areas accompanied by intense heat, which caused great inconvenience to people's lives.

In addition, the atmospheric circulation has also changed, affecting the trend of atmospheric circulation and causing extreme weather phenomena such as strong winds and dust storms in some regions. Therefore, the climate pattern in 2020 is slightly different and needs more attention and research to better cope with future climate change. This suggests that the increase in air temperature may lead to the melting of permafrost, which may result in the collapse of the ground and the formation of lakes, thus affecting the ecological environment. In addition, the frequency of extreme weather events may also affect the stability of permafrost, such as dust storms, desertification, etc., which may intensify the melting of permafrost and cause damage to the ground surface.

After a detailed analysis of the stability changes in the permafrost region, to ensure the validity and accuracy of the TLZ permafrost model, we constructed the MAGT permafrost model by combining the measured ground temperature data, and compared the TLZ permafrost model with the MAGT permafrost model by validating the temperature results at different depths. The results showed an average RMSE of 0.19°C between the TLZ-based and MAGT-based results. We then performed a comparative analysis by combining the validation results of previous similar studies. When studying the underground depth of 2.35 m of the Qinghai-Tibetan Plateau using the MAGT permafrost model and the TTOP permafrost model, Ran et al. (2022) obtained an average RMSE of 0.93 °C [46]. When utilizing the MAGT permafrost model and the TTOP permafrost model for the underground depth range of 0 to 2.99 m of the Qinghai-Tibetan Plateau, Ni et al. observed an average RMSE of 0.53 °C in 2021 [45]. When Yin et al. (2021) used the MAGT permafrost model and the TTOP permafrost model to study the underground depth range of 0.69 to 4.32 m of the Qinghai-Tibetan Plateau, they observed an average RMSE of 0.5 °C [47]. In comparison to their results, the RMSE result in our study is sufficiently low, only 0.19 °C showing that the TLZ permafrost model has more accuracy and smaller errors than traditional TTOP permafrost models.

After a comparative analysis with the results of the traditional TTOP permafrost model, we then compare and analyze the results with those of the traditional LST-zero-curtain permafrost model. Our study focuses more on the details of the zero-curtain effect and performs a more in-depth analysis. For example, we have used observations, experimental controls, and simulations in investigating the mechanism of the zero-curtain effect, and have obtained more information from them.

In addition, we propose the TLZ permafrost model approach for better description of the zero-curtain effect. It was discovered in the zero-curtain effect evaluation on the TLZ permafrost model that the zero-curtain effect only occurs in the active layer's freezing phase, which is from the middle of October to the middle of November each year, during this time period, the water on the surface of the permafrost layer is completely frozen, thus creating a stable permafrost structure that allows it to exist. Moreover, it is only during this time period that the stability of permafrost can be effectively studied, because only during this time period is the structure of permafrost stable enough and not susceptible to external factors.

The findings of this study are consistent with those of a prior one by Gillespie et al. The depth at which the zero-curtain effect manifests itself is where our research differs from the research of Gillespie et al. [49]. While the zero-curtain effect predominately appeared at 30 cm, 25 cm, and 15 cm in the prior work by Gillespie et al., our data, as shown in Figure 5.5, demonstrate that the zero-curtain effect happens at 60 cm, 50 cm, and 30 cm. The main reasons for this discrepancy are different approaches to calculating zero-curtain effects and different soil qualities between our research region (Asia's Qinghai-Tibetan Plateau area) and their research region (South-American's Chilean area). The Qinghai-Tibet Plateau region in Asia is mostly grassland with poorer soils and less support for plant growth, while the Chilean region in South America has higher quality soils and more support for plant growth. This most likely leads to different locations of subsurface energy balance points.

In addition, we used the TLZ hierarchical method to calculate the zero-curtain effect according to the combination of TTOP and LST, as opposed to Gillespie et al. who rated the zero-curtain effect just using LST. Because Gillespie et al. used the physics perspective ground surface temperature (LST) as a discriminating criterion, they used subsurface temperature to verify the accuracy of LST at 3 subsurface temperature monitoring stations with 2 cm depth subsurface temperature, illustrating that their approach can verify the existence of zero-curtain effect, thereby demonstrating the veracity of the zero-curtain effect theory in an indirect manner [49].

But in this research, we constructed the MAGT permafrost model with a large amount of measured ground temperature data to directly compare with the TLZ permafrost model at different depths. The validation methods used in the two researches were varied, and since Gillespie et al. did not disclose specific error precision validation figures in their previous investigation, we cannot measure the validation results of the two researches with specific error values such as RMSE,SE,MAE, etc. In contrast, the direct validation approach is typically more precise than the indirect validation approach.

Because to identify permafrost changes in the Qinghai-Tibetan Plateau area, Zhao et al. also researched the zero-curtain effect [52]. They pointed out that the variation of permafrost depth is one of the important factors affecting the regional climate, and we compared the error results at various depths with their findings . Their average errors at 245 cm, 105 cm, 40 cm, 10 cm, and 5 cm were greater than 0.4 °C [52], demonstrating that the TLZ permafrost model's average errors at various depths are lower than those of the traditional zero-curtain model, which has higher accuracy.

Although the validity and high accuracy of the TLZ permafrost model were verified in this research, the results in Table 5.3 show that the analytical error of the model for deep soils is smaller than that for shallow soils, which may be related to two major factors. The first is the use of a large amount of high-precision data and the introduction of a correction factor related to soil thermal conductivity in the determination of the lower limit temperature (TTOP) in this research, which results in a higher accuracy of the lower limit temperature part and is closer to the actual situation. The second is that there are some differences between the 0cm temperature and the LST even though the effects of snow and vegetation were taken into account and removed when determining the upper limit temperature (LST). These two points may be the main reasons for the difference between deep and shallow errors, which should be taken into account in future studies to investigate more reasonable conversion techniques. Moreover, when facing the area with more distribution of tall vegetation, more accurate removal methods can be adopted, such as coherent multi-frequency processing of synthetic aperture radar, etc. These are the spaces where the TLZ permafrost model can continue to be improved.

6.2 Conclusion

Permafrost is one of the most sensitive areas of global climate change, and it is of great theoretical and practical significance to analyze its change law. To this end, we can use the relevant properties of the zero-curtain effect to analyze the change pattern of permafrost to study the mechanism of permafrost change and provide theoretical guidance for the management of permafrost. Specifically, we can examine the influence of the zero-curtain effect on permafrost change, so as to explore the pattern of permafrost change, analyze the relationship between it and climate change and human activities, and propose corresponding policy recommendations based on this.

To address the shortcomings of the conventional TTOP permafrost model and the conventional LST-zero-curtain permafrost model, a new TLZ permafrost model was suggested to evaluate the zero-curtain effect of permafrost by setting the lower temperature as the TTOP value and the upper temperature as the LST value in this research. The depth, time, and duration of the zero-curtain effect derived from the TLZ permafrost model are used to analyze the change of permafrost in the central-eastern part of the Qinghai-Tibetan Plateau between 2012 and 2021. To obtain more accurate lower limit temperature (TTOP) values, the soil thermal conductivity in TTOP is corrected by introducing a new net soil water content factor (NWC).

The TLZ permafrost model is ingeniously reconstructed by using the correlation of temperature and soil heat between the traditional TTOP permafrost model and the LST zero-curtain permafrost model. Compared with the conventional TTOP model, the TLZ permafrost model utilizes LST instead of air temperature, which greatly reduces the spatial distance problem in the temperature analysis of the conventional TTOP model, and LST is more stable and easier to observe than the air temperature of the range of 2-10m. And compared with the traditional LST-zero-curtain permafrost model increases the curve change in terms of lower limit temperature for the zero-curtain effect analysis, which makes it more accurate for the zero-curtain effect and more consistent with the physical heat conversion principle of the active layer.

In addition to the above advantages, when we apply the TLZ permafrost model to the east-central part of the Qinghai-Tibetan Plateau in the research area for dynamic assessment and mapping, we can find that the TLZ permafrost model can not only distinguish the distribution and changes of permafrost and non-permafrost well at large and medium scales, but also make a very detailed ranking of the stability of permafrost areas at small scales. It is also possible to make a very detailed classification of the stability of permafrost areas at small scales and to accurately analyze information such as the conversion of changes in permafrost of different stability. This is a new breakthrough in the comprehensiveness of the permafrost analysis scale, which cannot be achieved by any previous permafrost analysis models. Moreover, when comparing and verifying with MAGT permafrost model, the error of the result is much less than 1℃, which well proves the validity and high accuracy of TLZ permafrost model.

In summary, the TLZ permafrost model can predict the deterioration of permafrost, periodic change model, stability change law, permafrost type conversion, future change prediction and so on. Compared with the traditional permafrost model, TLZ permafrost model opens up a new path in the field of permafrost model research.

Acknowledgement

This thesis is mainly the result of my research during my doctoral program in Social Systems Engineering at Ibaraki University, in addition to my personal research work and efforts.

First of all, I would like to thank my main supervisor, Prof. Tonooka, for his careful guidance from the identification of the research topic, data processing, algorithm analysis, to the revision of the dissertation, etc. I can say that without Prof. Tonooka's patient and rigorous teaching, I would not have been able to successfully complete this dissertation. I would like to express my deepest gratitude to Prof. Tonooka.

Secondly, I would like to express my gratitude to NASA and CMDC, the providers of the data, for the large amount of long-period satellite data and measured meteorological data used in this thesis.

Then, I would like to thank Prof. Wakabayashi for his valuable advice during the writing of this paper.

Also, Prof. Alan Gillespie, a famous American scholar, gave me very valuable advice on my subsequent research, and I would like to thank Prof. Alan Gillespie.

In addition, I would like to express my gratitude to Prof. Tonooka and my fellow researchers for their unfailing care during my doctoral studies.

Finally, I would like to thank my family in China for their encouragement and support in all aspects of my research.

Thank you all.

Zhao Zhijian

2023.02.22

References

1. Ma, W.; Cheng, G.; Wu, Q. Construction on permafrost foundations: Lessons learned from the Qinghai–Tibet railroad. Cold Reg. Sci. Technol. 2009, 59, 3–11.
2. Harris, C.; Davies, M.C.R.; Etzelmüller, B. The assessment of potential geotechnical hazards associated with mountain permafrost in a warming global climate. Permafr. Periglac. Process. 2001, 12, 145–156.
3. Gruber, S. Derivation and analysis of a high-resolution estimate of global permafrost zonation. Cryosphere. 2012, 6, 221–233.
4. Kimball, J.S.; McDonald, K.C.; Keyser, A.R.; Frolking, S.; Running, S.W. Application of the NASA Scatterometer (NSCAT) for Determining the Daily Frozen and Nonfrozen Landscape of Alaska. Remote Sens. Environ. 2001, 75, 113–126.
5. Briggs, M.A.; Walvoord, M.A.; McKenzie, J.M.; Voss, C.I.; Day-Lewis, F.D.; Lane, J.W. New permafrost is forming around shrinking Arctic lakes, but will it last? Geophys. Res. Lett. 2014, 41, 1585–1592.
6. Dobiński, W. Permafrost active layer. Earth-Sci. Rev. 2020, 208, 103301.
7. Mekonnen, Z.A.; Riley, W.J.; Grant, R.F.; Romanovsky, V.E. Changes in precipitation and air temperature contribute comparably to permafrost degradation in a warmer climate. Environ. Res. Lett. 2021, 16, 024008.
8. Romanovsky, V.E.; Osterkamp, T.E. Thawing of the Active Layer on the Coastal Plain of the Alaskan Arctic. Permafr. Periglac. Process. 1998, 8, 1–22.
9. Zhang, T.; Frauenfeld, O.W.; Serreze, M.C.; Etringer, A.; Oelke, C.; McCreight, J.L.; Barry, R.; Gilichinsky, D.; Yang, D.; Ye, H.; et al. Spatial and temporal variability in active layer thickness over the Russian Arctic drainage basin. J. Geophys. Res. 2005, 110, D16101.
10. Hinkel, K.M.; Outcalt, S.I.; Taylor, A.E. Seasonal patterns of coupled flow in the active layer at three sites in northwest North America. Can. J. Earth Sci. 1997, 34, 667–678.
11. Luo, D.; Jin, H.; Marchenko, S.S.; Romanovsky, V.E. Difference between near-surface air, land surface and ground surface temperatures and their influences on the frozen ground on the Qinghai-Tibet Plateau. Geoderma 2018, 312, 74–85.
12. Hachem, S.; Allard, M.; Duguay, C. Using the MODIS land surface temperature product for mapping permafrost: An application to northern Québec and Labrador, Canada. Permafr. Periglac. Process. 2009, 20, 407–416.
13. Zou, D.; Zhao, L.; Sheng, Y.; Chen, J.; Hu, G.; Wu, T.; Wu, J.; Xie, C.; Wu, X.; Pang, Q.; et al. A new map of permafrost distribution on the Tibetan Plateau. Cryosphere 2017, 11, 2527–2542.
14. Shen, X.; Liu, B.; Jiang, M.; Lu, X. Marshland loss warms local land surface temperature in China. Geophys. Res. Lett. 2020, 47, e2020GL087648.

15. Qin, Y.; Wu, T.; Zhao, L.; Wu, X.; Li, R.; Xie, C.; Pang, Q.; Hu, G.; Qiao, Y.; Zhao, G.; et al. Numerical modeling of the active layer thickness and permafrost thermal state across Qinghai-Tibetan Plateau. J. Geophys. Res. Atmos. 2017, 122, 11604–11620.
16. Sun, Z.; Zhao, L.; Hu, G.; Qiao, Y.; Du, E.; Zou, D; Xie, C. Modeling permafrost changes on the Qinghai-Tibetan Plateau from 1966 to 2100: A case study from two boreholes along the Qinghai-Tibet engineering corridor. Permafr. Periglac. Process. 2020, 31, 156–171.
17. Peng, X.; Zhang, T.; Frauenfeld, O.W.; Wang, K.; Luo, D.; Cao, B.; Su, H.; Jin, H.; Wu, Q. Spatiotemporal changes in active layer thickness under contemporary and projected climate in the Northern Hemisphere. J. Clim. 2018, 31, 251–266.
18. Zhao, L.; Zou, D.; Hu, G.; Du, E.; Pang, Q.; Xiao, Y.; Li, R.; Sheng, Y.; Wu, X.; Sun, Z.; et al. Changing climate and the permafrost environment on the Qinghai-Tibet （Xizang） Plateau. Permafr. Periglac. Process. 2020, 31, 396–405.
19. Wei, Y.; Lu, H.; Wang, J.; Wang, X.; Sun, J. Dual Influence of Climate Change and Anthropogenic Activities on the Spatiotemporal Vegetation Dynamics Over the Qinghai-Tibetan Plateau From 1981 to 2015. Earth′s Future 2022, 10, e2021EF002566.
20. Liu, Y.; Fang, P.; Guo, B.; Ji, M.; Liu, P.; Mao, G.; Xu, B.; Kang, S.; Liu, J. A comprehensive dataset of microbial abundance, dissolved organic carbon, and nitrogen in Tibetan Plateau glaciers. Earth Syst. Sci. Data 2022, 14, 2303–2314.
21. Mu, C.C.; Abbott, B.W.; Wu, X.D.; Zhao, Q.; Wang, H.J.; Su, H.; Wang, S.F.; Gao, T.G.; Guo, H.; Peng, X.Q.; et al. Thaw depth determines dissolved organic carbon concentration and biodegradability on the northern Qinghai-Tibetan Plateau. Geophys. Res. Lett. 2017, 44, 9389–9399.
22. McGuire, A.D.; Koven, C.; Lawrence, D.M.; Clein, J.S.; Xia, J.; Beer, C.; Burke, E.; Chen, G.; Chen, X.; Delire, C.; et al. Variability in the sensitivity among model simulations of permafrost and carbon dynamics in the permafrost region between 1960 and 2009. Glob. Biogeochem. Cycles 2016, 30, 1015–1037.
23. Nieberding, F.; Wille, C.; Fratini, G.; Asmussen, M.O.; Wang, Y.; Ma, Y.; Sachs, T. A long-term (2005–2019) eddy covariance data set of CO_2 and H_2O fluxes from the Tibetan alpine steppe. Earth Syst. Sci. Data 2020, 12, 2705–2724.
24. Wang, Y.; Wang, L.; Li, X.; Zhou, J.; Hu, Z. An integration of gauge, satellite, and reanalysis precipitation datasets for the largest river basin of the Tibetan Plateau. Earth Syst. Sci. Data 2020, 12, 1789–1803.
25. Huang, Z.; Zhong, L.; Ma, Y.; Fu, Y. Development and evaluation of spectral nudging strategy for the simulation of summer precipitation over the Tibetan Plateau using WRF (v4.0) Geosci. Model Dev. 2021, 14, 2827–2841.
26. Zhang, G.; Nan, Z.; Wu, X.; Ji, H.; Zhao, S. The role of winter warming in permafrost change over the Qinghai-Tibet Plateau. Geophys. Res. Lett. 2019, 46, 11261–11269.

27. Alempic, J.; Lartigue, A.; Goncharov, A.E.; Grosse, G.; Strauss, J.; Tikhonov, A.N.; Fedorov, A.N.; Poirot, O.; Legendre, M.; Santini, S.; Abergel, C.; Claverie, J.M. An update on eukaryotic viruses revived from ancient permafrost. bioRxiv. 2022, 11, 10.515937.
28. Nikiforoff, C. The perpetually frozen subsoil of siberia. Soil Sci. 1928, 26, 61–82.
29. Stefan, J. Ueber die Theorie der Eisbildung, insbesondere über die Eisbildung im Polarmeere. Ann. Phys. 1891, 278, 269–286.
30. Berggren, W.P. Prediction of temperature-distribution in frozen soils. Eos Trans. Am. Geophys. Union 1943, 24, 71–77.
31. Nelson, F.E.; Outcalt, S.I. A Computational Method for Prediction and Regionalization of Permafrost. Arct. Alp. Res. 1987, 19, 279–288.
32. Anisimov, O.A.; Nelson, F.E. Permafrost distribution in the Northern Hemisphere under scenarios of climatic change. Glob. Planet. Change 1996, 14, 59–72.
33. Nelson, F.E.; Shiklomanov, N.I.; Mueller, G.R.; Hinkel, K.M.; Walker, D.A.; Bockheim, J.G. Estimating Active-Layer Thickness over a Large Region: Kuparuk River Basin, Alaska, USA. Arct. Alp. Res. 1997, 29, 367–378.
34. Nelson, F.E.; Anisimov, O.A.; Shiklomanov, N.I. Climate Change and Hazard Zonation in the Circum-Arctic Permafrost Regions. Nat. Hazards 2002, 26, 203–225.
35. Nelson, F.E.; Shiklomanov, N.I.; Hinkel, K.M.; Christiansen, H.H. The Circumpolar Active Layer Monitoring (CALM) Workshop and THE CALM II Program. Polar Geogr. 2004, 28, 253–266.
36. Kudryavtsev, V.A.; Garagulya, L.S.; Kondratyeva, K.A.; Melamed, V.G. Fundamentals of Frost Forecasting in Geological Engineering Investigations; Moscow State University Press: Nakuka, Moscow, 1974; Volume 431.
37. Shiklomanov, N.I.; Nelson, F.E. Analytic representation of the active layer thickness field, Kuparuk River Basin, Alaska. Ecol. Model. 1999, 123, 105–125.
38. Nan, Z.; Li, S.; Cheng, G. Prediction of permafrost distribution on the Qinghai-Tibet Plateau in the next 50 and 100 years. Sci. China Ser. D-Earth Sci. 2005, 48, 797–804.
39. Aalto, J.; Karjalainen, O.; Hjort, J.; Luoto, M. Statistical forecasting of current and future circum-Arctic ground temperatures and active layer thickness. Geophys. Res. Lett. 2018, 45, 4889–4898.
40. Smith, M.W.; Riseborough, D.W. Permafrost monitoring and detection of climate change. Permafr. Periglac. Process. 1996, 7, 301–309.
41. Riseborough, D.W. The mean annual temperature at the top of permafrost, the TTOP model, and the effect of unfrozen water. Permafr. Periglac. Process. 2002, 13, 137–143.
42. Garibaldi, M.C.; Bonnaventure, P.P.; Lamoureux, S.F. Utilizing the TTOP model to understand spatial permafrost temperature variability in a High Arctic landscape, Cape Bounty, Nunavut, Canada. Permafr. Periglac. Process. 2021, 32, 19–34.
43. Juliussen, H.; Humlum, O.; Towards a TTOP ground temperature model for mountainous terrain in central-eastern Norway. Permafr. Periglac. Process. 2007, 18, 161–184.

44. Zhang, Y.; Zang, S.; Li, M.; Shen, X.; Lin, Y. Spatial Distribution of Permafrost in the Xing′an Mountains of Northeast China from 2001 to 2018. Land 2021, 10, 1127.
45. Ni, J.; Wu, T.; Zhu, X.; Hu, G.; Zou, D.; Wu, X.; Li, R.; Xie, C.; Qiao, Y.; Pang, Q.; et al. Simulation of the Present and Future Projection of Permafrost on the Qinghai-Tibet Plateau with Statistical and Machine Learning Models. JGR Atmos. 2021, 126, e2020JD033402
46. Ran, Y.; Li, X.; Che, T.; Wang, B.; Cheng, G. Current state and past changes in frozen ground at the Third Pole: A research synthesis. Adv. Clim. Change Res. 2022, 13, 632–641.
47. Yin, G.; Niu, F.; Lin, Z.; Luo, J.; Liu, M. Data-driven spatiotemporal projections of shallow permafrost based on CMIP6 across the Qinghai–Tibet Plateau at 1 km^2 scale. Adv. Clim. Change Res. 2021, 12, 814–827.
48. Obu, J.; Westermann, S.; Bartsch, A.; Berdnikov, N.; Christiansen, H.H.; Dashtseren, A.; Delaloye, R.; Elberling, B.; Etzelmüller, B.; Kholodov, A.; et al. Northern Hemisphere permafrost map based on TTOP modelling for 2000–2016 at 1 km^2 scale. Earth-Sci. Rev. 2019, 193, 299–316.
49. Batbaatar, J.; Gillespie, A.R.; Sletten, R.S.; Mushkin, A.; Amit, R.; Trombotto Liaudat, D.; Liu, L.; Petrie, G. Toward the Detection of Permafrost Using Land-Surface Temperature Mapping. Remote Sens. 2020, 12, 695.
50. Outcalt, S.I.; Nelson, F.E.; Hinkel, K.M. The zero-curtain effect: Heat and mass transfer across an isothermal region in freezing soil. Water Resour. Res. 1990, 26, 1509–1516.
51. Gillespie, A.R.; Batbaatar, J.; Sletten, R.S.; Trombotto, D.; O′Neal, M.; Hanson, B.; Mushkin, A. Monitoring and mapping soil ice/water phase transitions in arid regions. In Geological Society of America Abstracts with Programs; Geological Society of America: Boulder, CO, USA, 2017.
52. Zhao, Y.; Nan, Z.; Ji, H.; Zhao, L. Convective heat transfer of spring meltwater accelerates active layer phase change in Tibet permafrost areas. Cryosphere 2022, 16, 825–849.
53. Wang, C.; Zhang, Z.; Zhang, H.; Zhang, B.; Tang, Y.; Wu, Q. Active Layer Thickness Retrieval of Qinghai–Tibet Permafrost Using the TerraSAR-X InSAR Technique. IEEE J. Sel. Top. Appl. Earth Obs. Remote Sens. 2018, 11, 4403–4413.
54. Zhao, Z.; Tonooka, H. Analysis of Permafrost Distribution and Change in the Mid-East Qinghai–Tibetan Plateau during 2012–2021 Using the New TLZ Model. Remote Sens. 2022, 14, 6350.
55. Kersten, M. S. Thermal properties of soils. University of Minnesota institute of technology engineering experiment station. 1949, LII, 21.
56. Johansen, O. Thermal Conductivity of Soils. Ph.D. Thesis, University of Trondheim, Trondheim, Norway, 1975. (Draft English Translation 637, US Army Corps of Engineers, Cold Regions Research and Engineering Laboratory, Hanover, New Hampshire ed.)
57. Walvoord, M.A.; Kurylyk, B.L. Hydrologic Impacts of Thawing Permafrost—A Review. Vadose Zone J. 2016, 15, vzj2016.01.0010.

58. Ran, Y.; Li, X.; Cheng, G.; Zhang, T.; Wu, Q.; Jin, H.; Jin, R. Distribution of Permafrost in China: An Overview of Existing Permafrost Maps. Permafr. Periglac. Process. 2012, 23, 322–333.
59. Zhang, G.; Nan, Z.; Hu, N.; Yin, Z.; Zhao, L.; Cheng, G.; Mu, C. Qinghai-Tibet Plateau Permafrost at Risk in the Late 21st Century. Earth′s Future 2022, 10, e2022EF002652.
60. Feng, S.; Tang, M.; Wang, D. New evidence for the Qinghai-Xizang(Tibet)Plateau as a pilot region of climatic fluctuation in China. Chin. Sci. Bull. 1998, 43, 1745–1749.
61. Peng, J.; Liu, Z.; Liu, Y.; Wu, J.; Han, Y. Trend analysis of vegetation dynamics in Qinghai–Tibet Plateau using Hurst Exponent. Ecol. Indic. 2012, 14, 28–39.
62. Wang, Z.; Fan, H.; Wang, D.; Xing, T.; Wang, D.; Guo, Q.; Xiu, L. Spatial Pattern of Highway Transport Dominance in Qinghai–Tibet Plateau at the County Scale. ISPRS Int. J. Geo-Inf. 2021, 10, 304.
63. Kukkonen, I.T.; Suhonen, E.; Ezhova, E.; Lappalainen, H.; Gennadinik, V.; Ponomareva, O.; Gravis, A.; Miles, V.; Kulmala, M.; Melnikov, V.; et al. Observations and modelling of ground temperature evolution in the discontinuous permafrost zone in Nadym, north-west Siberia. Permafr. Periglac. Process. 2020, 31, 264–280.
64. Donato, G.; Belongie, S. Approximate Thin Plate Spline Mappings. In Proceedings of the Computer Vision—ECCV 2002, Copenhagen, Denmark, 28–31 May 2002; Heyden, A., Sparr, G., Nielsen, M., Johansen, P., Eds.; Spring: Berlin/Heidelberg, Germany, 2002; Volume 2352, pp. 21–31.
65. Deng, Z.; Lu, Z.; Wang, G.; Wang, D.; Ding, Z.; Zhao, H.; Xu, H.; Shi, Y.; Cheng, Z.; Zhao, X. Extraction of fractional vegetation cover in arid desert area based on Chinese GF-6 satellite. Open Geosci. 2021, 13, 416–430.
66. Jiang, L.; Pan, F.; Wang, G.; Pan, J.; Shi, J.; Zhang, C. MODIS Daily Cloud-Free Factional Snow Cover Data Set for Asian Water Tower Area (2000–2022); National Tibetan Plateau Data Center: Beijing, China, 2022.
67. Tarnawski, V.R.; Momose, T.; McCombie, M.L.; Leong, W.H. Canadian field soils III. Thermal-conductivity data and modeling. Int. J. Thermophys. 2015, 36, 119–156.
68. McInnes, K.J. Thermal Conductivities of Soils from Dryland Wheat Regions of Eastern Washington. Master′s Thesis, Washington State University, Washington, DC, USA, 1981.
69. Hopmans, J.W.; Dane, J.H. Thermal conductivity of two porous media as a function of water content, temperature, and density. Soil Sci. 1986, 142, 187–195.
70. Campbell, G.S.; Jungbauer, J.D., Jr.; Bidlake, W.R.; Hungerford, R.D. Predicting the effect of temperature on soil thermal conductivity. Soil Sci. 1994, 158, 307–313.
71. Côté, J.; Konrad, J.M. A generalized thermal conductivity model for soils and construction materials. Can. Geotech. J. 2005, 42, 443–458.

72. Kasubuchi, T.; Momose, T.; Tsuchiya, F.; Tarnawski, V.R. Normalized thermal conductivity model for three Japanese soils. Trans. Jpn. Soc. Irrig. Drain. Rural Eng. 2007, 75, 529–533.
73. Lu, S.; Ren, T.; Gong, Y.; Horton, R. An improved model for predicting soil thermal conductivity from water content at room temperature. Soil Sci. Soc. Am. J. 2007, 71, 8–14.
74. Chen, S.X. Thermal conductivity of sands. Heat Mass Transf. 2008, 44, 1241–1246.
75. Tarnawski, V.R.; McCombie, M.L.; Leong, W.H.; Wagner, B.; Momose, T.; Schönenberger, J. Canadian field soils II. Modeling of quartz occurrence. Int. J. Thermophys. 2012, 33, 843–863.
76. McCombie, M.L.; Tarnawski, V.R.; Bovesecchi, G.; Coppa, P.; Leong, W.H. Thermal conductivity of pyroclastic soil (Pozzolana) from the environs of Rome. Int. J. Thermophys. 2017, 38, 21.